Regenerable Composites for Removal of Organic Dye in Aqueous Media and Water in Heavy Oil and the Associated Interaction Mechanism

By

Jiawen Zhang

A thesis submitted in partial fulfillment of the requirements for the degree of

Doctor of Philosophy

In

Materials Engineering

Department of Chemical & Materials Engineering
University of Alberta

ABSTRACT

Water plays an indispensable role in all aspects of life, including farming, domestic and industrial uses. In industries, water has been extensively applied in mining, production and surface treatment, producing a large quantity of contaminated water that threatens human health, endangers environment and undermines sustainable development. Besides, in some cases, after the application of water, the remnant of water in products (e.g., heavy oil) can result in difficulties in refining and transport. Thus, technique development is immediately necessary to eliminate the contaminants in aqueous effluents and to remove water from products. Herein, in this dissertation, regenerable composites are designed, synthesized and employed for sustainable dye elimination from water and water removal from heavy oil, and the associated interaction mechanism has also been investigated.

Dyes, as a kind of most common pollutants existing in wastewater, can endanger the health of living creatures. The adsorbents nowadays for dye removal usually suffer from low adsorption capacity, sludge production and low regenerability. Herein, in this work, a poly (acrylic acid) (PAA) functionalized magnetic Fe_3O_4 nanoparticle-graphene oxide nanocomposite (PAA/MGO), with high adsorption capacity and rapid adsorption rate for dye (using methylene blue as a model compound), was synthesized by a facile method. It was found that PAA/MGO composite (291 mg/g) possessed elevated maximum adsorption capacity (pH ~7) compared with MGO (70 mg/g), and with the aid of magnetic separation, PAA/MGO composite showed remarkable regenerability for 5 times of usage. The adsorption mechanism was also surveyed by Langmuir and Freundlich isotherm models fitting and studying adsorption capacity difference at different pH (pH ~3-11).

Graphene oxide (GO), as a 2-dimentional nanomaterial, has been widely applied in dye removal via adsorption due to its affinity to dyes, high surface area and rich functional groups

available for further modification. However, the fundamental understanding of the effect of specific functional groups of GO on the interaction between GO and dyes is still unclear. Herein, single-molecular force spectroscopy (SMFS) and Density Functional Theory (DFT) calculations were applied to study the interaction between a single dye molecule and GO, which suggested that the carboxylic groups could interact with cationic dye by electrostatic interaction under ionized condition, whereas the epoxy groups on the basal plane of GO could enhance the π-π interaction between aromatic parts of GO and cationic dye under both ionized and unionized conditions of carboxylic groups on GO. The configuration of dye on GO was also investigated and discussed. This fundamental study can shed light to GO nanocomposites designing and enhance their performance in discoloration of wastewater.

Global demand for crude oil has constantly increased, which leads to a rising production of heavy oil. However, the water residue in heavy oil can be stabilized by asphaltenes, the heaviest components in heavy oil, and results in many problems in oil production and refining, which include corrosion and low petroleum recovery. Asphaltenes tend to aggregate, precipitate and lead to foulings on appliances and adsorbents, which can also undermine oil production and the process to remove water from heavy oil. In this work, inspired by the long-range attraction property of zwitterionic polyelectrolytes to water in oil, zwitterionic polyelectrolyte poly (3-[dimethyl(2-methacryloyloxyethyl) ammonium] propanesulfonate) (PMAPS) grafted polydopamine (PDA) coated silicon wafer substrates and sponges were fabricated, manifesting great underwater self-cleaning ability, anti- oil property and regenerability. After being soaked in model heavy oil (asphaltene toluene solution) under dry state, the PMAPS-PDA coating on silicon wafer substrates still showed underwater superoleophobicity after being cleaned by acidic, neutral and alkaline water, showing promises to minimize the fouling concerns in the handling and transport of heavy

oil. The PMAPS-PDA modified sponges could remove more than 90% of water from model heavy oil for ten cycles, showing promises for water removal from heavy oil. Single-charged polyelectrolytes cationic poly (2-(methacryloyloxy)ethyl trimethylammonium chloride) (PMTAC) and anionic poly (3-sulfopropyl acrylate potassium) (PSPAK) were used to fabricate coatings using the same method as PMAPS, and their performance in fouling cleaning-up and water removal from model heavy oil was not comparable to PMAPS, demonstrating the superiority of zwitterionic polyelectrolytes in anti-fouling and water removal applications in heavy oil industries.

PREFACE

Chapter 3 of this thesis was published as Jiawen Zhang, Md. Shafiul Azam, Chen Shi, Jun Huang, Bin Yan, Qingxia Liu, and Hongbo Zeng, "Poly (acrylic acid) Functionalized Magnetic Graphene Oxide Nanocomposite for Removal of Methylene Blue," RSC Advances, 2015, vol. 5, issue 41, 32272-32282. I was responsible for materials synthesis, adsorption tests, zeta potential measurements, recycling tests, data analysis and the manuscript composition. Dr. Jun Huang contributed to the AFM imaging of graphene oxide. Dr. Md. Shafiul Azam, Dr. Chen Shi, Dr. Bin Yan and Dr. Qingxia Liu contributed to manuscript revision. Dr. Hongbo Zeng was the corresponding author who was involved in concept formation and manuscript composition.

Chapter 4 of this thesis was composited by Jiawen Zhang. I was responsible for AFM work, density functional theory simulations, materials synthesis and data analysis. Dr. Chen Shi, Lu Gong and Jing Liu assisted with some of AFM force measurements. Dr. Bin Yan, Dr. Xi Lu and Jingsi Chen gave suggestions for revising the manuscript. Li Xiang, Dr. Jingyi Wang and Dr. Qingxia Liu contributed to the manuscript edits. Dr. Hongbo Zeng was the supervisor and involved in concept formation and manuscript composition.

Chapter 5 of this thesis was composited by Jiawen Zhang. I was responsible for materials synthesis, contact angle measurements, underwater self-cleaning tests and water removal ability tests, and data analysis. Lu Gong and Li Xiang was responsible for AFM imaging. Dr. Ling Zhang was responsible for the SEM measurement. Dr. Chen Shi helped with the materials synthesis. Wenjihao Hu gave suggestions for the manuscript revision. Dr. Qingxia Liu contributed to the manuscript edits. Dr. Hongbo Zeng was the supervisor and involved in concept formation and manuscript composition.

Chapter 1, Chapter 2 and Chapter 6 are written by Jiawen Zhang originally.

ACKNOWLEDGEMENT

First and foremost, I would like to express my sincere gratitude to Dr. Hongbo Zeng, a scholarly, responsible and respective supervisor, who has given me essential guidance and invaluable support during my Ph.D. study. Prof. Zeng has introduced me to the field of surface science and helped me to develop logical thinking and writing skills, which would be the tremendous wealth for my future study. I also wish to thank Dr. Qingxia Liu for his informative and valuable advices. Prof. Liu is highly experienced in both academic and industrial fields, who has greatly broadened my knowledge.

Second, I would like to thank my group members for their helpful support throughout my whole Ph.D. study.

Third, I would like to acknowledge the financial support from the Natural Sciences and Engineering Research Council of Canada (NSERC), Canadian Centre for Clean Coal/Carbon and Mineral Processing Technologies (C5MPT) and the Canada Foundation for Innovation (CFI).

Finally, I would like to thank my beloved parents, my husband and other family members. They have offered me generous encouragement and reliable support that I can finish my Ph.D. study.

Dedicated to

My parents, my husband Li Xiang, and my other family members

LIST OF TABLES

LIST OF FIGURES

SYMBOLS AND NOMENCLATURE

GO	graphene oxide
2-D	2-dimensional
MGO	magnetic graphene oxide
AOCs	aromatic organic compounds
FTIR	Fourier transform infrared spectroscopy
W/O	water-in-oil
SMFS	single-molecule force spectroscopy
PAA/MGO	poly (acrylic acid) modified magnetic graphene oxide
PMAPS	poly (3-[methacryloyloxyethyl)ammonium] propanesulfonate)
PDA	polydopamine
PMTAC	poly (2-(methacryloyloxy)ethyl trimethylammonium chloride)
PSPAK	poly (3-sulfopropyl acrylate potassium)
AFM	atomic force microscope
PEG	polyethylene glycol
F	bond dissociation force
ΔG	bond dissociation energy, kcal mol^{-1}
Δx	bond dissociation distance, Å

EDL	electrical double layer
MB	methylene blue
PAA	poly (acrylic acid)
EDC	1-(3-Dimethylaminopropyl)-3-ethylcarbodiimide hydrochloride
DI	deionization
TGA	thermogravimetric analysis
TEM	transmission electron microscopy
XPS	X-ray photoelectron spectroscopy
q_t	adsorption capacity, mg g^{-1}
$p\%$	removal percentage
C_0, C_t	initial concentration and concentration at selective time, mg L^{-1}
t	time
m	mass of the adsorbent used, g
V_0, V_t	initial volume and volume at selective t of solutions, mL
B. E.	binding energy, eV
R^2	correlation coefficient values
C_e	equilibrium concentration of MB, mg L^{-1}
q_m	maximum Langmuir monolayer adsorption capacity, mg g^{-1}

b	related to the energy of the adsorption.
K_f, n	indicators of adsorption capacity and adsorption intensity
UV spectroscopy	ultraviolet spectroscopy
EDS	energy-dispersive X-ray spectroscopy
DFT	density functional theory
TBO	toluidine blue o
TA	DL-thioctic acid
DMAP	4-(dimethylamino)pyridine
DCC	N,N'-dicyclohexylcarbodiimide
E-FJC	extended freely jointed chain
R	loading rate
k_B	Boltzmann constant
T	absolute temperature
k_0	spontaneous dissociation rate of the bond
R	gas constant
A	Arrhenius prefactor or the frequency factor
PCM	polarizable continuum model
E_{ad}	adsorption energies, kcal mol^{-1}

$E_{ad,\ vacuum}$	adsorption energy in vacuum, kcal mol^{-1}
$E_{ad,\ water}$	adsorption energy in water, kcal mol^{-1}
ESP	electrostatic potential, kcal mol^{-1}
ESP_{min}	minimum ESP, kcal mol^{-1}
ESP_{max}	maximum ESP, kcal mol^{-1}
PU	polyurethane
V501	4,4'- azobis(4-cyanopentanoic acid)
RAFT agent	4-cyanopentanoic acid dithiobenzoate
WCA-A	water contact angles in air
OCA-W	oil contact angles in water

Chapter 1 Introduction

As the most abundant solvent existing in the world, water has been widely applied in most kinds of industries, such as mining, paper and pulp, textile and oil sands industries,[1-4] which have benefited and greatly enriched human life. However, the discharged effluents containing various pollutants might jeopardize the life of human beings and environment. Besides, the water residue in the products may lead to process and transport difficulties.

Dyes are a kind of most common pollutants existing in wastewater, which are used to colourize the products in many industries and their usage produces substantial amount of coloured wastewater. Dyes discharged in environment can reduce the light penetration in water and impair the photosynthetic activity of aquatic organisms.[5-6] Moreover, many dyes are toxic to living creatures and not easy to be degraded by microorganisms. Therefore, economic and efficient techniques are highly required to remove dye pollutants from wastewater.

The increasing global demand for crude oil and conventional oil resources depletion lead to a rising production of heavy oil. In the production process of heavy oil, the formation water will be stabilized by asphaltenes (the heaviest components with aromatic structures and heteroatoms) in the heavy oil and form water-in-oil (W/O) emulsions, in which the water can corrode the appliances and impair the refined petroleum production.[7] Thus, it is urgent to develop cost-effective method to remove water from the emulsions.

1.1 Industrial pollutants review

1.1.1 Industrial pollutants

The pollutants in industrial wastewater contain organic and inorganic substances, which come from manufacturing and energy productions. The pollutants may be toxic or carcinogenic, thus the wastewater treatment is imperative to protect human and ecological health. The discharged

pollutants include medicines, surfactants, heavy metals, pesticides, phenols, dyes, food additives, oils and so on.[1, 8]

1.1.2 Dyes in wastewater and their toxicity

As one of the most common pollutants, dyes are extensively used in many industries, such as dye productions, paper and pulp, textile and plastics industries. More than one hundred thousand kinds of commercial dyes are produced annually, and the total mass of dyes is over 700,000 tons.[9] Dyes are a group of organic compounds, containing chromophore groups and conjugated structures, which can adsorb visible lights and exhibit specific colors.[10] In industries, dyes are applied to impart color to substrates, such as papers, textiles and leathers, for a permanent coloration.[11] During the productions and applications of dyes, about 10-15% of dyes cannot bind to the substrates and then discharged to the environment as effluent.[12] Some dyes can lead to allergy, skin irritation and even cancer in human beings.[13] Besides, even a trace amount of dyes can cause evident coloration of water, which can lead to the adsorption and reflection of visible lights, reduce the light penetration in water for aquatic organism's photosynthetic activity, and then deteriorate healthy aquatic ecosystems.[5-6] Therefore, it is highly imperative to decolorize the dye-contaminated water.

1.1.3 Technologies to remove dyes from wastewater

Numerous efforts have been devoted to the remediation of dye-contaminated aqueous effluents, and the current technologies applied to dye removal can be classified as: chemical, biological and physical methods.[14]

Chemical methods include the techniques involving chemical reactions, such as irradiation, precipitation-flocculation, electrokinetic coagulation, electroflotation, electrochemical and oxidation.[14-16] These techniques are usually costly, and might produce sludges, causing disposal

problems. Besides, due to the excessive chemical disposal, secondary pollution may happen.

Recently, biological methods for dye removal have attracted enormous attention, in which the microorganisms (e.g., fungi, algae, bacterial) are used to degrade and adsorb dyes from the aqueous effluents.[17] Employing biological methods for dye wastewater treatment possesses many advantages, such as relatively economical efficient, generating less sludges and environmentally friendly.[18] However, the application of biological treatment is restricted by high land requirements (large area, sensitive to sunshine duration),[19] low efficiency for some toxic or stubborn dyes[19-20] and inadequate discoloration.[16]

Physical methods are extensively used in industries for dye removal due to high dye removal efficiency and easy application, such as adsorption, membrane filtration, electrodialysis and ion-exchange.[21-22] Membrane filtration can continuously separate dye, but this technique requires pre-treatment of wastewater to avoid membrane blockage and the periodic replacement of membrane is costly.[23-25] In ion exchange process, wastewater containing dyes passes through the ion exchange resin, and then the charged dyes can be fixed on resin. The shortcomings of this technique include high cost and only effective for some specific species of dyes.[24, 26] Adsorption, as an easy and economic process for dye removal, recently has attracted more and more attentions and is considered to be superior compared to other techniques.

1.1.4 Adsorbent choices

As a treatment process with long history, adsorption possess flexibility, high removal ability and recyclability for the adsorbates, thus it has been widely applied for wastewater remediation.[14, 16] A large variety of of natural and artificial adsorbents have been designed and applied for wastewater treatment, such as silica gel, fly ash and coal, natural clay and activated carbon. Activated carbon is the most achievable and commonly used adsorbent for dye removal.[27]

Its porous structure endows itself with high surface area, resulting high adsorption capacity. The drawback of activated carbon is that its activation needs high energy and its reactivation after usage leads to 10-15% loss of itself.[16] The porous structure of activated carbon might also lead to the pore blockage, and then result in desorption and recycling difficulty. The remained challenging issues of conventional adsorbents, such as relatively low removal efficiency and recyclability, and separation difficulty, call for the development of new adsorbents. Graphene oxide (GO), with unique 2-dimensional (2-D) structure, high surface area and rich functional groups, has attracted many attentions recently for wastewater treatment. Its 2-D structure promises GO's application in fabricating composites for dye removal with good recyclability due to easy accessing and desorption of dyes.

1.1.5 Graphene oxide-based composites used in adsorption applications

The rich functional groups on GO, such as carboxylic, epoxy and carbonyl groups, endow GO with good water dispersibility and capability for further modification.[28-29] To achieve specific applications of GO in different fields, GO has been modified by various chemical and physical methods for certain functionalities. Magnetic particles have been used to modify GO for easy separation and recyclability.[30-32] However, the decoration of magnetic nanoparticles on GO sheets usually results in relatively low adsorption capacity (mg/g) for adsorbates. One possible feasible way to solve the problem is to graft functional polymers to the magnetic graphene oxide (MGO) to increase its adsorption capacity. Polymers contain numerous kinds of rich functional groups, such as carboxylic and amino groups, which can have strong affinity for specific kinds of pollutants. However, most efforts being devoted to the fabrication of graphene/polymer composites focus on their mechanical and electric performance, whereas the adsorption capacity enhancement via the combination of polymer on GO is rarely studied. Only limited studies have employed polymers to

modify GO targeting dye removal, including cellulose[33] and chitosan.[34]

1.1.6 Graphene oxide adsorption mechanism

GO is known to have affinities to aromatic organic compounds (AOCs) (e.g. dyes, drugs, biomolecules), via a noncovalent approach which retains its structure and tremendous properties.[35-37] Besides, π−π stacking between GO and AOCs can lead to effective quenching of the fluorescence of dye.[36, 38] Hence, GO has been widely applied in wastewater treatment,[37, 39-43] drug delivery,[44-45] biosensors,[44, 46-47] catalysis[36, 48] and so on. Gaining a detailed knowledge of GO-AOCs interactions would greatly contribute to performance enhancement and extend GO's application scope.

Via Hummer's method, GO can be produced in relatively large scale by chemical oxidation and exfoliation of graphite flake, which makes its large-scale applications in various fields possible. A great amount of oxygen-containing functional groups are introduced on GO sheets[37]: epoxy and carbonyl groups existing on GO surface, carboxylic groups locating on the edge of GO flakes and the broken holes on GO's surface.[49-53] The complex surface properties of GO lead to its various types of interactions with the AOCs.[36] Macroscopic experimental techniques, such as ultraviolet (UV) spectroscopy,[54-55] Fourier transform infrared spectroscopy (FTIR)[55] and fluorescence spectroscopy,[38] have been employed to provide overall information about the aggregation types between GO and AOCs. It was reported that GO carries negatively charges when dispersed in water, which favors its adsorption for cationic AOCs.[28] The proposed interaction mechanisms between GO and cationic AOCs include the π-π interaction and hydrophobic interaction due to the remained sp^2 zones on GO's surface,[54, 56] and the electrostatic interaction introduced by the negatively charged carboxylic groups of GO.[57-58] However, using the macroscopic techniques is difficult to survey the influence of specific kinds of functional groups

on GO-AOCs interactions, and the fundamental mechanism remains unclear. There has been no experimental and theoretical study on exploring the interaction mechanism of GO-AOCs interaction at nanoscale and single molecular level to our best knowledge.

1.2 Water relevant problems in heavy oil industries

The industrial development leads to significant burdens on energy sources. Due to the decreasing conventional oil supply all over the world, unconventional oil sources, such as heavy oil, receive more and more attention and investments nowadays.[7, 59] The heaviest fractions (asphaltenes) of heavy oil are easy to precipitate and form foulings on furnaces, reservoirs, pipelines and other appliances, resulting in troubles in handling, transport and refining of the high asphaltenic heavy oil.[60-63] Water, as the cheapest and most abundant solvent, is generally applied for surface cleaning for fouled surface,[64] which might be not effective in cleaning heavy oil contaminated surfaces due to the adhesion of asphaltenes to solids.[65] Besides, the involvement of water during heavy oil production and transportation will lead to water-in-oil (W/O) emulsions stabilized by asphaltenes, which will undermine petroleum recovery and cause corrosion problems.[66-68]

Nowadays, due to the oil spills from now and then, oil/water separation and anti-oil fouling coatings have attracted a lot of attentions. The oils separated from water include a large variety of light oils, such as organic solvents, soybean oil and even light crude oil, but water removal from heavy oil by adsorption has not been successfully achieved before as far as we know. It is imperative to develop effective method to clean the heavy oil fouled surface and remove water from heavy oil.

1.2.1 Common water-in-oil (W/O) separation methods

Due to frequent oil leakage and increased production of industrial oily wastewater, great

efforts have been devoted for the separation of light oils/water mixture. Conventional methods for oil/water separation can meet most separation requirements by combining different comprehensive approaches, such as centrifugation, gravity separation, coagulation, electric field separation and biological treatment. However, theses techniques usually suffer from low separation efficiency, production of secondary fouling and large field requirements.[69-75] Recently, oil/water separation by manipulating surface wettability has attracted more and more attention. Wettability is the property of a surface that determines the liquid wetting behavior on the surface, resulted from intermolecular interaction. If the surface shows different wettability for oil and water, then the selective separation of oil/water mixture is possibly to be achieved. Superoleophilic and superhydrophobic materials can be used to selectively remove oil from water, while superoleophobic and superhydrophilic materials can be applied for separating water from oil. The superoleophilic materials, due to their intrinsic property, are easy to be fouled by oil. The oil fouling can block the pore of porous adsorbents and membrane, resulting separation failure. Therefore, heavy oil/water separation is highly possible to be undermined by the asphaltenes foulings. Superhydrophilic materials should be advantageous in heavy oil/water separation, which is because that superhydrophilic materials could have strong affinity to water, and the bound water molecules are possible to repel heavy oil foulings The underwater oil contact angle θ can be calculated by the following equation derived from Young's equation (Figure 1.1):[76-77]

$$cos\theta = \frac{\gamma_{o-g}cos\theta_O - \gamma_{w-g}cos\theta_w}{\gamma_{o-w}} \qquad (1.1)$$

where γ_{o-g}, γ_{w-g} and γ_{o-w} are oil-air, water-air and oil-water interfacial tensions, respectively. θ_O and θ_w are the contact angles of oil in air and water in air, respectively.

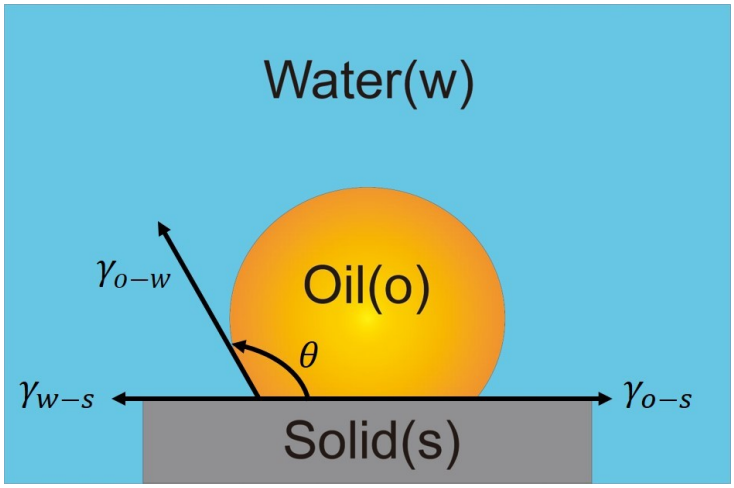

Figure 1.1 Diagram illustrates the underwater contact angle determined by surface tensions.

The involved technologies in oil/water separation are mainly based on filtration (commonly using meshes and membranes) and adsorption (typically using porous adsorptive materials).[78] In filtration, the oil/water mixture need to be collected and then flow through the meshes or membranes by gravity or pressure. Oil/water separation by adsorption is more practical in some cases due to its easy application.

1.2.2 Zwitterionic polyelectrolytes used in anti-fouling and oil/water separation

The underwater superhydrophilic property of the solid substrates can be achieved by grafting various polymers on their surfaces, such as polyethylene glycol,[79] poly (acrylic acid)[80-81] and zwitterionic polyelectrolytes, and constructing surfaces with high roughness.[79]

Zwitterionic materials are a class of materials that are composed of both positive and negative ionic groups and remain charge neutral,[82-83] which extensively exist in living creatures, such as cell membranes,[84] peptides,[85] proteins[86] and osmolytes.[87] The utilization of zwitterions' antifouling property was inspired by the zwitterionic phospholipids headgroups in external face of the mammalian cell membranes, resulting the cell's nonfouling property.[88] The antifouling of zwitterions is attributed to the ionic groups of zwitterions that can bind water molecules, which

can prevent fouling adhesion. [89-90] Zwitterionic polyelectrolytes, the polymeric form of zwitterions, possessing superiorly binding water ability compared with single-charged polyelectrolytes and other hydrophilic species[87, 91] and have been widely applied for surface modifications to achieve underwater superoleophobicity[92] and oil/water separation.[93] In oil/water separation, the oils include a large variety of light oils, such as ether, toluene, hexane, hexadecane, soybean oil and even light crude oil.[92-95] Besides, it is observed that zwitterionic polyelectrolytes possess a stronger long-range attraction for water under oil compared with single-charged (cationic and anionic) polyelectrolytes, which is likely due to their large dipole moment.[96] Thus, it is promising to apply zwitterionic polyelectrolytes as anti-fouling coatings for heavy oil fouling cleaning-up and the removal of water from heavy oil by adsorption.

1.3 Objectives

As discussed above, the traditional adsorbents for dyes often suffer from low adsorption capacity and regenerability problems. GO and its composites have been proved as effective adsorbents for dyes, as well as a large group of aromatic organic compounds. Our objective is to rationally design and fabricate GO-based adsorbent for dyes that have high adsorption capacity and outstanding regenerability, and to understand the interaction mechanism between GO and dyes.

In heavy oil industries, it is challenging to overcome the heavy oil fouling and remove the produced water from heavy oil. Our objective is to fabricate regenerable coating with underwater self-cleaning property and coated sponge with water removal ability.

The detailed objectives are listed as follows.

(1) Fabricate poly (acrylic acid) modified magnetic graphene oxide (PAA/MGO) composite for cationic dye removal using methylene blue as model compound. Survey its adsorption capacity and regenerability performance.

(2) Combine single-molecule force spectroscopy (SMFS) and density functional theory (DFT) simulations to study the interaction between GO and AOC molecule at single-molecule level, which will provide information about adsorption energy and configuration of AOC molecule on GO affected by specific kinds of functional groups.

(3) Fabricate zwitterionic polyelectrolytes modified dopamine (PDA) coated silicon wafer substrates and sponges. The underwater self-cleaning ability and regenerability of the coated substrates after fouled by model heavy oil (asphaltene toluene solution) under dry state will be investigated. The water removal ability (removal efficiency and regenerability) from model heavy oil (asphaltene toluene solution) of the coated sponges will be studied. And the performance of zwitterionic polyelectrolyte-PDA coating for water removal and underwater self-cleaning will be compared with that of single-charged polyelectrolytes-PDA coatings.

1.4 Structure of the thesis

Chapter 1 reviews related literature and introduces the water-related challenges in wastewater treatment and heavy oil industries. The objectives in this work are given.

Chapter 2 describes the primary techniques used in this study.

Chapter 3 demonstrates the adsorption capacity and regenerability for MB (a model cationic dye) adsorption of PAA/MGO nanocomposite synthesized by a facile and effective method, compared to MGO. The effect of pH and the mechanism involved in the adsorption process has been studied, of which the results are presented and discussed.

In Chapter 4, the interaction mechanism between GO and AOC molecule (using MB as a model compound) has been investigated in depth, analyzed by SMFS and DFT simulations at single molecule level and elucidated.

In Chapter 5, zwitterionic polyelectrolyte poly (3-[dimethyl(2-methacryloyloxyethyl)

ammonium] propanesulfonate) (PMAPS) has been grafted on PDA deposited silicon wafer substrates and sponges. The PMAPS-PDA coating's performance in underwater self-cleaning after being fouled in dry state by model heavy oil (asphaltene toluene solution) and its regenerability has been investigated and compared with that of single-charged polyelectrolytes cationic poly (2-(methacryloyloxy)ethyl trimethylammonium chloride) (PMTAC) and anionic poly (3-sulfopropyl acrylate potassium) (PSPAK)-PDA coatings. The effect of pH on their underwater self-cleaning ability and anti-oil property has also been studied and demonstrated. The water removal performance from model heavy oil of PMAPS-PDA coated sponges has been surveyed and compared with that of PMTAC-PDA and PSPAK-PDA coated sponges.

In Chapter 6, major conclusions and contributions of this work are presented. The suggestions for future work are also outlined.

References

1. Kelly, E. N.; Schindler, D. W.; Hodson, P. V.; Short, J. W.; Radmanovich, R.; Nielsen, C. C., Oil Sands Development Contributes Elements Toxic at Low Concentrations to the Athabasca River and Its Tributaries. *Proc. Natl. Acad. Sci. U. S. A.* **2010,** *107*, 16178-16183.

2. Kelly, E. N.; Short, J. W.; Schindler, D. W.; Hodson, P. V.; Ma, M.; Kwan, A. K.; Fortin, B. L., Oil Sands Development Contributes Polycyclic Aromatic Compounds to the Athabasca River and Its Tributaries. *Proc. Natl. Acad. Sci. U. S. A.* **2009,** *106*, 22346-22351.

3. Allen, E. W., Process Water Treatment in Canada's Oil Sands Industry: I. Target Pollutants and Treatment Objectives. *J. Environ. Eng. Sci.* **2008,** *7*, 123-138.

4. Bajpai, P., *Bleach Plant Effluents from the Pulp and Paper Industry*. Springer: 2013.

5. Ozcan, A.; Ozcan, A.; Gok, O., Adsorption Kinetics and Isotherms of Anionic Dye of Reactive Blue 19 from Aqueous Solutions onto Dtma-Sepiolite. In *Hazardous Materials and Wastewater—Treatment, Removal and Analysis*, Nova Science Publishers: New York, 2007.

6. Prasad, A. L.; Santhi, T., Adsorption of Hazardous Cationic Dyes from Aqueous Solution onto Acacia Nilotica Leaves as an Eco Friendly Adsorbent. *Sustain. Environ. Res.* **2012,** *22*, 113-122.

7. Martínez-Palou, R.; de Lourdes Mosqueira, M.; Zapata-Rendón, B.; Mar-Juárez, E.; Bernal-Huicochea, C.; de la Cruz Clavel-López, J.; Aburto, J., Transportation of Heavy and Extra-Heavy Crude Oil by Pipeline: A Review. *J. Pet. Sci. Eng.* **2011,** *75*, 274-282.

8. Grassi, M.; Kaykioglu, G.; Belgiorno, V.; Lofrano, G., Removal of Emerging Contaminants from Water and Wastewater by Adsorption Process. In *Emerging Compounds Removal from Wastewater*, Springer: 2012; pp 15-37.

9. Singh, S. N., *Microbial Degradation of Synthetic Dyes in Wastewaters*. Springer: 2014.

10. Abrahart, E. N., *Dyes and Their Intermediates*. Chemical Publishing: New York, 1977.

11. Pereira, L.; Alves, M., Dyes—Environmental Impact and Remediation. In *Environmental Protection Strategies for Sustainable Development*, Springer: 2012; pp 111-162.

12. Vaidya, A.; Datye, K., Environmental-Pollution During Chemical-Processing of Synthetic-Fibers. *Colourage* **1982,** *29*, 3-10.

13. Bhatnagar, A.; Jain, A., A Comparative Adsorption Study with Different Industrial Wastes as Adsorbents for the Removal of Cationic Dyes from Water. *J. Colloid Interface Sci.* **2005,** *281*, 49-55.

14. Garg, V. K., Green Chemistry for Dyes Removal from Waste Water. *Green Process. Synth.* **2015,** *4*, 507-508.

15. Raghavacharya, C., Colour Removal from Industrial Effluents: A Comparative Review of Available Technologies. *Chem. Eng. World* **1997,** *32*, 53-54.

16. Robinson, T.; McMullan, G.; Marchant, R.; Nigam, P., Remediation of Dyes in Textile Effluent: A Critical Review on Current Treatment Technologies with a Proposed Alternative. *Bioresour. Technol.* **2001,** *77*, 247-255.

17. Ding, Z.; Hu, X.; Zimmerman, A. R.; Gao, B., Sorption and Cosorption of Lead (II) and Methylene Blue on Chemically Modified Biomass. *Bioresour. Technol.* **2014,** *167*, 569-573.

18. Forgacs, E.; Cserhati, T.; Oros, G., Removal of Synthetic Dyes from Wastewaters: A Review. *Environ. Int.* **2004,** *30*, 953-971.

19. Bhattacharyya, K. G.; Sarma, A., Adsorption Characteristics of the Dye, Brilliant Green, on Neem Leaf Powder. *Dyes Pigm.* **2003,** *57*, 211-222.

20. Kumar, V.; Wati, L.; Nigam, P.; Banat, I.; Yadav, B.; Singh, D.; Marchant, R., Decolorization and Biodegradation of Anaerobically Digested Sugarcane Molasses Spent Wash Effluent from Biomethanation Plants by White-Rot Fungi. *Process Biochem.* **1998,** *33*, 83-88.

21. Dąbrowski, A., Adsorption—from Theory to Practice. *Adv. Colloid Interface Sci.* **2001,** *93*, 135-224.

22. Iqbal, M. J.; Ashiq, M. N., Adsorption of Dyes from Aqueous Solutions on Activated Charcoal. *J. Hazard. Mater.* **2007,** *139*, 57-66.

23. Xu, Y.; Lebrun, R. E.; Gallo, P.-J.; Blond, P., Treatment of Textile Dye Plant Effluent by Nanofiltration Membrane. *Sep. Sci. Technol.* **1999,** *34*, 2501-2519.

24. Mishra, G.; Tripathy, M., A Critical Review of the Treatments for Decolourization of Textile Effluent. *Colourage* **1993,** *40*, 35-35.

25. Mantzavinos, D.; Hellenbrand, R.; Livingston, A. G.; Metcalfe, I. S., Beneficial Combination of Wet Oxidation, Membrane Separation and Biodegradation Processes for Treatment of Polymer Processing Wastewaters. *Can. J. Chem. Eng.* **2000,** *78*, 418-422.

26. Slokar, Y. M.; Le Marechal, A. M., Methods of Decoloration of Textile Wastewaters. *Dyes Pigm.* **1998,** *37*, 335-356.

27. Namasivayam, C.; Kavitha, D., Removal of Congo Red from Water by Adsorption onto Activated Carbon Prepared from Coir Pith, an Agricultural Solid Waste. *Dyes Pigm.* **2002,** *54*, 47-58.

28. Ramesha, G.; Kumara, A. V.; Muralidhara, H.; Sampath, S., Graphene and Graphene Oxide as Effective Adsorbents toward Anionic and Cationic Dyes. *J. Colloid Interface Sci.* **2011,** *361*, 270-277.

29. Hamilton, C. E. Functionalization, Coordination, and Coating of Carbon Nanomaterials. Rice University, 2009.

30. Ai, L.; Zhang, C.; Chen, Z., Removal of Methylene Blue from Aqueous Solution by a Solvothermal-Synthesized Graphene/Magnetite Composite. *J. Hazard. Mater.* **2011,** *192*, 1515-1524.

31. Xie, G.; Xi, P.; Liu, H.; Chen, F.; Huang, L.; Shi, Y.; Hou, F.; Zeng, Z.; Shao, C.; Wang, J., A Facile Chemical Method to Produce Superparamagnetic Graphene Oxide–Fe_3O_4 Hybrid Composite and Its Application in the Removal of Dyes from Aqueous Solution. *J. Mater. Chem.* **2012,** *22*, 1033-1039.

32. He, F.; Fan, J.; Ma, D.; Zhang, L.; Leung, C.; Chan, H. L., The Attachment of Fe 3 O 4 Nanoparticles to Graphene Oxide by Covalent Bonding. *Carbon* **2010,** *48*, 3139-3144.

33. Shi, H.; Li, W.; Zhong, L.; Xu, C., Methylene Blue Adsorption from Aqueous Solution by Magnetic Cellulose/Graphene Oxide Composite: Equilibrium, Kinetics, and Thermodynamics. *Ind. Eng. Chem. Res.* **2014,** *53*, 1108-1118.

34. Li, L.; Fan, L.; Luo, C.; Duan, H.; Wang, X., Study of Fuchsine Adsorption on Magnetic Chitosan/Graphene Oxide. *RSC Adv.* **2014,** *4*, 24679-24685.

35. Kang, T. W.; Jeon, S. J.; Kim, H. I.; Park, J. H.; Yim, D.; Lee, H. R.; Ju, J. M.; Kim, M. J.; Kim, J. H., Optical Detection of Enzymatic Activity and Inhibitors on Non-Covalently Functionalized Fluorescent Graphene Oxide. *ACS Nano* **2016,** *10*, 5346-5353.

36. Georgakilas, V.; Tiwari, J. N.; Kemp, K. C.; Perman, J. A.; Bourlinos, A. B.; Kim, K. S.; Zboril, R., Noncovalent Functionalization of Graphene and Graphene Oxide for Energy Materials, Biosensing, Catalytic, and Biomedical Applications. *Chem. Rev.* **2016,** *116*, 5464-5519.

37. Yan, H.; Wu, H.; Li, K.; Wang, Y.; Tao, X.; Yang, H.; Li, A.; Cheng, R., Influence of the Surface Structure of Graphene Oxide on the Adsorption of Aromatic Organic Compounds from Water. *ACS Appl. Mater. Interfaces* **2015,** *7*, 6690-6697.

38. Wang, Y.; Li, Z.; Hu, D.; Lin, C.-T.; Li, J.; Lin, Y., Aptamer/Graphene Oxide Nanocomplex for in Situ Molecular Probing in Living Cells. *J. Am. Chem. Soc.* **2010,** *132*, 9274-9276.

39. Chen, X.; Chen, B., Macroscopic and Spectroscopic Investigations of the Adsorption of Nitroaromatic Compounds on Graphene Oxide, Reduced Graphene Oxide, and Graphene Nanosheets. *Environ. Sci. Technol.* **2015,** *49*, 6181-6189.

40. Kyzas, G. Z.; Deliyanni, E. A.; Matis, K. A., Graphene Oxide and Its Application as an Adsorbent for Wastewater Treatment. *J. Chem. Technol. Biotechnol.* **2014,** *89*, 196-205.

41. Sharma, P.; Hussain, N.; Borah, D. J.; Das, M. R., Kinetics and Adsorption Behavior of the Methyl Blue at the Graphene Oxide/Reduced Graphene Oxide Nanosheet–Water Interface: A Comparative Study. *J. Chem. Eng. Data* **2013,** *58*, 3477-3488.

42. Yang, S.-T.; Chen, S.; Chang, Y.; Cao, A.; Liu, Y.; Wang, H., Removal of Methylene Blue from Aqueous Solution by Graphene Oxide. *J. Colloid Interface Sci.* **2011,** *359*, 24-29.

43. Zhang, J.; Azam, M. S.; Shi, C.; Huang, J.; Yan, B.; Liu, Q.; Zeng, H., Poly(Acrylic Acid) Functionalized Magnetic Graphene Oxide Nanocomposite for Removal of Methylene Blue. *RSC Adv.* **2015,** *5*, 32272-32282.

44. Wang, Y.; Li, Z.; Wang, J.; Li, J.; Lin, Y., Graphene and Graphene Oxide: Biofunctionalization and Applications in Biotechnology. *Trends Biotechnol.* **2011,** *29*, 205-212.

45. Yang, K.; Feng, L.; Liu, Z., The Advancing Uses of Nano-Graphene in Drug Delivery. *Expert Opin. Drug Deliv.* **2015,** *12*, 601-612.

46. Lee, J.; Kim, J.; Kim, S.; Min, D. H., Biosensors Based on Graphene Oxide and Its Biomedical Application. *Adv. Drug Deliv. Rev.* **2016**.

47. Liu, J.; Liu, Z.; Barrow, C. J.; Yang, W., Molecularly Engineered Graphene Surfaces for Sensing Applications: A Review. *Anal. Chim. Acta* **2015,** *859*, 1-19.

48. Kong, X.-k.; Chen, Q.-w.; Lun, Z.-y., Probing the Influence of Different Oxygenated Groups on Graphene Oxide's Catalytic Performance. *J. Mater. Chem. A* **2014,** *2*, 610-613.

49. Compton, O. C.; Jain, B.; Dikin, D. A.; Abouimrane, A.; Amine, K.; Nguyen, S. T., Chemically Active Reduced Graphene Oxide with Tunable C/O Ratios. *ACS Nano* **2011,** *5*, 4380-4391.

50. Lerf, A.; He, H.; Forster, M.; Klinowski, J., Structure of Graphite Oxide Revisited. *J. Phys. Chem. B* **1998,** *102*, 4477-4482.

51. Szabó, T.; Berkesi, O.; Dékány, I., Drift Study of Deuterium-Exchanged Graphite Oxide. *Carbon* **2005,** *43*, 3186-3189.

52. Cai, W.; Piner, R. D.; Stadermann, F. J.; Park, S.; Shaibat, M. A.; Ishii, Y.; Yang, D.; Velamakanni, A.; An, S. J.; Stoller, M., Synthesis and Solid-State Nmr Structural Characterization of 13c-Labeled Graphite Oxide. *Science* **2008,** *321*, 1815-1817.

53. Szabó, T.; Berkesi, O.; Forgó, P.; Josepovits, K.; Sanakis, Y.; Petridis, D.; Dékány, I., Evolution of Surface Functional Groups in a Series of Progressively Oxidized Graphite Oxides. *Chem. Mater.* **2006,** *18*, 2740-2749.

54. Montes-Navajas, P.; Asenjo, N. G.; Santamaria, R.; Menendez, R.; Corma, A.; Garcia, H., Surface Area Measurement of Graphene Oxide in Aqueous Solutions. *Langmuir* **2013,** *29*, 13443-13448.

55. Haubner, K.; Murawski, J.; Olk, P.; Eng, L. M.; Ziegler, C.; Adolphi, B.; Jaehne, E., The Route to Functional Graphene Oxide. *Chemphyschem* **2010,** *11*, 2131-2139.

56. Chen, L.; Yang, J.; Zeng, X.; Zhang, L.; Yuan, W., Adsorption of Methylene Blue in Water by Reduced Graphene Oxide: Effect of Functional Groups. *Mater. Express* **2013,** *3*, 281-290.

57. Ramesha, G. K.; Kumara, A. V.; Muralidhara, H. B.; Sampath, S., Graphene and Graphene Oxide as Effective Adsorbents toward Anionic and Cationic Dyes. *J. Colloid Interface Sci.* **2011,** *361*, 270-277.

58. Balapanuru, J.; Yang, J. X.; Xiao, S.; Bao, Q.; Jahan, M.; Polavarapu, L.; Wei, J.; Xu, Q. H.; Loh, K. P., A Graphene Oxide–Organic Dye Ionic Complex with DNA-Sensing and Optical-Limiting Properties. *Angew. Chem.* **2010,** *122*, 6699-6703.

59. Ferreira, S. R.; Louzada, H. F.; Dip, R. M. M.; González, G.; Lucas, E. F., Influence of the Architecture of Additives on the Stabilization of Asphaltene and Water-in-Oil Emulsion Separation. *Energy Fuels* **2015,** *29*, 7213-7220.

60. Goual, L.; Sedghi, M.; Zeng, H.; Mostowfi, F.; McFarlane, R.; Mullins, O. C., On the Formation and Properties of Asphaltene Nanoaggregates and Clusters by Dc-Conductivity and Centrifugation. *Fuel* **2011,** *90*, 2480-2490.

61. Hoepfner, M. P.; Vilas Bôas Fávero, C. u.; Haji-Akbari, N.; Fogler, H. S., The Fractal Aggregation of Asphaltenes. *Langmuir* **2013,** *29*, 8799-8808.

62. González, G.; Sousa, M. A.; Lucas, E. F., Asphaltenes Precipitation from Crude Oil and Hydrocarbon Media. *Energy Fuels* **2006,** *20*, 2544-2551.

63. Syunyaev, R.; Balabin, R.; Akhatov, I.; Safieva, J., Adsorption of Petroleum Asphaltenes onto Reservoir Rock Sands Studied by near-Infrared (Nir) Spectroscopy. *Energy Fuels* **2009,** *23*, 1230-1236.

64. He, K.; Duan, H.; Chen, G. Y.; Liu, X.; Yang, W.; Wang, D., Cleaning of Oil Fouling with Water Enabled by Zwitterionic Polyelectrolyte Coatings: Overcoming the Imperative Challenge of Oil–Water Separation Membranes. *ACS Nano* **2015,** *9*, 9188-9198.

65. Sztukowski, D. M.; Yarranton, H. W., Oilfield Solids and Water-in-Oil Emulsion Stability. *J. Colloid Interface Sci.* **2005,** *285*, 821-833.

66. Czarnecki, J.; Moran, K., On the Stabilization Mechanism of Water-in-Oil Emulsions in Petroleum Systems. *Energy Fuels* **2005,** *19*, 2074-2079.

67. Kallevik, H.; Kvalheim, O. M.; Sjöblom, J., Quantitative Determination of Asphaltenes and Resins in Solution by Means of near-Infrared Spectroscopy. Correlations to Emulsion Stability. *J. Colloid Interface Sci.* **2000,** *225*, 494-504.

68. Dai, Q.; Chung, K. H., Hot Water Extraction Process Mechanism Using Model Oil Sands. *Fuel* **1996,** *75*, 220-226.

69. Chen, G., Electrochemical Technologies in Wastewater Treatment. *Sep. Purif. Technol.* **2004,** *38*, 11-41.

70. Kwon, W.-T.; Park, K.; Han, S. D.; Yoon, S. M.; Kim, J. Y.; Bae, W.; Rhee, Y. W., Investigation of Water Separation from Water-in-Oil Emulsion Using Electric Field. *J Ind. Eng. Chem.* **2010,** *16*, 684-687.

71. Eow, J. S.; Ghadiri, M., Electrostatic Enhancement of Coalescence of Water Droplets in Oil: A Review of the Technology. *Chem. Eng. J.* **2002,** *85*, 357-368.

72. P. Kajitvichyanukul, Y.-T. H., L. Wang, *Handbook of Environmental Engineering*. 2006; Vol. 4, p 521.

73. Chan, Y. J.; Chong, M. F.; Law, C. L.; Hassell, D., A Review on Anaerobic–Aerobic Treatment of Industrial and Municipal Wastewater. *Chem. Eng. J.* **2009,** *155*, 1-18.

74. Suzuki, Y.; Maruyama, T., Removal of Emulsified Oil from Water by Coagulation and Foam Separation. *Sep. Sci. Technol.* **2005,** *40*, 3407-3418.

75. Xue, Z.; Cao, Y.; Liu, N.; Feng, L.; Jiang, L., Special Wettable Materials for Oil/Water Separation. *J. Mater. Chem. A* **2014,** *2*, 2445-2460.

76. Liu, M.; Wang, S.; Wei, Z.; Song, Y.; Jiang, L., Bioinspired Design of a Superoleophobic and Low Adhesive Water/Solid Interface. *Adv. Mater.* **2009,** *21*, 665-669.

77. Jung, Y. C.; Bhushan, B., Wetting Behavior of Water and Oil Droplets in Three-Phase Interfaces for Hydrophobicity/Philicity and Oleophobicity/Philicity. *Langmuir* **2009,** *25*, 14165-14173.

78. Gupta, R. K.; Dunderdale, G. J.; England, M. W.; Hozumi, A., Oil/Water Separation Techniques: A Review of Recent Progresses and Future Directions. *J. Mater. Chem. A* **2017**.

79. Huang, W.; Lei, M.; Huang, H.; Chen, J.; Chen, H., Effect of Polyethylene Glycol on Hydrophilic Tio 2 Films: Porosity-Driven Superhydrophilicity. *Surf. Coat. Technol.* **2010,** *204*, 3954-3961.

80. Xu, L.; Liu, N.; Cao, Y.; Lu, F.; Chen, Y.; Zhang, X.; Feng, L.; Wei, Y., Mercury Ion Responsive Wettability and Oil/Water Separation. *ACS Appl. Mater. Interfaces* **2014,** *6*, 13324-13329.

81. Zhang, W.; Zhu, Y.; Liu, X.; Wang, D.; Li, J.; Jiang, L.; Jin, J., Salt-Induced Fabrication of Superhydrophilic and Underwater Superoleophobic Paa-G-Pvdf Membranes for Effective Separation of Oil-in-Water Emulsions. *Angew. Chem. Int. Ed.* **2014,** *53*, 856-860.

82. Kobayashi, M.; Terayama, Y.; Kikuchi, M.; Takahara, A., Chain Dimensions and Surface Characterization of Superhydrophilic Polymer Brushes with Zwitterion Side Groups. *Soft Matter* **2013,** *9*, 5138-5148.

83. Murakami, D.; Kobayashi, M.; Moriwaki, T.; Ikemoto, Y.; Jinnai, H.; Takahara, A., Spreading and Structuring of Water on Superhydrophilic Polyelectrolyte Brush Surfaces. *Langmuir* **2013,** *29*, 1148-1151.

84. Xue, Q.; Cao, H.; Meng, F.; Quan, M.; Gong, Y.-K., Cell Membrane Mimetic Coating Immobilized by Mussel-Inspired Adhesion on Commercial Ultrafiltration Membrane to Enhance Antifouling Performance. *J. Membr. Sci.* **2017**.

85. Garbis, S. D.; Roumeliotis, T. I.; Tyritzis, S. I.; Zorpas, K. M.; Pavlakis, K.; Constantinides, C. A., A Novel Multidimensional Protein Identification Technology Approach Combining Protein Size Exclusion Prefractionation, Peptide Zwitterion− Ion Hydrophilic Interaction Chromatography, and Nano-Ultraperformance Rp Chromatography/Nesi-Ms2 for the in-Depth Analysis of the Serum Proteome and Phosphoproteome: Application to Clinical Sera Derived from Humans with Benign Prostate Hyperplasia. *Anal. Chem.* **2010,** *83*, 708-718.

86. Harris, L. J.; Birch, T. W., Zwitterions: Proof of the Zwitterion Constitution of the Amino-Acid Molecule. Ii. Amino-Acids, Polypeptides, Etc., and Proteins as Zwitterions, with Instances of Non-Zwitterion Ampholytes. *Biochem. J.* **1930,** *24*, 1080.

87. Eiberweiser, A.; Nazet, A.; Kruchinin, S. E.; Fedotova, M. V.; Buchner, R., Hydration and Ion Binding of the Osmolyte Ectoine. *J. Phys. Chem. B* **2015,** *119*, 15203-15211.

88. Bretscher, M. S., Mammalian Plasma Membranes. *Nature* **1975,** *258*, 43-49.

89. Zhang, P.; Lin, L.; Zang, D.; Guo, X.; Liu, M., Designing Bioinspired Anti-Biofouling Surfaces Based on a Superwettability Strategy. *Small* **2016**.

90. Jiang, S.; Cao, Z., Ultralow-Fouling, Functionalizable, and Hydrolyzable Zwitterionic Materials and Their Derivatives for Biological Applications. *Adv. Mater.* **2010,** *22*, 920-932.

91. Chen, S.; Li, L.; Zhao, C.; Zheng, J., Surface Hydration: Principles and Applications toward Low-Fouling/Nonfouling Biomaterials. *Polymer* **2010,** *51*, 5283-5293.

92. Liu, Q.; Patel, A. A.; Liu, L., Superhydrophilic and Underwater Superoleophobic Poly (Sulfobetaine Methacrylate)-Grafted Glass Fiber Filters for Oil–Water Separation. *ACS Appl. Mater. Interfaces* **2014,** *6*, 8996-9003.

93. Zhu, Y.; Zhang, F.; Wang, D.; Pei, X. F.; Zhang, W.; Jin, J., A Novel Zwitterionic Polyelectrolyte Grafted Pvdf Membrane for Thoroughly Separating Oil from Water with Ultrahigh Efficiency. *J. Mater. Chem. A* **2013,** *1*, 5758-5765.

94. Gao, S.; Sun, J.; Liu, P.; Zhang, F.; Zhang, W.; Yuan, S.; Li, J.; Jin, J., A Robust Polyionized Hydrogel with an Unprecedented Underwater Anti-Crude-Oil-Adhesion Property. *Adv. Mater.* **2016,** *28*, 5307-5314.

95. Huang, K.-T.; Yeh, S.-B.; Huang, C.-J., Surface Modification for Superhydrophilicity and Underwater Superoleophobicity: Applications in Antifog, Underwater Self-Cleaning, and Oil–Water Separation. *ACS Appl. Mater. Interfaces* **2015,** *7*, 21021-21029.

96. Shi, C.; Yan, B.; Xie, L.; Zhang, L.; Wang, J.; Takahara, A.; Zeng, H., Long-Range Hydrophilic Attraction between Water and Polyelectrolyte Surfaces in Oil. *Angew. Chem. Int. Ed.* **2016,** *55*, 15017-15021.

Chapter 2 Experimental techniques

2.1 Atomic force microscope (AFM)

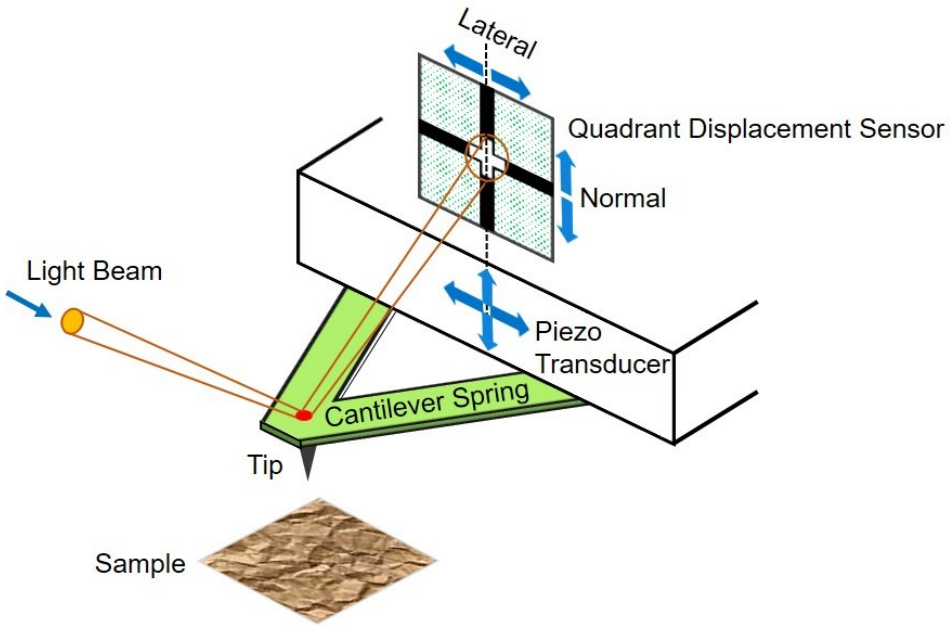

Figure 2.1 Typical AFM configuration[1]

Invented in 1986,[2] atomic force microscope has been applied in numerous disciplines and applications by obtaining images with subnanometer resolution[3] and performing force measurements.[4] It can be observed on Figure 2.1 that AFM is mainly composed of a piezo transducer oscillating the cantilever for precise movements, a cantilever with a sharp tip interacting with sample, a laser beam and quadrant displacement sensor recording the motion of the cantilever. Tapping mode and ScanAsyst mode have been used in our work for samples' AFM imaging. In tapping mode, the probe is manipulated to oscillate around its resonance frequency, and it can intermittently interact with the surface of sample. To maintain a constant tip-sample separation distance, the oscillation amplitude is kept constant and the feedback generates the topography of

the sample surface. ScanAsyst imaging mode is an image-optimization scanning mode that continuously and appropriately adjusts parameters by using peak force of the force curves at every pixel as feedback signal.

The principle of single-molecule force (SMF) spectroscopy is shown in Figure 2.2. To study the interaction of molecule A and B of interest, a single molecule A is bound to AFM tip using polyethylene glycol (PEG) as a linker to isolate the contribution of molecule A, and molecule B is bound or coated on substrate. In a single force measurement, the tip is first brought toward to the surface of B (1 and 2 in Figure 2.2), where a single molecule A-B complex is formed, and then the tip is retracted (3 and 4 in Figure 2.2), the PEG linker is stretched and behaves like a spring. When the applied force is equal to the bond dissociation force (F), the interaction bond breaks. By applying different separation rates and obtaining the corresponding most probable F, the bond dissociation energy (ΔG) and distance (Δx) can be estimated.[5-6]

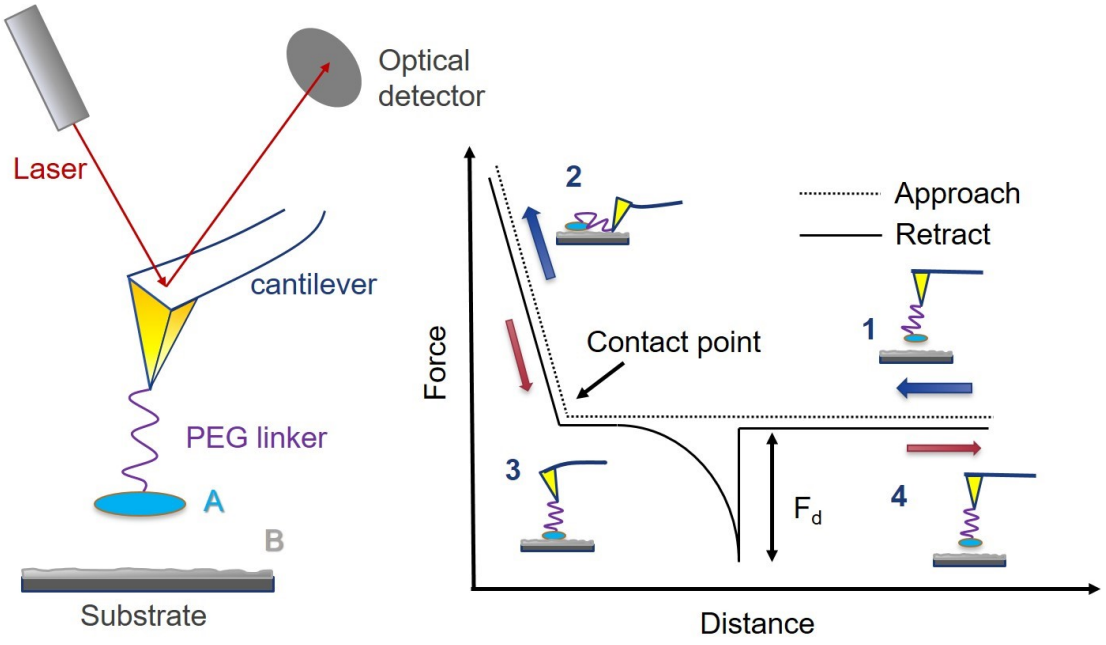

Figure 2.2 Scheme of SMF measurement setup to investigate the interaction between A and B.[7]

2.2 Contact angle measurement

Using a standard contact angle goniometer (Ramé-hart, Model 250), water-in-air (W/A) and oil-in-water (O/W) contact angles on different sample surfaces have been measured by sessile and pendant drop method, respectively. A droplet of water or oil is placed on the surface of sample by gravity or buoyancy, and its contact angle is obtained by fitting the drop outline using image processing software.

2.3 Ultraviolet-visible (UV-vis) spectroscopy

UV-vis spectroscopy characterizes the adsorption or reflectance of lights in the range of UV-vis spectral of the substances. The adsorption wavelength of lights is related to the electron transitions from the ground state to the excited state. The concentrations of molecule in the aqueous solution can be obtained by linear fitting of the characteristic peak adsorption intensity at specific wavelength versus the concentrations of a series of aqueous solutions with different known concentrations. In this work, the adsorption peaks of aqueous solutions have been characterized by an Evolution 300 UV–Vis spectrophotometer (Thermo Fisher Scientific).[8]

2.4 Fourier-transform infrared (FTIR) spectroscopy

A Thermo Nicolet 8700 FTIR Spectrometer has been used to identify the functional groups in the samples. FTIR spectroscopy is a technique applied to identify the existence of specific functional groups in substances (gas, liquid or solid) by characterizing their adsorption bands in the range of IR region (from 12800 to 10 cm^{-1}). Instead of repeatedly measuring the adsorption of IR lights at each different wavelength, FTIR spectroscopy characterizes the adsorption bands under the irradiation of lights with different combinations of wavelengths using interferometer. Then the adsorption spectrum can be obtained by converting via Fourier transformation.

2.5 X-ray photoelectron spectroscopy (XPS)

XPS is a spectroscopic method to characterize the elemental composition, and the electronic environment of the elements in the surface of samples (0 to 10 nm) for measurement. Monochromatic X-ray beam with known energy is used to irradiate a sample, and the energy of escaped electrons from the sample can be given by analyzing the information obtained by the electron detector. The electron binding energy $E_{binding}$ (eV) can be given using the following equation:[9]

$$E_{binding} = E_{photon} - (E_{kinetic} + E_{\emptyset}) \qquad (2.1)$$

where E_{photon} is the energy of X-ray photons used, $E_{kinetic}$ is the photoelectron kinetic energy and $E_{\emptyset}$ is solid effects correction.

$E_{binding}$ is determined by the electron configuration of the element's electrons. The typical spectrum can be obtained by plotting the detected electron number versus their $E_{binding}$. By analyzing the XPS spectrum, the atomic and bond percentages can be calculated. In this study, a Kratos Axis Ultra spectrometer has been used to characterize the as-prepared materials.

2.6 Thermogravimetric analysis (TGA)

TGA is a technique to monitor the mass of sample changing with increasing temperature, which rises linearly as a function of time. The gas atmosphere during the measurement can be controlled. Mass changes during measurements can be related to the physical and chemical properties of the samples.[10] TGA has been used in this work to evaluate the composition of the as-prepared materials (TA instruments Q500).

2.7 Zeta potential measurement

When a colloidal particle with a net surface charge is dispersed in aqueous solution, it will be surrounded by oppositely charged ions as shown in Figure 2.3 (using a negatively charged particle as an example). The surface charge layer and the oppositely charged layer together are

called as electrical double layer (EDL), which moves with the particle in the solution. Zeta potential is defined as the potential difference between the bulk fluid and the stationary layer attached to the particle.[11] The value of zeta potential of colloidal particles can indicate the electrostatic interaction between kinds of colloidal particles and also the stability of charged particles in liquid dispersion. A Malvern Nanosizer Nano ZSP has been used to characterize zeta potential of colloidal particles.

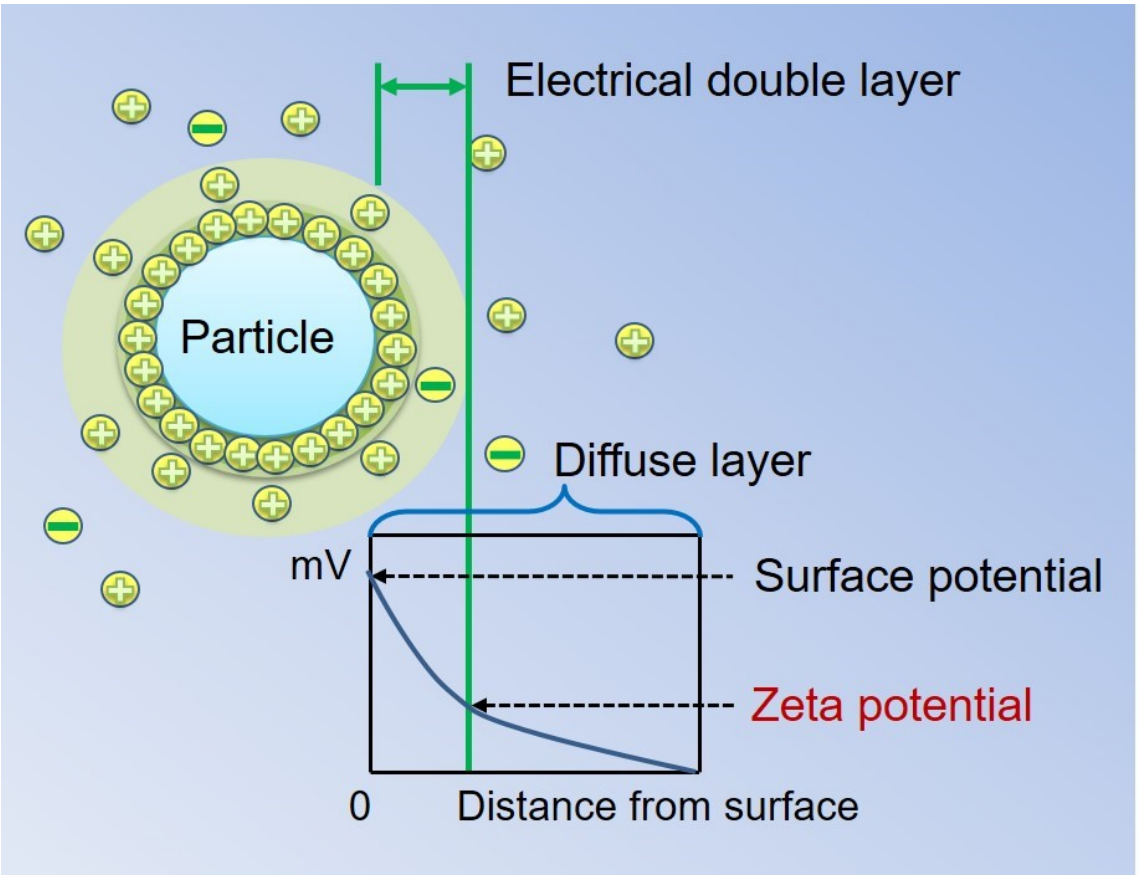

Figure 2.3 Diagram illustrates the electrical double layer (EDL) at the surface of a colloidal particle in solution.

2.8 Coulometric Karl Fischer titration

Invented in 1935 and named by Karl Fisher, coulometric Karl Fisher titration is used in this work to determine the trace amount of water (measuring range: 1 ppm – 5%) in a sample by

using coulometric titration.[12] During the titration process, iodine is generated electrochemically and then reacts with water stoichiometrically.[13] The titration end-point is determined by an abrupt voltage drop due to excess iodine and the amount of charges that consumed to generate iodine during titration is used to calculate the water content in the original sample.

References

1. Zeng, H., *Polymer Adhesion, Friction, and Lubrication*. John Wiley & Sons: 2013.

2. Bennig, G. K., Atomic Force Microscope and Method for Imaging Surfaces with Atomic Resolution. U.S. Patent: 1988.

3. Zhang, L.; Zeng, H.; Liu, Q., Probing Molecular and Surface Interactions of Comb-Type Polymer Polystyrene-Graft-Poly (Ethylene Oxide)(Ps-G-Peo) with an SFA. *J. Phys. Chem. C* **2012,** *116*, 17554-17562.

4. Wang, J.; Li, J.; Xie, L.; Shi, C.; Liu, Q.; Zeng, H., Interactions between Elemental Selenium and Hydrophilic/Hydrophobic Surfaces: Direct Force Measurements Using AFM. *Chem. Eng. J.* **2016,** *303*, 646-654.

5. Bell, G. I., Models for the Specific Adhesion of Cells to Cells. *Science* **1978,** *200*, 618-627.

6. Evans, E.; Ritchie, K., Strength of a Weak Bond Connecting Flexible Polymer Chains. *Biophys. J.* **1999,** *76*, 2439-2447.

7. Puntheeranurak, T.; Neundlinger, I.; Kinne, R. K.; Hinterdorfer, P., Single-Molecule Recognition Force Spectroscopy of Transmembrane Transporters on Living Cells. *Nat. Protoc.* **2011,** *6*, 1443.

8. Skoog, D. A.; Holler, F. J.; Crouch, S. R., *Principles of Instrumental Analysis*. Cengage learning: 2017.

9. Hollander, J. M.; Jolly, W. L., X-Ray Photoelectron Spectroscopy. *Acc. Chem. Res.* **1970,** *3*, 193-200.

10. Coats, A.; Redfern, J., Thermogravimetric Analysis. A Review. *Analyst* **1963,** *88*, 906-924.

11. Kirby, B. J., *Micro-and Nanoscale Fluid Mechanics: Transport in Microfluidic Devices*. Cambridge University Press: 2010.

12. Fischer, K., Neues Verfahren Zur Maßanalytischen Bestimmung Des Wassergehaltes Von Flüssigkeiten Und Festen Körpern. *Angew. Chem.* **1935,** *48*, 394-396.

13. Tavčar, E.; Turk, E.; Kreft, S., Simple Modification of Karl-Fischer Titration Method for Determination of Water Content in Colored Samples. *J Anal. Methods Chem.* **2012,** *2012*.

Chapter 3 Poly (acrylic acid) Functionalized Magnetic Graphene Oxide Nanocomposite for Removal of Methylene Blue

3.1 Introduction

Dyes are widely used in many industries like textile, paper and pulp, dyestuffs and plastics industries. The dye contaminants extensively exist in wastewater discharged by miscellaneous industrial activities which cause various environmental problems.[1-2] A trace amount of water-soluble dyes can cause noticeable colorization of water, which will reduce the light penetration and thus interfere with the photosynthetic activity of aquatic organisms.[3-4] Moreover, dyes are generally toxic to living creatures and cannot be easily degraded by microorganisms.[1-2, 5] Therefore, economic techniques to efficiently remove dye contaminants from wastewater are highly desirable. To date, various technologies have been invented and applied for the removal of dyes from wastewater, including coagulation/flocculation,[6-7] photocatalysis,[8-10] ultrafiltration,[11-12] and adsorption.[13-14] Among these methods, adsorption has received much attention due to its high efficiency, simplicity and economy.[13, 15-17] A variety of adsorbents such as clay,[18] zeolite[19] and carbon materials,[20] have been developed to remove colored organic pollutants. Yet, challenging issues like relatively low removal efficiency and separation difficulty still remain for most conventional adsorbents.

Graphene oxide (GO) has unique 2-D structure with high surface area and rich functional groups, such as carboxylic, epoxide and hydroxide groups, which endow its good dispersibility in water and availability for further modification,[21-22] attracting considerable attention for wastewater treatment.[23-29] Inherently, the basal plane of GO is able to interact with the aromatic rings of

organics by π-π stacking,[30-31] contributing to its adsorption of organic dye pollutants. To expand the practical applicability of GO, various chemical and physical modifications have been applied to decorate GO with specific functionalities, such as photocatalysis ability,[10] improved adsorption capacity for specific pollutants [32] and recyclability.[14] Magnetic particles have also been introduced to GO sheets to enhance the separation efficiency. [33-36] It is noted, however, the introduction of magnetic particles to GO commonly leads to a relatively low adsorption capacity of the composite materials. One possible way to cope with this dilemma is to graft the magnetic graphene oxide (MGO) with functional polymers, which contain abundant functional groups such as carboxyl and amino groups and can adsorb pollutants through electrostatic interaction or chelation.[37] Although much effort has been devoted to the fabrication and characterization of graphene-polymer composites, most of the attempts focused on their mechanical and electric performance instead of the adsorptive property in wastewater treatment.[38-39] The role of polymers in most MGO-polymer composites reported was usually to strengthen the mechanical property of the composites.[40-41] Among the limited studies on polymer modified graphene oxide targeting dye removal, cellulose and chitosan have been chosen as the functional polymers to eliminate methylene blue (MB) and fuchsine from wastewater, respectively.[17, 42] Functionalization of MGO composites using polymers containing abundant carboxylic groups (like poly (acrylic acid)), which have strong affinity to positively charged organic pollutants and the ability to enhance water dispersibility, has not been reported.

Herein, we report a facile and effective method to prepare poly (acrylic acid) (PAA) modified magnetic graphene oxide composite (PAA/MGO). Magnetic graphene oxide composite (MGO) was first synthetized using a co-precipitation method,[21] and PAA was then introduced to the as-prepared MGO through carbodiimide activation under sonication at room temperature.[43-46]

The carboxylic groups of PAA can be bound to GO surfaces, and also have electrostatic affinity to cationic pollutants, which is expected to synergistically enhance the adsorption performance.[47] In this work, PAA/MGO was utilized to remove organic dye pollutants (i.e. methylene blue), and a higher adsorption capacity with excellent recyclability was achieved as compared to that of magnetic graphene oxide or graphene oxide composites reported previously.[33-35, 48-50] The adsorption mechanism was also investigated and proposed.

3.2 Materials and experimental methods

3.2.1. Chemicals and materials

$FeCl_3 \cdot 6H_2O$ and $FeCl_2 \cdot 4H_2O$ were purchased from Sigma-Aldrich. $KMnO_4$, $NaNO_3$, methylene blue (MB), NaOH, HCl, ammonium hydroxide and hydrogen peroxide were purchased from Fisher Scientific. Graphite flake (325 mesh), H_2SO_4 (98%), 1-(3-Dimethylaminopropyl)-3-ethylcarbodiimide hydrochloride (EDC) and poly (acrylic acid) (25%, Average M.W. 240,000) were obtained from Alfa Aesar. All chemicals used in this study were analytical grade and used as received.

3.2.2. Preparation of graphene oxide (GO)

A modified Hummer's method was applied to synthetize GO.[51] Briefly, graphite (2 g) and $NaNO_3$ (1.5 g) were mixed in a 250 ml three-necked flask in an ice bath, and H_2SO_4 (98%, 150 mL) was added into the mixture with stirring. Then, $KMnO_4$ (9 g) was slowly added to the mixture over about 1 h. Stirring and ice bath were maintained during the addition of $KMnO_4$, which were kept for another 2 h after the addition. The ice bath was removed afterwards while the stirring was kept vigorously for 5 days at room temperature. H_2O_2 solution (6 mL) was then added into the mixture with another 2 hours agitation. Sequentially, 250 mL solution of deionization (DI) water

mixed with H_2SO_4 (98%, 7.5 mL) and H_2O_2 (30 wt%, 4.17 mL) was added to dilute and wash the mixture. The resulted mixture was thoroughly washed by DI water, centrifuged, and then dialyzed for 5 days. Finally, the GO aqueous solution was lyophilized and fluffy black dried GO was obtained.

3.2.3. Preparation of Magnetic Graphene Oxide (MGO)

MGO was synthetized following a modified co-precipitation method.[52] The procedure of a typical synthesis experiment is as follows. Firstly, 100 mg GO was dispersed into 100 mL DI water by ultrasonication until fully dispersed. Then the GO solution was added into a 250 mL three-necked flask and stirred vigorously. Secondly, $FeCl_3 \cdot 6H_2O$ (0.819 g) and $FeCl_2 \cdot 4H_2O$ (0.294 g) were dissolved in DI water (25 mL), and the solution was dropped into the GO solution in the flask under severe agitation for 20 min. Afterwards, the mixture was heated to 50 ºC, and the pH was adjusted to 10 with the observation of black precipitate. The solution was further heated to 85 ºC and the heat was maintained for an hour. The as-prepared MGO was magnetically separated and washed for more than 3 times. Finally, black MGO powder was obtained by freeze-drying.

3.2.4. Preparation of PAA/MGO

PAA/MGO composite was synthesized based on a modified synthetic method for PAA/Fe_3O_4.[37] Briefly, MGO (50 mg) was dispersed in 1 ml of buffer (3 mM phosphate, pH = 6.0, 0.1 M NaCl) by sonication in a centrifuge tube. Afterwards, 0.25 mL of carbodiimide solution (0.025 g mL^{-1} in buffer) was added to the MGO solution. After 10 min sonication, 0.286 mL of PAA solution (25 wt%.) was mixed with 0.963 mL buffer. The PAA mixture was then added to the MGO mixture. The reaction was carried out under sonication for another 30 min. Finally,

PAA/MGO was magnetically separated and washed by DI water for over 3 times. Grey powder of PAA/MGO was obtained after freeze-drying.

3.2.5. Sample Characterizations

Fourier transform infrared (FTIR) spectra were recorded on a Thermo Nicolet 8700 FTIR Spectrometer. Thermogravimetric analysis (TGA) was carried out using a TA instruments Q500 under Ar flow (5.0 $mL \cdot min^{-1}$) and Air (200.0 $mL \cdot min^{-1}$) at a heating rate of 10 $^{o}C\ min^{-1}$. Transmission electron microscopy (TEM) images were recorded by CM20 FEG transmission electron microscope operated at 200 kV. Atomic force microscopy (AFM) imaging was conducted using an Asylum MFP-3D AFM to characterize the morphology and thickness of GO in tapping mode. GO sample was prepared by dropping GO aqueous solution on a freshly cleaved mica surface, followed by overnight drying. X-ray photoelectron spectroscopy (XPS) measurements were carried out on a Kratos Axis Ultra spectrometer using Al Ka radiation, operated at 12 mA, 14 kV, of which the peak fitting was performed by CasaXPS software. Zeta potential was measured using a Malvern Nanosizer Nano ZSP. The concentrations of MB in aqueous solutions during adsorption tests were characterized using an Evolution 300 UV–Vis spectrophotometer (Thermo Fisher Scientific). The Magnetic hysteresis measurements were conducted at room temperature under a maximum applied field of 60000 Oe on a Quantum Design 9T-PPMS magnetometer.

3.2.6. Adsorption tests

The adsorption of MB in aqueous solutions using MGO and PAA/MGO composites was carried out in batch experiments. Solutions of adsorbents (4 mg) dispersed in deionized (DI) water (0.5 mL) were mixed with different concentrations of MB solutions (25 ml) in centrifuge tubes (pH =7, pH was adjusted using 0.1 M HCl and 0.1 NaOH). The adsorption experiments were

performed by putting the centrifuge tubes in a shaker (300 RPM) and monitored with time. Portions of the mixture were taken out at different time intervals, of which the adsorbents were magnetically removed and the residue concentrations of MB were determined with UV-visible spectrophotometer.[33, 53] The adsorption kinetics and isotherms of MB on the as-prepared adsorbents were obtained under aforementioned condition.

The effect of pH on the adsorption of MB on MGO and PAA/MGO was also investigated. Solutions of MGO or PAA/MGO (4 mg) dispersed in DI water (0.5 mL) and 20 mg L^{-1} MB solutions (25 mL) were mixed and adjusted to different pH (pH=3, 5, 7, 9, 11). The mixtures were left in shaker (300 RPM) for 24 h to reach adsorption equilibrium. The adsorption capacity q_t (mg g^{-1}) and removal percentage $p\%$ can be calculated by Equation 3.1[33] and Equation 3.2[54], where C_0 and C_t (mg L^{-1}) are the initial concentration and concentration at time t of residual MB in the solutions, respectively, m (g) stands for the mass of the adsorbent used, V_0 (mL) and V_t (mL) are initial volume and volume at time t of solutions, respectively.

$$q_t = \frac{C_0V_0 - C_tV_t}{m} \qquad (3.1)$$

$$p = \frac{C_0 - C_e}{c_0} \times 100 \qquad (3.2)$$

3.2.7. Zeta potential measurements

MGO or PAA/MGO (5 mg) was added into 10 mM NaCl solutions (10 ml) and the suspensions were sonicated until fully dispersed. The pH of the supernatants of the suspensions was adjusted to pH~3 to 11 using 0.1 M NaOH or HCl, and the zeta potential was then determined using a Malvern Nanosizer Nano ZSP. The measurements for each type of samples were repeated for 3 times.

3.2.8. Recyclable usage

MGO and PAA/MGO (8 mg) aqueous solutions (0.5 mL) were added to 20 mg L^{-1} MB solutions (25 mL) respectively and then the pH of the mixtures was adjusted to pH~7 using 0.1 M NaOH or HCl. The solutions were then left in the shaker (300 rpm) for 5 h. After adsorption, the adsorbents were collected by external magnet and MB concentrations in the residue solutions were measured by UV spectroscopy. For desorption, the recycled adsorbents were dispersed in 10 mL ethanol solution (5 % vol. acetic acid), sonicated for 15 min and recovered magnetically. The desorption process was repeated for 3 times. After magnetic separation, the adsorbents were washed with 2 mL DI water and then magnetically separated for reuse.

3.3 Results and discussion

3.3.1. Synthesis and characterizations of nanocomposite adsorbents

Figure 3.1 shows the synthesis route of PAA/MGO composite. GO was first prepared from graphite based on a modified Hummers method.[51] $FeCl_2$ and $FeCl_3$ solution (Fe^{2+}: Fe^{3+}= 2:1) was dropped to GO solutions as iron source, with Fe^{2+} and Fe^{3+} ions attracted to the negative-charged oxygen atoms of GO. The solution was adjusted to alkaline condition (pH=10) and Fe_3O_4 particles were formed *in situ* by co-precipitation.[55] PAA was then bound to the surfaces of GO by a "grafting from" method.[37, 56]

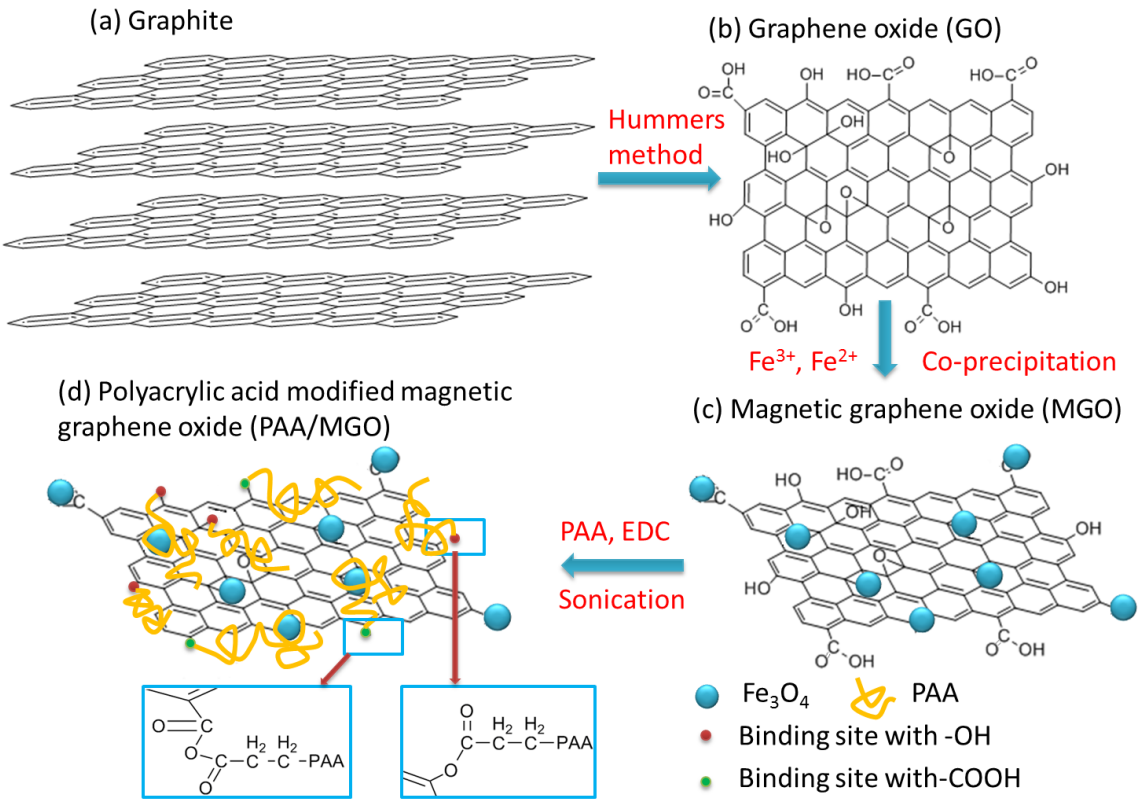

Figure 3.1 Schematic of synthesis process for PAA/MGO composite. Note, the binding of PAA and –COOH groups on GO by forming acid anhydride groups as illustrated in (d) may not be very stable in aqueous solution, and the binding between PAA and –OH groups on GO would dominate the grafting interaction.

AFM topography and height profile of GO are shown in Figure 3.2a and 3.2b, respectively, indicating a single layer of GO sheet with thickness of ~0.91 nm which is consisted with literature value.[57] Single layer of GO sheet is thicker than pristine graphene monolayer that is atomically flat with a well-known van der Waals thickness of ~0.34 nm, which is mainly due to the covalently bonded groups on the carbon atoms and distorted sp^3-hybridized geometry transformed from the planar sp^2-hybridized geometry.[54] The single layer structure of GO obtained contributes to its high surface area allowing further surface modification.

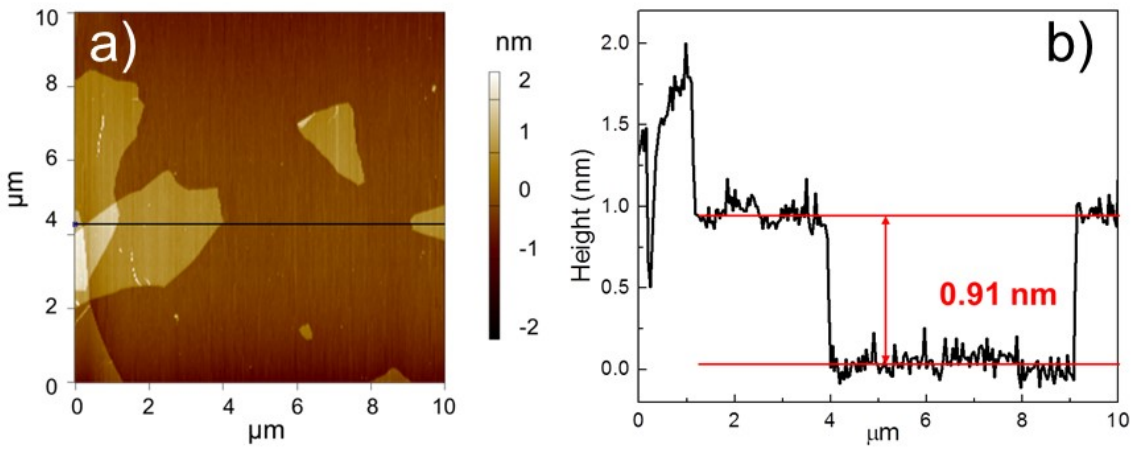

Figure 3.2 (a) AFM topographic image of GO sheets, and **(b)** height profile for monolayer GO.

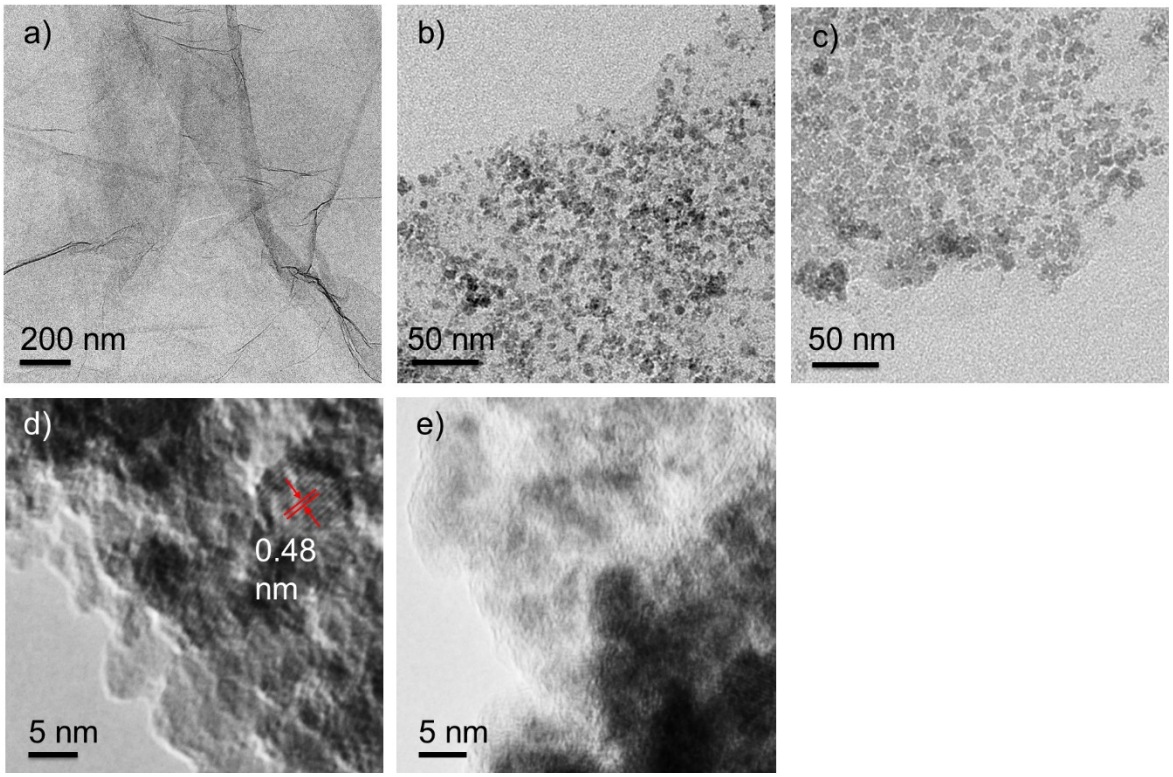

Figure 3.3 TEM images of **(a)** GO, **(b)** MGO and **(c)** PAA/MGO, HRTEM images of **(d)** MGO, and (e) PAA/MGO.

The TEM image of GO (Figure 3.3a) reveals that GO possesses a transparent sheet structure. TEM image of MGO (Figure 3.3b) shows that the magnetic nanoparticles (with an average diameter of ~7 nm) disperse evenly on the transparent graphene oxide sheets and have a crystal structure with a lattice spacing of 0.48 nm, corresponding to the (111) plane of spinel-structured iron oxide, as shown in the HRTEM image of MGO (Figure 3.3d).[58] The modification of PAA on MGO shows no significant change of the morphology of iron oxide nanoparticles on graphene oxide sheets in TEM image of PAA/MGO (Figure 3.3c). It is noted that after the binding of PAA on MGO, the crystal structure of the magnetic nanoparticles on PAA/MGO is much less visible in the HRTEM image (Figure 3.3e) as compared to that in the HRTEM image of MGO (Figure 3.3d), which is most likely due to the electron scattering and energy loss in the grafted PAA.[59, 60-61]

Powder X-ray diffraction (XRD) was employed to characterize the crystalline structure of magnetic iron oxide nanoparticles in the MGO and PAA/MGO composites, and the XRD patterns are shown in Figure 3.4a and are in accordance with the standard XRD spectra for Fe_3O_4 (PDF#01-071-6336). The XRD results confirm the successful deposition of Fe_3O_4 nanoparticles on GO sheets and that the addition of PAA does not change the crystalline structure of these nanoparticles.

The FTIR spectra of GO, PAA, MGO and PAA/MGO are shown in Figure 4.4b. For the FTIR spectrum of GO, the peaks from 1000 to 1300 cm^{-1} can be ascribed to the C-O vibration of hydroxyl groups and C-O-C vibration of epoxy groups; the peaks around 3436 and 3625 cm^{-1} can be attributed to the O-H vibration of hydroxyl groups and the peak at 1739 cm^{-1} is due to –C=O vibration of carboxylic groups,[62-63] indicating that the oxidized product of graphite (i.e. GO) via the modified Hummers' method possesses various oxygen-containing functional groups. With the deposition of Fe_3O_4 nanoparticles on GO sheets, the intensity of the peaks for the hydroxyl, epoxy

and carboxylic groups was weakened, which is most likely because the oxygen of these groups can interact with iron ions to form oxide. For PAA/MGO, the appearance of $–CH_2$ vibration at 1455 and 2923 cm^{-1} and the enhanced –C=O vibration peak of carboxylic groups confirm the deposition of PAA on the composite surfaces.[64]

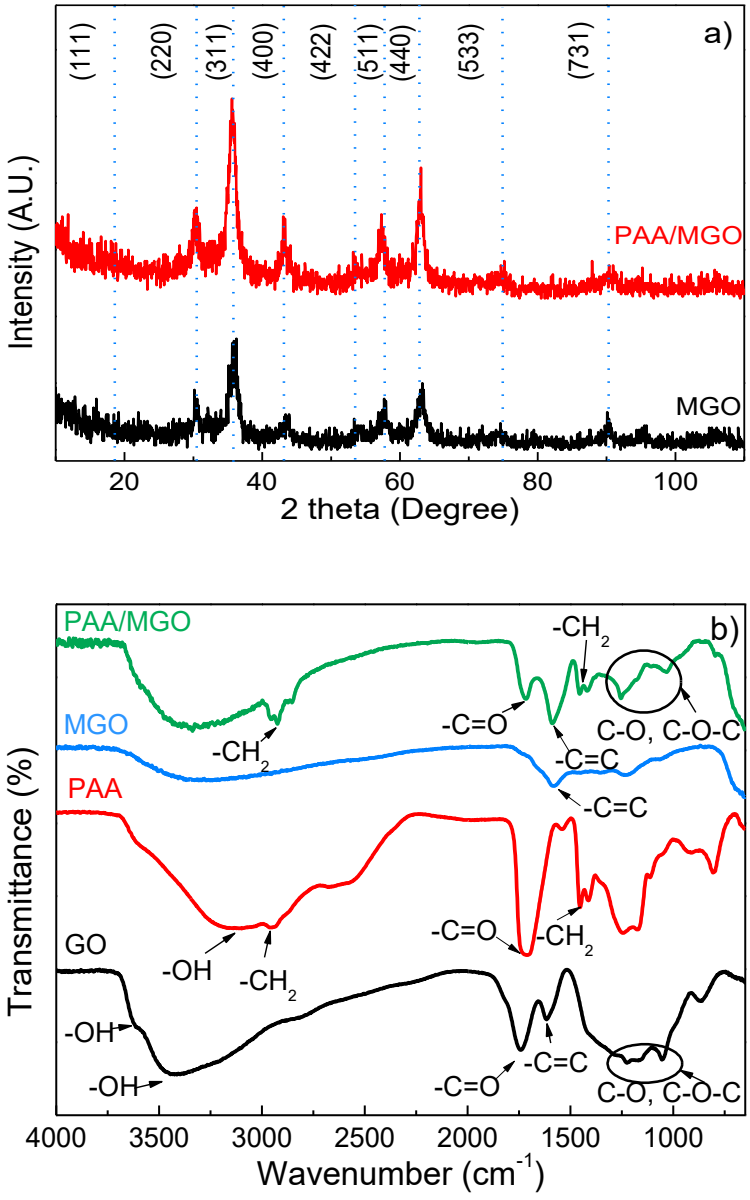

Figure 3.4 (a) XRD patterns of MGO and PAA/MGO, **(b)** FTIR spectra of GO, PAA, MGO and PAA/MGO.

The C1s XPS spectra of GO, MGO and PAA/MGO are shown in Figure 3.5a, 3.5b and 3.5c, respectively. The spectra were calibrated using the binding energy of the adventitious C1s at 284.6 eV. In Figure 3.5, the deconvolution of C1s XPS spectra of GO, MGO and PAA/MGO shows four peaks at 284.6 eV, 286.5 eV, 287.7 eV and 288.3 eV, which can be assigned to saturated C-C bonding of graphene, the carbon-linking hydroxyl groups (C-OH) and epoxy groups (C-O-C), carbonyl groups (C=O), and carboxyl groups (-COOH), respectively.[65-66] The bond percentage and binding energy (B. E.) of different bonds based on the C1s spectra for GO, MGO and PAA/MGO are summarized in Table 3-1. Table 3-1 shows that after the co-precipitation of magnetic particles, the relative intensity of peaks corresponding to oxygen-containing groups significantly decreases, agreeing with FTIR results, which supports the hypothesis that the oxygen-containing groups reacted with iron ions to form Fe_3O_4 nanoparticles. Compared to MGO, the intensity of C=O peak of PAA/MGO dramatically increases, suggesting the successful deposition of PAA on MGO.

Table 3-1 XPS C1s peak information for four types of C bonds in GO, MGO and PAA/MGO.

Materials	COOH		C=O		C-O		C-C	
	%	B.E.	%	B.E.	%	B.E.	%	B.E.
GO	7.4	288.4	4.29	287.3	44.5	286.6	43.9	284.6
MGO	5.6	288.7	2.11	287.7	31.2	286.4	61.1	284.6
PAA/MGO	13.8	288.7	2.11	287.9	25.8	286.4	58.3	284.6

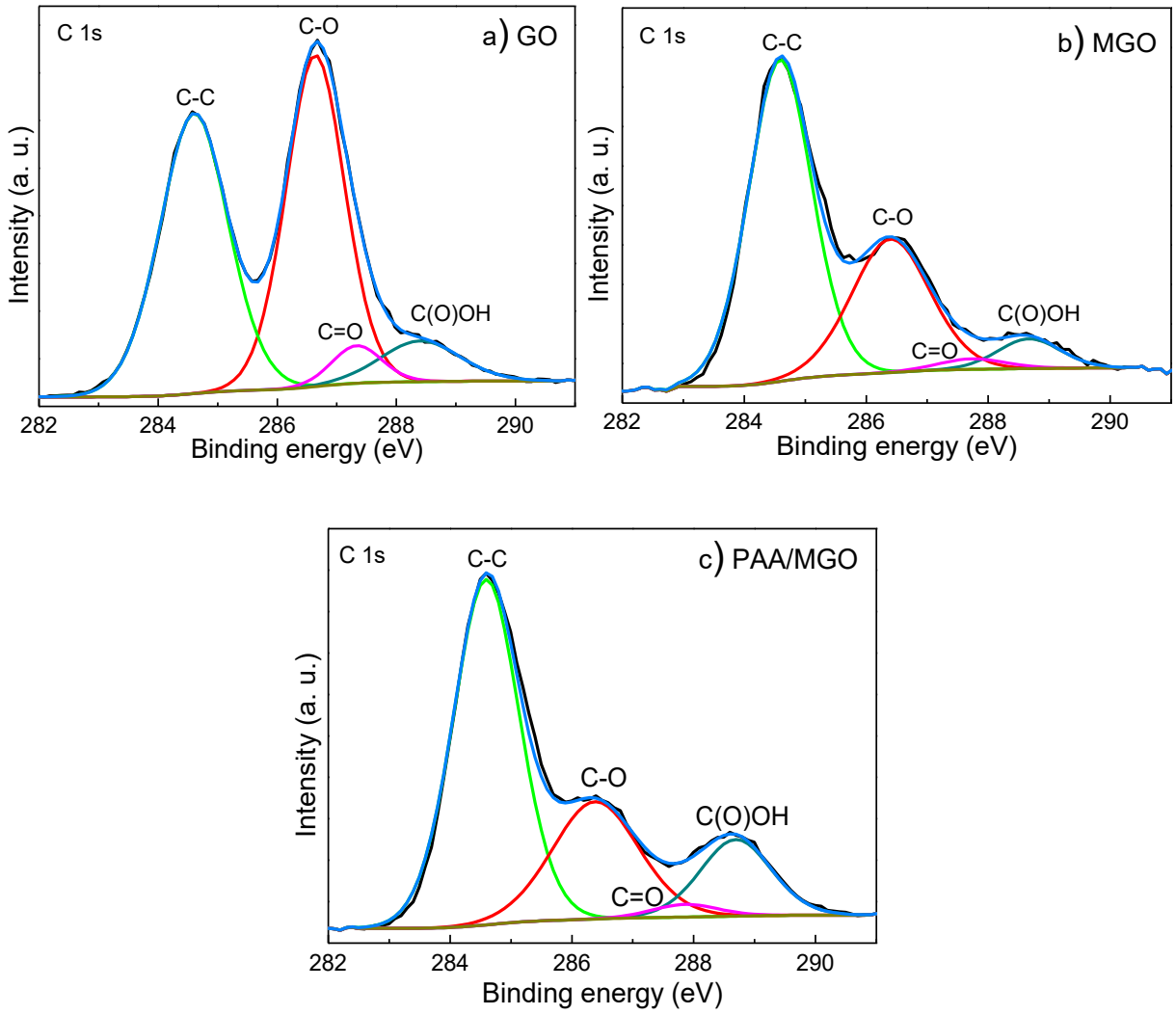

Figure 3.5 C1s XPS spectra of (a) GO, (b) MGO and (c) PAA/MGO.

The thermal behaviors of GO, MGO, PAA/MGO and Fe_3O_4 were characterized by thermogravimetric analysis and the TGA results are shown in Figure 3-6. For the TGA curve of GO, the weight loss below 120 ºC is due to the loss of physically adsorbed water. The weight loss from 120 ºC to ~300 ºC is ascribed to the loss of oxygen-containing functional groups. The final weight loss from 430 ºC to 530 ºC is mainly attributed to the burning of carbon.[67] For Fe_3O_4, a slight weight gain below 200 ºC is due to the oxidization of Fe_3O_4 to γ-Fe_2O_3.[34] In contrast, the weight gain of MGO and PAA/MGO owing to the oxidization of Fe_3O_4 was overwhelmed by the

decomposition of oxygen-containing groups, thus these two composites showed gradual weight loss with increasing temperature till 400 °C. Based on the mass loss of the composite materials in TGA tests shown in Figure 3-6, the mass fraction of Fe_3O_4 in MGO was evaluated to be ~71% and the mass fraction of PAA in PAA/MGO composite was estimated as ~15%.

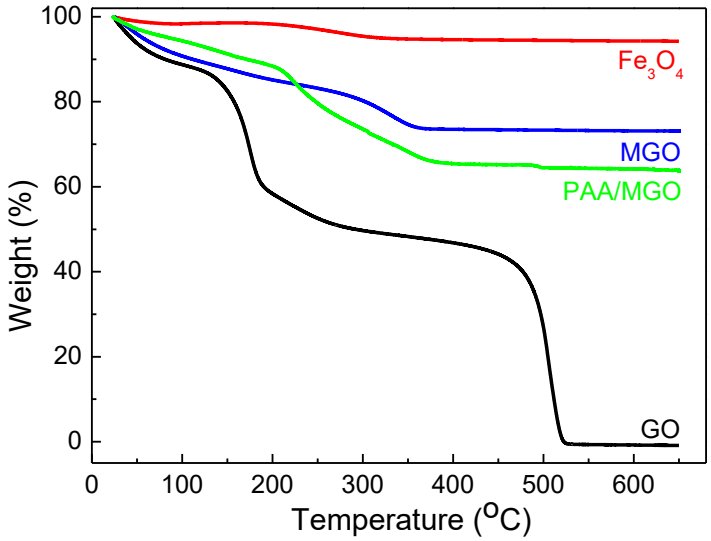

Figure 3.6 TGA curves of GO (black), MGO (blue), PAA/MGO (green) and Fe_3O_4 (red).

3.3.2. Magnetization tests

Figure 3.7 shows the magnetic responses of MGO and PAA/MGO composites, both of which show typical superparamagnetic behavior. The saturation magnetizations of MGO and PAA/MGO are 27.7 emu g^{-1} and 12.3 emu g^{-1}, respectively. The reduced saturation magnetization of PAA/MGO as compared to MGO could be attributed to the less mass fraction of magnetic component in the composite. The inset in Figure 3.7 shows a picture of the mixtures (pH = 7) of 20 mg L^{-1} MB solutions (5 mL) with (a) 0.5 mL of DI water, (b) 0.5 mL of MGO (2 mg) solution and (c) 0.5 mL of PAA/MGO (2 mg) solution. Under an external magnetic field, both MGO and PAA/MGO can be easily separated, but only the residue solution for the PAA/MGO case can be

totally discolored (in ~ 2 minutes), which demonstrates the magnetism and different adsorption capacity of the nanocomposite adsorbents.

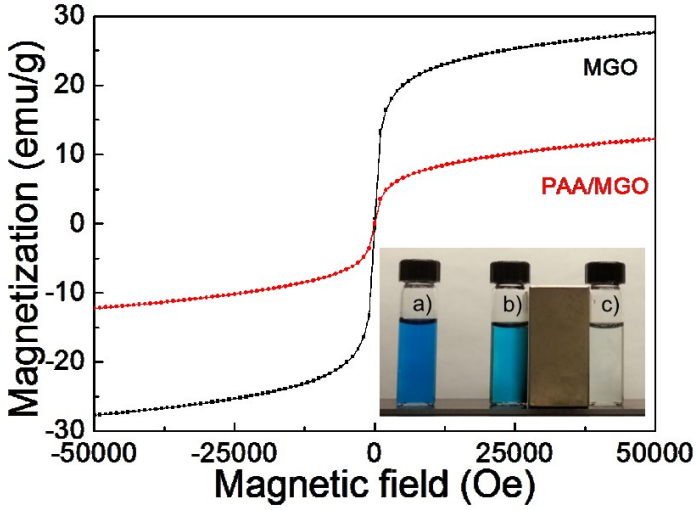

Figure 3.7 Magnetic hysteresis loops of MGO and PAA/MGO. The inset shows the mixtures of 20 mg L-1 MB solutions (5 mL) and (a) 0.5 mL of DI water, (b) 0.5 mL of MGO (2 mg) solution and (c) 0.5 mL of PAA/MGO (2 mg) solution.

3.3.3. Adsorption tests

The adsorption capacity of MB on MGO and PAA/MGO composites was investigated by batch tests. Figure 3.8 shows the adsorption capacity q_t of MB on MGO and PAA/MGO as a function of adsorption time t. Figure 3.8 exhibits that the adsorption of MB drastically increases with time in the first few minutes, and then gradually reaches equilibrium. The adsorption capacity q_t at time t of MB on PAA/MGO was much higher than that on MGO. For example, q_t =100 mg/g and 37 mg/g at t=20 min for PAA/MGO and MGO, respectively, showing that the functionalization of PAA on MGO significantly improved the adsorption capacity of MB of the composite materials.

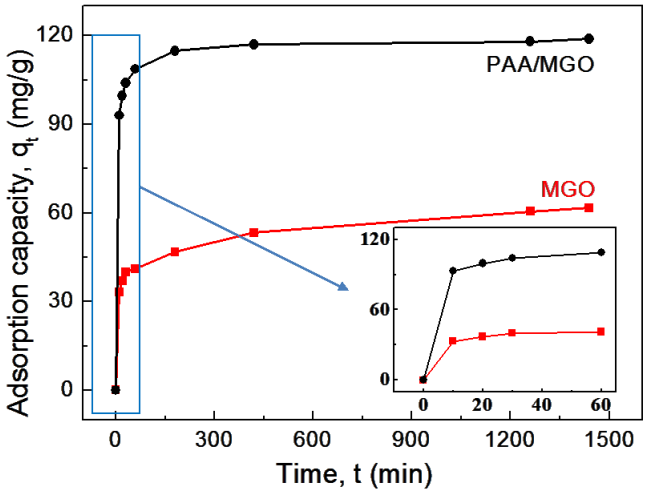

Figure 3.8 Adsorption capacity q_t of MB on MGO and PAA/MGO as a function of adsorption time t, with 20 mg L^{-1} initial concentration of MB, pH =7. Inset shows the adsorption profile of MB on MGO and PAA/MGO in the initial adsorption stage.

The pseudo-first-order and pseudo-second-order kinetic models were used to study the adsorption kinetics of MB on MGO and PAA/MGO.[68-69] The pseudo-first-order kinetic model assumes that the adsorption rate is proportional to the available number of adsorption sites; while the pseudo-second-order kinetic model assumes that the adsorption rate is proportion to the square of available number of adsorption sites.[50]

Pseudo-first-order kinetic model: $log(q_e - q_t) = logq_e - \frac{k_1 t}{2.303}$ (3.3)

Pseudo-second-order kinetic model: $\frac{t}{q_t} = \frac{1}{q_e^2 k_2} + \frac{t}{q_e}$ (3.4)

q_e and q_t (mg g^{-1}) represent the amounts of MB adsorbed at equilibrium and at any adsorption time t. k_1 (min^{-1}) and k_2 (g mg^{-1} min^{-1}) are pseudo-first and pseudo-second order rate constants, respectively. Figure 3.9a and 3.9b show the fitting for the adsorption of MB on MGO and

PAA/MGO using the pseudo-first-order kinetics and pseudo-second-order kinetics, respectively. All kinetic parameters obtained by linear regression of the two kinetic models are summarized in Table 3-2. The higher correlation coefficient values (R^2) in Table 3-2 and the good agreement between the measured $q_{e,exp}$ and the calculated $q_{e,cal}$ indicate a better fitting of the data using the pseudo-second-order kinetic model than the pseudo-first-order model for the adsorption behaviors of MB on MGO and PAA/MGO.

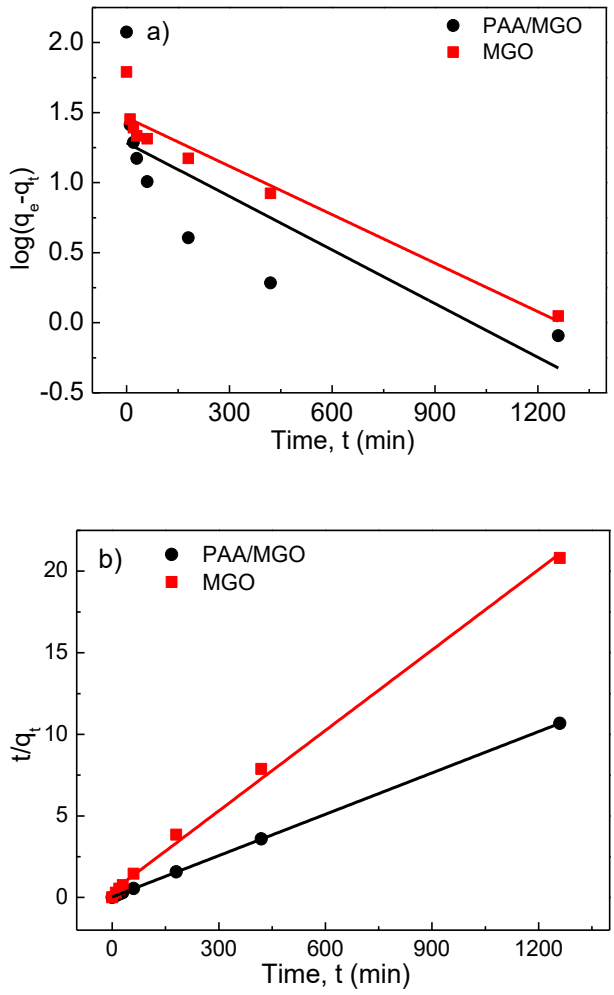

Figure 3.9 Fitting of the adsorption kinetics of MB on MGO and PAA/MGO using **(a)** the pseudo-first-order kinetic model and **(b)** pseudo-second-order kinetic model. Symbols are experimental values and solid lines are the fittings using the two kinetic models.

Table 3-2 Parameters for the fitting of the adsorption of MB on MGO and PAA/MGO using the pseudo-first-order and pseudo-second-order kinetic models.

Adsorbents	$q_{e,\ exp}$ (mg g^{-1})	Pseudo-second-order kinetics			pseudo-second-order kinetics		
		k_1 (min^{-1})	$q_{e,\ cal}$ (mg g^{-1})	R^2	k_2 (g mg^{-1} min^{-1})	$q_{e,\ cal}$ (mg g^{-1})	R^2
MGO	61.2	0.0027	19.26	0.58862	0.0023	60.9	0.99687
PAA/MGO	117.5	0.0030	19.26	0.91559	0.0007	118.3	0.99998

To better understand the interactions between the adsorbents and MB, the adsorption data has been analyzed using Langmuir and Freundlich isotherm models, as shown in Equation 3.5 and Equation 3.6, respectively.[70-71] Langmuir model assumes monolayer adsorption of adsorbate on a homogeneous surface of adsorbent. C_e (mg L^{-1}) is the equilibrium concentration of the MB. q_m (mg g^{-1}) is the maximum Langmuir monolayer adsorption capacity. b is related to the energy of the adsorption.[72] q_m and b can be obtained from the fitting of experimental data by Equation 3.5. The Freundlich isotherm model is an empirical model assuming a heterogeneous surface of adsorbent. K_f and n are the indicators of adsorption capacity and adsorption intensity, respectively, which can be determined from the fitting of experimental data by Equation 3.6.

Langmuir isotherm equation: $\frac{C_e}{q_e} = \frac{1}{bq_m} + \frac{C_e}{q_m}$ (3.5)

Freundlich isotherm equation: $logq_e = logK_f + \frac{1}{n}logC_e$ (3.6)

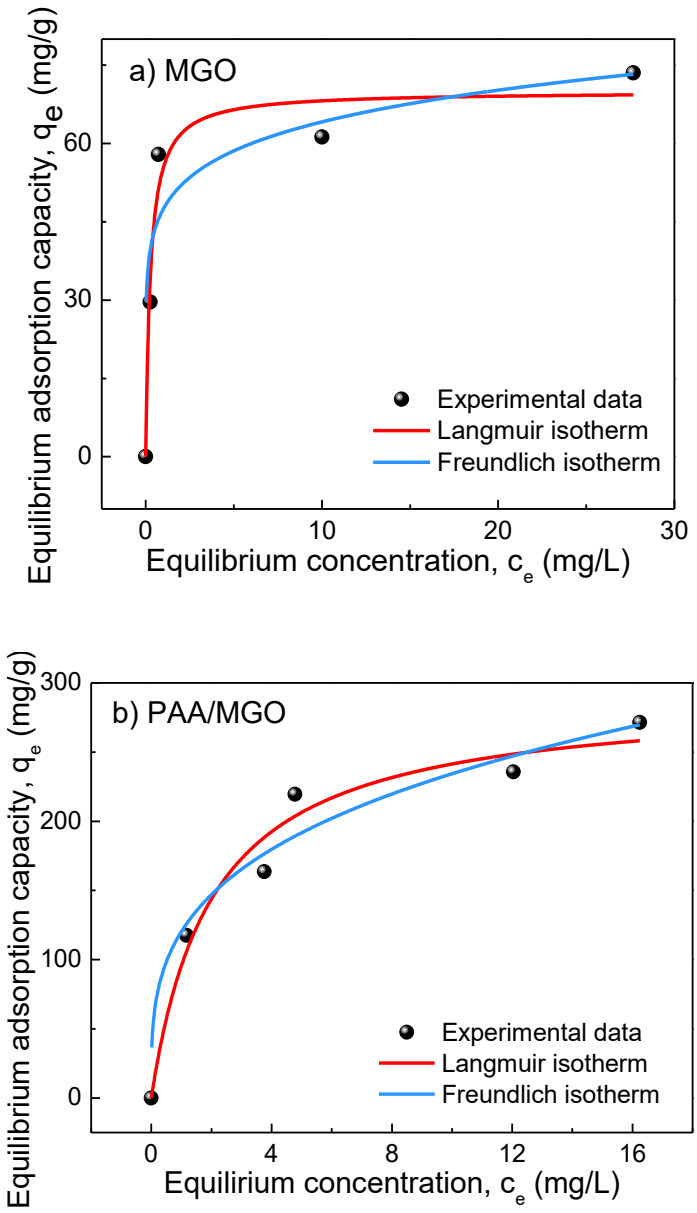

Figure 3.10 Isotherms of the adsorption of MB on **(a)** MGO and **(b)** PAA/MGO, with a contact time of 24 h.

Figure 3.10a and 3.10b show the fitting of adsorption data using the Langmuir and Freundlich models for the adsorption of MB on MGO and PAA/MGO, respectively and the fitting parameters are summarized in Table 3-3. The regression coefficients (R^2) suggest that the Langmuir model fits the adsorption better, which implies that both MGO and PAA/MGO likely

possess homogeneous adsorption surface and the adsorption of MB on these two adsorbents is likely monolayer. However, it should be noted previous studies have shown that certain heterogeneous materials/surfaces and heterogeneous adsorption could also obey the Langmuir model.[70, 73] The q_m of MB on PAA/MGO (290.7 mg g^{-1}) is much higher than q_m of MB on MGO (70.0 mg g^{-1}) due to the incorporation of PAA. At pH 7 for the adsorption tests, the deprotonated carboxylic groups of PAA grafted on MGO can have electrostatic attraction with cationic MB. The hydrophilicity of PAA also facilitates the dispersion of PAA/MGO composite and enhances the stability of the suspension, facilitating the exposure of adsorbent surfaces to contact with MB molecules.

Table 3-3 Fitting parameters of the adsorption of MB on MGO and PAA/MGO using Langmuir and Freundlich isotherm models.

	Langmuir model			Freundlich model		
	b (mg L^{-1})	q_m (mg g^{-1})	R^2	K_f	n	R^2
MGO	3.80	70.0	0.95	47.48	7.66	0.62
PAA/MGO	0.49	290.7	0.97	120.24	3.45	0.88

3.3.4. Effects of pH

The effects of pH on zeta potential of MGO and PAA/MGO and the adsorption capacity, q, of MB on MGO and PAA/MGO were also investigated and the results are shown in Figure 3.11. Figure 3.11a shows that with increasing pH=3 to 11 the zeta potential of both MGO and

PAA/MGO decreases, and the zeta potential of PAA/MGO is lower than that of MGO over the whole pH range. The decreased zeta potential can be attributed to that the carboxylic groups on MGO and on the PAA chains of PAA/MGO deprotonate as pH increases leading to more negatively charged surfaces. The lower zeta potential of PAA/MGO compared with MGO is due to its higher content of carboxylic groups. Figure 3.11b shows that adsorption capacity of MB on MGO increases with increasing pH over the whole range (pH=3 to 11); while adsorption capacity of MB on PAA/MGO increases from pH=3 to 7 achieving almost complete adsorption from pH=7 to 11 (viz. PAA/MGO removed almost all the dye in the solutions). It is noted that PAA/MGO exhibits much higher adsorption capacity of MB than MGO over the whole pH range investigated. As MB molecule contains chloridion that can deionize in aqueous solution and carry positive charge, MB shows electrostatic attraction with negatively charged carboxylic groups.[74] Therefore more negative zeta potential of MGO and PAA/MGO leads to higher adsorption capacity of MB. It is noted that the zeta potential of MGO at pH=3 is ~ -6.1 mV and is almost neutral with negligible electrostatic attraction with MB. The limited adsorption capacity of MB on MGO and PAA/MGO even at pH 3 indicates that π-π interaction between GO surface and MB also plays a role in the adsorption process.

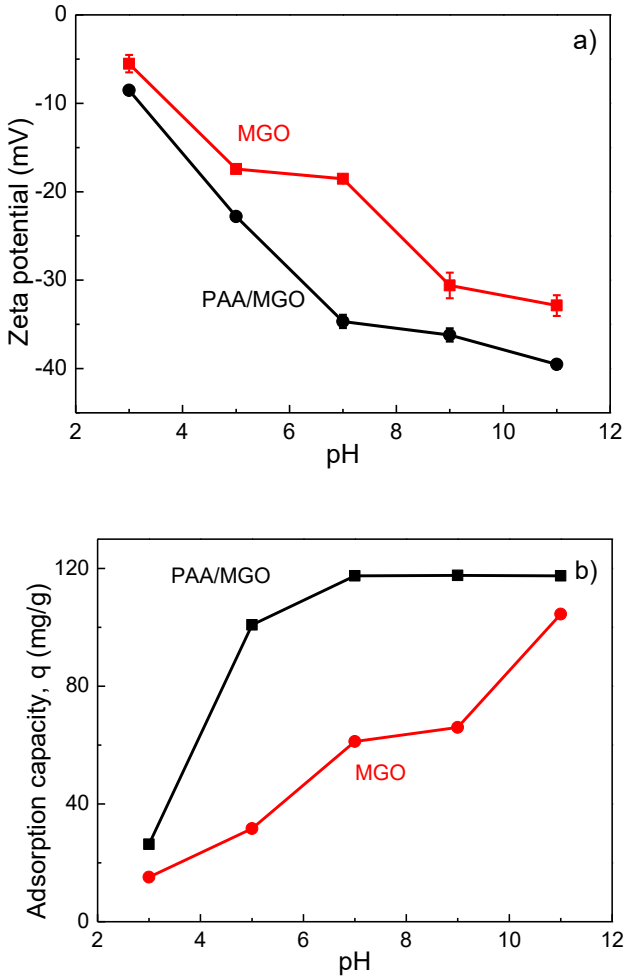

Figure 3.11 (a) Zeta potential of MGO and PAA/MGO and **(b)** adsorption capacity of MB on MGO and PAA/MGO under various pH conditions.

3.3.5. Recyclable usage tests

The recyclability of adsorbents is an important factor for their practical application in water treatment. Adsorption-desorption cycles were carried out to test the recyclable usage of MGO and PAA/MGO on the removal of MB. Figure 3.12 shows that after 5 cycles, the removal percentage of MB by PAA/MGO still remains >98%, while the removal percentage of MB by MGO drops

gradually to about 31%. The better recyclability of PAA/MGO is likely due to the better dispersity of the adsorbents owing to the functionalization of hydrophilic PAA on MGO.

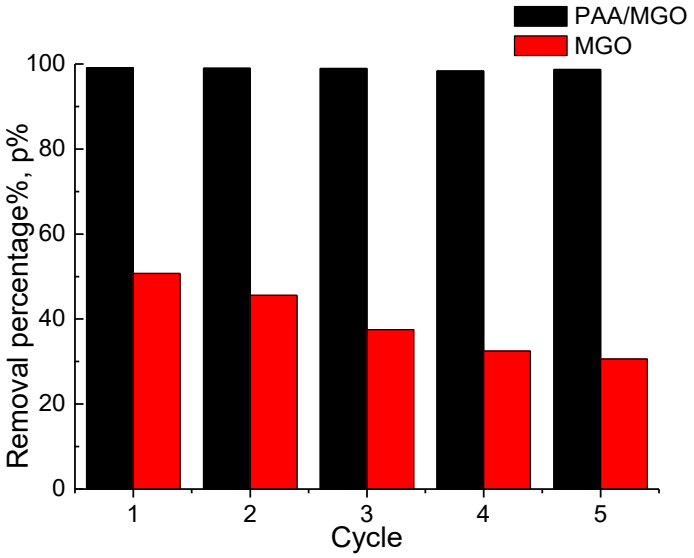

Figure 3.12 Removal percentages *p*% of MB by MGO and PAA/MGO for 5 cycles.

3.4 Conclusions

In this work, we report a facile method for the synthesis of poly (acrylic acid) functionalized magnetic Fe_3O_4 nanoparticle-graphene oxide nanocomposite (PAA/MGO). The structure and surface properties of MGO and PAA/MGO composites were characterized by various techniques including FTIR, XPS, TEM, HRTEM, TGA and zeta potential determinations. The adsorption behaviors of a model dye pollutant, methylene blue, on MGO and PAA/MGO were evaluated in batch tests. At pH 7, MGO and PAA/MGO nanocomposites show a maximum adsorption capacity of MB ~70 mg g^{-1} and ~291 mg g^{-1}, respectively. The higher adsorption capacity of MB on PAA/MGO compared to MGO was attributed to the enhanced electrostatic attraction between positively charged MB molecules and negatively charged nanocomposite surfaces due to the higher content of deprotonated carboxyl groups on PAA/MGO. The removal

capacity of MB by both MGO and PAA/MGO adsorbents also increases with increasing solution pH, and the zeta potential of both MGO and PAA/MGO decreases with increasing the solution pH which enhances the electrostatic attraction between MB and the composite surfaces. At pH 3, MGO and PAA/MGO become almost neutral with zeta potential close to 0 mV, both of which still show limited adsorption capacity to MB, indicating that π-π interaction between GO surface and MB also contributes to the adsorption process. Our results show that the PAA/MGO possesses rapid adsorption rate and higher adsorption capacity of MB than previously reported magnetic graphene or magnetic graphene oxide composites (~44 to ~190 mg g^{-1}) under similar experimental conditions.[33, 75-76] PAA/MGO also can be easily separated under an external magnetic field with excellent recyclability and reusability. The PAA/MGO nanocomposite has great potential application as a novel adsorbent for the removal of cationic organic pollutants from wastewater.

References

1. Zhu, S.; Jiao, S.; Liu, Z.; Pang, G.; Feng, S., High Adsorption Capacity for Dye Removal by Cuzn Hydroxyl Double Salts. *Environ. Sci.: Nano* **2014,** *1*, 172-180.

2. Crini, G., Non-Conventional Low-Cost Adsorbents for Dye Removal: A Review. *Bioresour. Technol.* **2006,** *97*, 1061-1085.

3. Ozcan, A.; Ozcan, A. S.; Gok, O., *Adsorption Kinetics and Isotherms of Anionic Dye of Reactive Blue 19 from Aqueous Solutions onto Dtma-Sepiolite*. 2007; p 25.

4. Prasad, A. L.; Santhi, T., Adsorption of Hazardous Cationic Dyes from Aqueous Solution onto Acacia Nilotica Leaves as an Eco Friendly Adsorbent. *Sustain. Environ. Res.* **2012,** *22*, 113-122.

5. Garg, V. K.; Gupta, R.; Bala Yadav, A.; Kumar, R., Dye Removal from Aqueous Solution by Adsorption on Treated Sawdust. *Bioresour. Technol.* **2003,** *89*, 121-124.

6. Shi, B.; Li, G.; Wang, D.; Feng, C.; Tang, H., Removal of Direct Dyes by Coagulation: The Performance of Preformed Polymeric Aluminum Species. *J. Hazard. Mater.* **2007,** *143*, 567-574.

7. Guibal, E.; Roussy, J., Coagulation and Flocculation of Dye-Containing Solutions Using a Biopolymer (Chitosan). *React. Funct. Polym.* **2007,** *67*, 33-42.

8. Lachheb, H.; Puzenat, E.; Houas, A.; Ksibi, M.; Elaloui, E.; Guillard, C.; Herrmann, J.-M., Photocatalytic Degradation of Various Types of Dyes (Alizarin S, Crocein Orange G, Methyl Red, Congo Red, Methylene Blue) in Water by Uv-Irradiated Titania. *Appl. Catal., B* **2002,** *39*, 75-90.

9. Zhao, D.; Sheng, G.; Chen, C.; Wang, X., Enhanced Photocatalytic Degradation of Methylene Blue under Visible Irradiation on Graphene@ TiO_2 Dyade Structure. *Appl. Catal., B* **2012,** *111*, 303-308.

10. Zhang, N.; Zhang, Y.; Xu, Y.-J., Recent Progress on Graphene-Based Photocatalysts: Current Status and Future Perspectives. *Nanoscale* **2012,** *4*, 5792-5813.

11. Purkait, M.; DasGupta, S.; De, S., Removal of Dye from Wastewater Using Micellar-Enhanced Ultrafiltration and Recovery of Surfactant. *Sep. Purif. Technol.* **2004,** *37*, 81-92.

12. Zaghbani, N.; Hafiane, A.; Dhahbi, M., Separation of Methylene Blue from Aqueous Solution by Micellar Enhanced Ultrafiltration. *Sep. Purif. Technol.* **2007,** *55*, 117-124.

13. Zhuang, X.; Wan, Y.; Feng, C.; Shen, Y.; Zhao, D., Highly Efficient Adsorption of Bulky Dye Molecules in Wastewater on Ordered Mesoporous Carbons. *Chem. Mater.* **2009,** *21*, 706-716.

14. Wang, C.; Feng, C.; Gao, Y.; Ma, X.; Wu, Q.; Wang, Z., Preparation of a Graphene-Based Magnetic Nanocomposite for the Removal of an Organic Dye from Aqueous Solution. *Chem. Eng. J.* **2011,** *173*, 92-97.

15. Iram, M.; Guo, C.; Guan, Y.; Ishfaq, A.; Liu, H., Adsorption and Magnetic Removal of Neutral Red Dye from Aqueous Solution Using Fe_3o_4 Hollow Nanospheres. *J. Hazard. Mater.* **2010,** *181*, 1039-1050.

16. Gupta, V. K., Application of Low-Cost Adsorbents for Dye Removal--a Review. *J. Environ. Manage.* **2009,** *90*, 2313-2342.

17. Li, L.; Fan, L.; Luo, C.; Duan, H.; Wang, X., Study of Fuchsine Adsorption on Magnetic Chitosan/Graphene Oxide. *RSC Adv.* **2014,** *4*, 24679-24685.

18. Li, Q.; Yue, Q.-Y.; Sun, H.-J.; Su, Y.; Gao, B.-Y., A Comparative Study on the Properties, Mechanisms and Process Designs for the Adsorption of Non-Ionic or Anionic Dyes onto Cationic-Polymer/Bentonite. *J. Environ. Manage.* **2010,** *91*, 1601-1611.

19. Alpat, S. K.; Özbayrak, Ö.; Alpat, Ş.; Akçay, H., The Adsorption Kinetics and Removal of Cationic Dye, Toluidine Blue O, from Aqueous Solution with Turkish Zeolite. *J. Hazard. Mater.* **2008,** *151*, 213-220.

20. Hameed, B.; Din, A. M.; Ahmad, A., Adsorption of Methylene Blue onto Bamboo-Based Activated Carbon: Kinetics and Equilibrium Studies. *J. Hazard. Mater.* **2007,** *141*, 819-825.

21. Ramesha, G.; Vijaya Kumara, A.; Muralidhara, H.; Sampath, S., Graphene and Graphene Oxide as Effective Adsorbents toward Anionic and Cationic Dyes. *J. Colloid Interface Sci.* **2011,** *361*, 270-277.

22. Hamilton, C. E. Functionalization, Coordination, and Coating of Carbon Nanomaterials Ph.D Thesis, University of Rice, 2009.

23. Zhao, G.; Wen, T.; Chen, C.; Wang, X., Synthesis of Graphene-Based Nanomaterials and Their Application in Energy-Related and Environmental-Related Areas. *RSC Adv.* **2012,** *2*, 9286-9303.

24. Wang, H.; Yuan, X.; Wu, Y.; Huang, H.; Peng, X.; Zeng, G.; Zhong, H.; Liang, J.; Ren, M., Graphene-Based Materials: Fabrication, Characterization and Application for the Decontamination of Wastewater and Wastegas and Hydrogen Storage/Generation. *Adv. Colloid Interface Sci.* **2013,** *195*, 19-40.

25. Wang, S.; Sun, H.; Ang, H. M.; Tadé, M. O., Adsorptive Remediation of Environmental Pollutants Using Novel Graphene-Based Nanomaterials. *Chem. Eng. J.* **2013,** *226*, 336-347.

26. Zhao, G.; Jiang, L.; He, Y.; Li, J.; Dong, H.; Wang, X.; Hu, W., Sulfonated Graphene for Persistent Aromatic Pollutant Management. *Adv. Mater.* **2011,** *23*, 3959-3963.

27. Zhang, W.; Zhou, C.; Zhou, W.; Lei, A.; Zhang, Q.; Wan, Q.; Zou, B., Fast and Considerable Adsorption of Methylene Blue Dye onto Graphene Oxide. *Bull. Environ. Contam. Toxicol.* **2011,** *87*, 86-90.

28. Stankovich, S.; Piner, R. D.; Chen, X.; Wu, N.; Nguyen, S. T.; Ruoff, R. S., Stable Aqueous Dispersions of Graphitic Nanoplatelets Via the Reduction of Exfoliated Graphite Oxide in the Presence of Poly(Sodium 4-Styrenesulfonate). *J. Mater. Chem.* **2006,** *16*, 155.

29. Stankovich, S.; Dikin, D. A.; Piner, R. D.; Kohlhaas, K. A.; Kleinhammes, A.; Jia, Y.; Wu, Y.; Nguyen, S. T.; Ruoff, R. S., Synthesis of Graphene-Based Nanosheets Via Chemical Reduction of Exfoliated Graphite Oxide. *Carbon* **2007,** *45*, 1558-1565.

30. Travlou, N. A.; Kyzas, G. Z.; Lazaridis, N. K.; Deliyanni, E. A., Functionalization of Graphite Oxide with Magnetic Chitosan for the Preparation of a Nanocomposite Dye Adsorbent. *Langmuir* **2013,** *29*, 1657-1668.

31. Yang, S.-T.; Chen, S.; Chang, Y.; Cao, A.; Liu, Y.; Wang, H., Removal of Methylene Blue from Aqueous Solution by Graphene Oxide. *J. Colloid Interface Sci.* **2011,** *359*, 24-29.

32. Madadrang, C. J.; Kim, H. Y.; Gao, G.; Wang, N.; Zhu, J.; Feng, H.; Gorring, M.; Kasner, M. L.; Hou, S., Adsorption Behavior of Edta-Graphene Oxide for Pb (II) Removal. *ACS Appl. Mater. Interfaces* **2012,** *4*, 1186-1193.

33. Ai, L.; Zhang, C.; Chen, Z., Removal of Methylene Blue from Aqueous Solution by a Solvothermal-Synthesized Graphene/Magnetite Composite. *J. Hazard. Mater.* **2011,** *192*, 1515-1524.

34. Xie, G.; Xi, P.; Liu, H.; Chen, F.; Huang, L.; Shi, Y.; Hou, F.; Zeng, Z.; Shao, C.; Wang, J., A Facile Chemical Method to Produce Superparamagnetic Graphene Oxide–Fe_3O_4 Hybrid

Composite and Its Application in the Removal of Dyes from Aqueous Solution. *J. Mater. Chem.* **2012,** *22*, 1033-1039.

35. He, F.; Fan, J.; Ma, D.; Zhang, L.; Leung, C.; Chan, H. L., The Attachment of Fe_3o_4 Nanoparticles to Graphene Oxide by Covalent Bonding. *Carbon* **2010,** *48*, 3139-3144.

36. Meral, K.; Metin, Ö., Graphene Oxide--Magnetite Nanocomposite as an Efficient and Magnetically Separable Adsorbent for Methylene Blue Removal from Aqueous Solution. *Turk. J. Chem.* **2014,** *38*, 775-782.

37. Huang, S.-H.; Chen, D.-H., Rapid Removal of Heavy Metal Cations and Anions from Aqueous Solutions by an Amino-Functionalized Magnetic Nano-Adsorbent. *J. Hazard. Mater.* **2009,** *163*, 174-179.

38. Kan, L.; Xu, Z.; Gao, C., General Avenue to Individually Dispersed Graphene Oxide-Based Two-Dimensional Molecular Brushes by Free Radical Polymerization. *Macromolecules* **2010,** *44*, 444-452.

39. Yang, Y.; Xie, Y.; Pang, L.; Li, M.; Song, X.; Wen, J.; Zhao, H., Preparation of Reduced Graphene Oxide/Poly(Acrylamide) Nanocomposite and Its Adsorption of Pb(II) and Methylene Blue. *Langmuir* **2013,** *29*, 10727-10736.

40. Liu, J.; Cao, H.; Xiong, J.; Cheng, Z., Ferromagnetic Hematite@ Graphene Nanocomposites for Removal of Rhodamine B Dye Molecules from Water. *CrystEngComm* **2012,** *14*, 5140-5144.

41. Chandra, V.; Park, J.; Chun, Y.; Lee, J. W.; Hwang, I.-C.; Kim, K. S., Water-Dispersible Magnetite-Reduced Graphene Oxide Composites for Arsenic Removal. *ACS Nano* **2010,** *4*, 3979-3986.

42. Shi, H.; Li, W.; Zhong, L.; Xu, C., Methylene Blue Adsorption from Aqueous Solution by Magnetic Cellulose/Graphene Oxide Composite: Equilibrium, Kinetics, and Thermodynamics. *Ind. Eng. Chem. Res.* **2014,** *53*, 1108-1118.

43. Neises, B.; Steglich, W., Simple Method for the Esterification of Carboxylic Acids. *Angew. Chem., Int. Ed. Engl.* **1978,** *17*, 522-524.

44. Durdureanu-Angheluta, A.; Ardeleanu, R.; Pinteala, M.; Harabagiu, V.; Chiriac, H.; Simionescu, B., Silane Covered Magnetite Particles. Preparation and Characterisation. *Dig. J. Nanomater. Bios.* **2008,** *3*, 33-40.

45. Everaerts, F.; Torrianni, M.; Hendriks, M.; Feijen, J., Biomechanical Properties of Carbodiimide Crosslinked Collagen: Influence of the Formation of Ester Crosslinks. *J. Biomed. Mater. Res. A* **2007,** *85*, 547-555.

46. Liao, M.-H.; Chen, D.-H., Preparation and Characterization of a Novel Magnetic Nano-Adsorbent. *J. Mater. Chem.* **2002,** *12*, 3654-3659.

47. Mak, S.-Y.; Chen, D.-H., Fast Adsorption of Methylene Blue on Polyacrylic Acid-Bound Iron Oxide Magnetic Nanoparticles. *Dyes Pigm.* **2004,** *61*, 93-98.

48. Yao, Y.; Miao, S.; Yu, S.; Ma, L. P.; Sun, H.; Wang, S., Fabrication of Fe_3o_4/Sio_2 Core/Shell Nanoparticles Attached to Graphene Oxide and Its Use as an Adsorbent. *J. Colloid Interface Sci.* **2012,** *379*, 20-26.

49. Yao, Y.; Miao, S.; Liu, S.; Ma, L. P.; Sun, H.; Wang, S., Synthesis, Characterization, and Adsorption Properties of Magnetic Fe_3o_4@Graphene Nanocomposite. *Chem. Eng. J.* **2012,** *184*, 326-332.

50. Li, L.; Liu, X. L.; Gao, M.; Hong, W.; Liu, G. Z.; Fan, L.; Hu, B.; Xia, Q. H.; Liu, L.; Song, G. W.; Xu, Z. S., The Adsorption on Magnetic Hybrid Fe_3o_4/Hkust-1/Go of Methylene Blue from Water Solution. *J. Mater. Chem. A* **2014,** *2*, 1795.

51. Paek, S.-M.; Yoo, E.; Honma, I., Enhanced Cyclic Performance and Lithium Storage Capacity of Sno_2/Graphene Nanoporous Electrodes with Three-Dimensionally Delaminated Flexible Structure. *Nano Lett.* **2009,** *9*, 72-75.

52. Ramesha, G.; Kumara, A. V.; Muralidhara, H.; Sampath, S., Graphene and Graphene Oxide as Effective Adsorbents toward Anionic and Cationic Dyes. *J. Colloid Interface Sci.* **2011,** *361*, 270-277.

53. Xie, Y.; Yan, B.; Xu, H.; Chen, J.; Liu, Q.; Deng, Y.; Zeng, H., Highly Regenerable Mussel-Inspired Fe3o4@ Polydopamine-Ag Core-Shell Microspheres as Catalyst and Adsorbent for Methylene Blue Removal. *ACS Appl. Mater. Interfaces* **2014,** *6*, 8845-8852.

54. Fu, Y.; Wang, J.; Liu, Q.; Zeng, H., Water-Dispersible Magnetic Nanoparticle–Graphene Oxide Composites for Selenium Removal. *Carbon* **2014,** *77*, 710-721.

55. Wang, G.; Yang, S.; Wei, Z.; Dong, X.; Wang, H.; Qi, M., Facile Preparation of Poly(E-Caprolactone)/Fe_3o_4@Graphene Oxide Superparamagnetic Nanocomposites. *Polym. Bull.* **2013,** *70*, 2359-2371.

56. Yang, Z.; Chen, X.-H.; Xia, S.-Z.; Pu, Y.-X.; Xu, H.-Y.; Li, W.-H.; Xu, L.-S.; Yi, B.; Pan, W.-Y., Covalent Attachment of Poly (Acrylic Acid) onto Multiwalled Carbon Nanotubes Functionalized with Formaldehyde Via Electrophilic Substitution Reaction. *J. Mater. Sci.* **2007,** *42*, 9447-9452.

57. Zhang, J.; Yang, H.; Shen, G.; Cheng, P.; Zhang, J.; Guo, S., Reduction of Graphene Oxide Via L-Ascorbic Acid. *Chem. Commun.* **2010,** *46*, 1112-1114.

58. Dong, Y.; Hu, M.; Ma, R.; Cheng, H.; Yang, S.; Li, Y. Y.; Zapien, J. A., Evaporation-Induced Synthesis of Carbon-Supported Fe_3O_4 Nanocomposites as Anode Material for Lithium-Ion Batteries. *CrystEngComm* **2013,** *15*, 1324-1331.

59. Jin, Y.; Jia, C.; Huang, S.-W.; O'Donnell, M.; Gao, X., Multifunctional Nanoparticles as Coupled Contrast Agents. *Nat. Commun.* **2010,** *1*, 41.

60. Reimer, L.; Kohl, H., *Transmission Electron Microscopy: Physics of Image Formation*. Springer Science & Business Media: 2008; Vol. 36.

61. Gentsch, P.; Gilde, H.; Reimer, L., Measurement of the Top Bottom Effect in Scanning Transmission Electron Microscopy of Thick Amorphous Specimens. *J. Microsc.* **1974,** *100*, 81-92.

62. Socrates, G., *Infrared and Raman Characteristic Group Frequencies: Tables and Charts*. John Wiley & Sons: 2004.

63. Larkin, P., *Infrared and Raman Spectroscopy; Principles and Spectral Interpretation*. Elsevier: 2011.

64. Shimanouchi, T. *Tables of Molecular Vibrational Frequencies Consolidated. Volume I*; DTIC Document: 1972.

65. Some, S.; Kim, Y.; Yoon, Y.; Yoo, H.; Lee, S.; Park, Y.; Lee, H., High-Quality Reduced Graphene Oxide by a Dual-Function Chemical Reduction and Healing Process. *Sci. Rep.* **2013,** *3*, 1929.

66. Fu, Y. Water-Dispersible Magnetic Particle-Graphene Oxide Composites: Synthesis, Characterization and Application in the Removal of Selenium. Master Thesis, University of Alberta, 2014.

67. Novoselov, K. S.; Geim, A. K.; Morozov, S. V.; Jiang, D.; Zhang, Y.; Dubonos, S. V.; Grigorieva, I. V.; Firsov, A. A., Electric Field Effect in Atomically Thin Carbon Films. *Science* **2004,** *306*, 666-669.

68. Connors, K. A., *Chemical Kinetics: The Study of Reaction Rates in Solution*. John Wiley & Sons: 1990.

69. Toth, J., *Adsorption*. CRC Press: 2002.

70. Langmuir, I., The Constitution and Fundamental Properties of Solids and Liquids. Part I. Solids. *J. Am. Chem. Soc.* **1916,** *38*, 2221-2295.

71. Freundlich, H., Uber Die Adsorption in Losungen. *Zeitschrift für Physikalische* **1906,** *57*, 384-470.

72. Masel, R. I., *Principles of Adsorption and Reaction on Solid Surfaces*. John Wiley & Sons: 1996; Vol. 3.

73. Dąbrowski, A., Adsorption—from Theory to Practice. *Adv. Colloid Interface Sci.* **2001,** *93*, 135-224.

74. Tuite, E. M.; Kelly, J. M., New Trends in Photobiology: Photochemical Interactions of Methylene Blue and Analogues with DNA and Other Biological Substrates. *J. Photochem. Photobiol., B* **1993,** *21*, 103-124.

75. He, F.; Fan, J.; Ma, D.; Zhang, L.; Leung, C.; Chan, H. L., The Attachment of Fe_3O_4 Nanoparticles to Graphene Oxide by Covalent Bonding. *Carbon* **2010,** *48*, 3139-3144.

76. Li, L.; Liu, X. L.; Gao, M.; Hong, W.; Liu, G. Z.; Fan, L.; Hu, B.; Xia, Q. H.; Liu, L.; Song, G. W., The Adsorption on Magnetic Hybrid Fe_3O_4/Hkust-1/Go of Methylene Blue from Water Solution. *J. Mater. Chem. A* **2014,** *2*, 1795-1801.

Chapter 4 Unraveling the Interaction between Graphene Oxide and Aromatic Organic Compounds

4.1 Introduction

Over the past decade, graphene oxide (GO) and its derivatives, one type of the graphene-based nanomaterials, have received much attention in many research areas and engineering applications, due to their unique physicochemical, mechanical, electronic, optical and structural properties.[1-8] In bioengineering, the atomically thin 2-D structure renders GO with extremely high specific surface area coupled with conjugated basal plane structure, serving as a platform or nanocarrier for a large quantity and variety of molecules containing aromatic functional groups, such as drugs,[9-11] genes[12] and fluorescent molecules[12-13]. The affinity of fluorescent molecules with aromatic functional groups to GO can lead to their effective quenching,[13-14] contributing to biosensing application.[15-17] Therefore, it is of great interest and importance to understand the interaction mechanism between the aromatic organic compounds (AOCs) and GO surfaces that determines their interaction energies and the configurations of the interfacial nanostructures for enhanced functionality.

By chemical oxidation and exfoliation of graphite flakes, GO can be produced in relatively large scale following modified Hummers' method,[18] with epoxy and carbonyl groups on GO's basal plane, carboxylic groups on GO flakes' edge while part of the sp^2 domain structure being retained from pristine graphite.[19-24] The complex chemical constitution of GO leads to various interactions between its surface and AOCs,[14] which have been characterized by many experimental techniques on bulk samples at relatively macroscopic scale, such as ultraviolet (UV) spectroscopy[25-26] and energy-dispersive X-ray spectroscopy (EDS). [25] Batch adsorption tests showed that negatively charged GO favors the adsorption of cationic AOCs.[27] The interactions

between GO and cationic AOCs are generally believed to include electrostatic interaction introduced by the negatively charged carboxylic groups on GO,[27-29] and π- π interaction due to the remained sp^2 zones on GO's surface.[25, 30] However, the understanding of the role of the specific functional groups in the interactions of GO with AOCs and their binding strength still remains unclear. To the best of our knowledge, there has been no experimental and theoretical study on characterizing the interaction mechanism of GO-AOCs at the single molecular level and nanoscale.

In this work, for the *first* time, we unveil the nanomechanical interaction mechanism between a model aromatic organic molecule and GO surface by using both single-molecule force spectroscopy (SMFS) measurements based on atomic force microscopy (AFM) and density functional theory (DFT) simulations. Our results provide new insights into the interaction mechanisms of GO-AOCs with useful implications on the design of advanced GO-based nanocomposites with tunable nanostructures and performance for a broad range of bioengineering and engineering applications.

4.2 Materials and methods

4.2.1 Materials

Potassium permanganate, sodium nitrate, methylene blue (MB), toluidine blue o (TBO) and hydrogen peroxide were purchased from Fisher Scientific. Graphite flake (325 mesh), sulfuric acid (98%), DL-thioctic acid (TA), poly(ethylene glycol) (HO-PEG_{4000}-OH, Mn 4000 g/mol), 4-(dimethylamino)pyridine (DMAP) and poly(ethylene glycol) methyl ether (CH_3-PEG_{1900}-OH, Mn 1900 g/mol) were obtained from Alfa Aesar. Succinic anhydride, N,N'-dicyclohexylcarbodiimide (DCC), N-hydroxysuccinimide (NHS) and dichloromethane (DCM) were purchased from Sigma-Aldrich. 1,4-dioxane were obtained from ACROS. All chemicals used in this study were analytical grade and used as received.

4.2.2 Preparation of graphene oxide (GO)

Graphene oxide was prepared by a modified Hummer's method.[31] Graphite (2 g) and sodium nitrate (1.5 g) were first added to a 500 ml 3-neck flask, and then sulfuric acid (98%, 150 mL) was added into the mixture in an ice bath with stirring. Then potassium permanganate (9 g) was slowly added into the mixture during a period of 1 h. Stirring was kept for 2 h in the ice-water bath and then kept for another 5 days at room temperature. After that, hydrogen peroxide solution (30 wt. %, 6 mL) was added into the mixture under agitation and the stirring was kept for 2 h. 250 mL solution (98 wt. %, 7.5 mL sulfuric acid and 30 wt. %, 4.17 mL hydrogen peroxide solution in deionized water) was added to dilute and wash the mixture. The resulted compound was thoroughly washed by deionized water, centrifuged and then dialyzed for 5 days. Eventually, the graphene oxide powder was obtained by freeze drying after sonication. The surface chemistry of GO was characterized using an X-ray photoelectron spectrometer (Kratos Axis Ultra, NY) with Al Kα radiation (12 mA, 14 kV).

4.2.3 Atomic force microscopy (AFM) imaging tests

The silicon wafer substrates used for topography measurements were prepared as follows. First, the silicon wafer substrates were rinsed by mili-Q water, ethanol, dried by Argon, and, subsequently, cleaned through UV-ozone treatment. Then, GO solution (20 mg/L) or mixture of equal-volume GO (20 mg/L) and MB (0.5 mg/L) aqueous solutions was dropped on the silicon wafer substrates. After fully dried, tapping mode AFM was carried out to characterize the surface topography of the samples using an Asylum MFP-3D AFM (Asylum Research, Santa Barbara, CA).

4.2.4 Single-molecule force spectroscopy (SMFS) measurements

Silicon wafer substrates were extensively rinsed by mili-Q water and ethanol, dried by Argon gas, and further cleaned through UV-ozone treatment. Then, a drop of GO solution (20 mg/mL) was spread on each substrate using pipet tip. The substrates were naturally dried overnight before single-molecule force measurement. The synthesis method of CH_3-PEG_{1900}-TA and TBO-PEG_{4000}-TA is described in Supporting Information. For tip modification, silicon nitride cantilevers with gold coated tips (NPG-10 probes, Bruker, Santa Barbara, CA) were first cleaned by UV-ozone treatment for 15 min and then transferred into an aqueous solution with a TBO-PEG_{4000}-TA/CH_3-PEG_{1900}-TA mass ratio of 1:2.

Single-molecule force spectroscopy experiments were carried out on a Dimension Icon AFM (Bruker, Santa Barbara, CA) and conducted in water (pH 5.6, natural pH; or pH=2, adjusted by 0.1 M HCl). The spring constants of cantilevers were determined to be ~0.15 N/m using the Hutter and Bechhoefer method.[32-33]

4.3 Experimental results and discussion

Methylene blue (MB), as a typical cationic aromatic dye, was chosen as a model AOC compound in this study, which has been applied in cell staining,[34] anti-microbial[35] and medicinal photosensitizer.[35-36] The affinity between MB and GO makes GO as a good carrier and adsorbent for MB, contributing to their applications in biosensor[37] and MB removal from wastewater.[38] AFM topography imaging of pure GO and MB/GO complex has been conducted and the results are shown in Figure 4.1. MB molecules were adsorbed to GO in aqueous solution and then the mixture solution was deposited on silicon wafer substrate to prepare the MB/GO complex sample for AFM imaging. The typical topographic AFM images of pure GO (Figure 4.1a and 4.1b) show that the GO sheets are smooth and flat. The height profile of pure GO (Figure 4.1c) demonstrates that the

GO surface is smooth with a ~0.1 nm height fluctuation and the thickness of GO is ~0.8 nm, indicating a single layer structure, which is in agreement with the literature.[39-41] The topographic AFM images of MB/GO complex (Figure 4.1d and 4.1e) show obvious difference with a large number of nanoaggregates of MB molecules adsorbed on the GO surface. The height profile of the MB/GO complex (Figure 4.1f) shows that the thickness of the flake is ~0.9 nm, suggesting the single layer structure of GO is not changed and the slightly increased thickness might be due to the presence of MB molecules between GO and the silicon wafer substrate. Owing to the adsorption of MB on GO surface, the MB/GO surface is evidently rougher, as compared to GO, with a height fluctuation of ~0.4 nm.

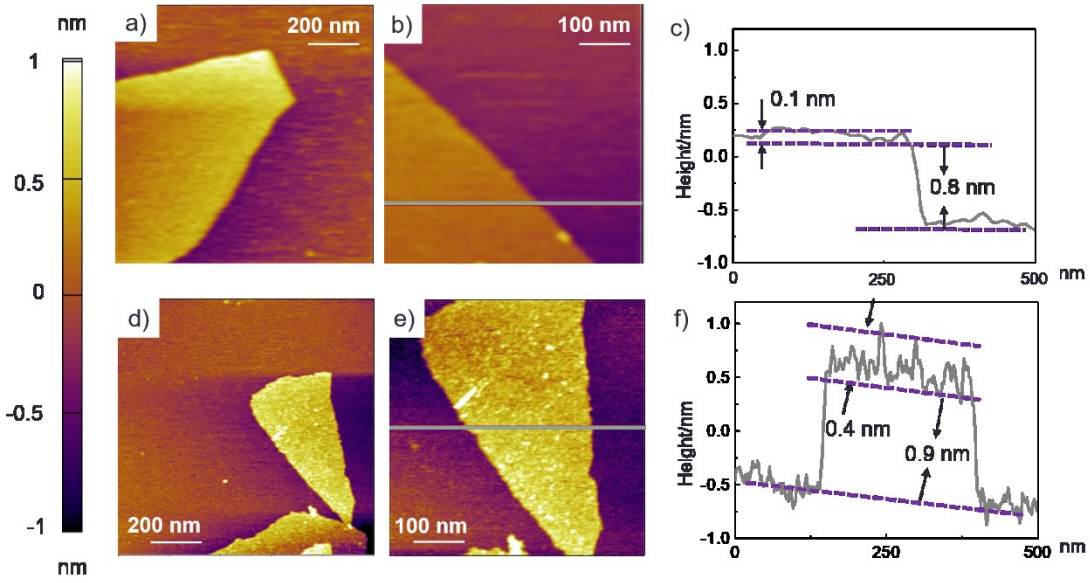

Figure 4.1 (a, b) Topographic atomic force microscopy (AFM) images and (c) height profile of graphene oxide (GO) on silicon wafer substrate. (d, e) Topographic AFM images and (f) height profile of methylene blue (MB)/GO complex on silicon wafer substrate.

The surface chemistry of GO was characterized using X-ray photoelectron spectroscopy (XPS). The C1s XPS spectrum of GO has been calibrated using the binding energy (B. E.) of the adventitious C1s at 284.6 eV and is shown in Figure 4.2. The deconvolution of the C1s XPS spectrum of GO shows four peaks at 284.6, 286.6, 287.3 and 288.3 eV, which can be assigned to sp^3 carbon (C-C) and sp^2 carbon (C=C), epoxy groups (C-O-C), carbonyl groups (C=O), and carboxylic groups (-COOH), respectively.[42-43] Epoxy groups are the dominative functional groups on GO with a content of 44.5%, and the content of carboxylic groups is much less (7.4%), while the carbonyl group content is 4.3%, which is even less. However, surprisingly little attention has been paid to study the role of epoxy groups in GO, of which the content is ~6 times that of carboxylic groups, in GO's interactions with AOCs.

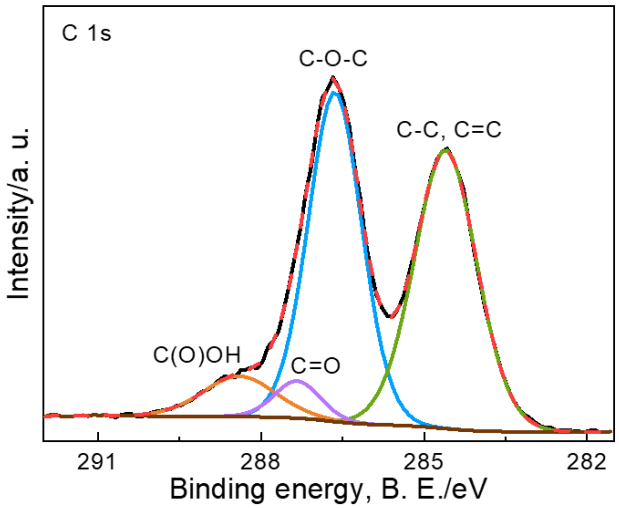

Figure 4.2 X-ray photoelectron spectroscopy (XPS) C1s spectrum of GO.

The different functional groups on GO can lead to various interactions for GO-AOCs in aqueous solution. Single molecular force measurements were conducted at both pH 2 (Figure 4.3a, with carboxylic groups remaining neutral) and pH 5.6 (Figure 4.3b, with carboxylic groups ionized).[44] The ionized carboxylic groups could introduce electrostatic interaction between GO and cationic AOC molecule. As shown in Figure 4.3c-3d, toluidine blue O (TBO) is employed in

SMFS experiments due to its highly similar chemical structure to MB with the amino group to be end-tethered to polyethylene glycol (PEG), which is used as a linker and flexible spacer to isolate the contribution of TBO from the AFM tip.[45-46] Force measurements were conducted over the different regions of GO surface using the TBO modified tip to qualify the interactions with various functional groups via the force-distance curves.[47-48]

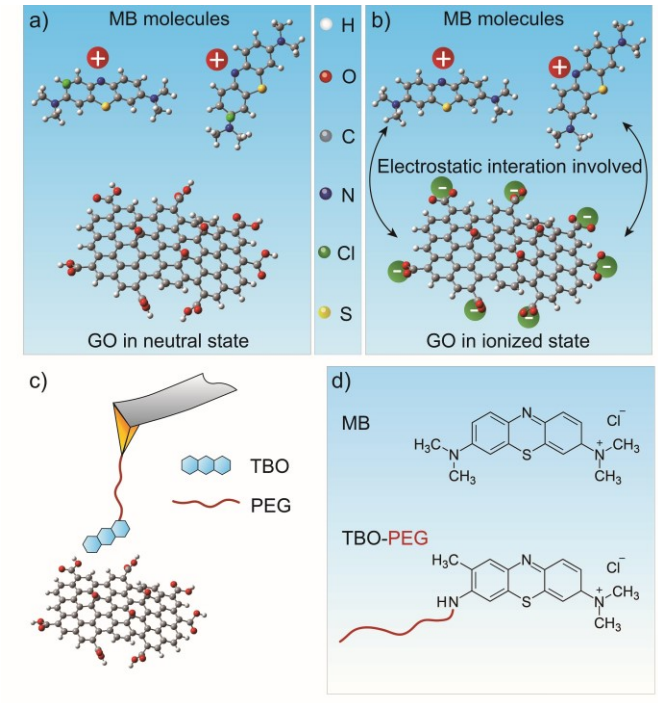

Figure 4.3 Schematic illustrations of free MB and GO molecules under (a) neutral (unionized) and (b) ionized conditions. The ionization of carboxylic groups of GO would introduce electrostatic interaction between GO and cationic MB, which is absent under neutral condition. (c) Scheme of experimental setup for single-molecular force (SMF) measurement (conducted under both neutral (pH 2) and ionized conditions (pH 5.6) of GO) to study the interaction between GO and toluidine blue O (TBO). TBO possesses highly similar chemical structure to MB with amino group to be end-tethered to polyethylene glycol (PEG), which is used as a linker between AFM tip and TBO. (d) Illustration of the chemical structures of MB and TBO-PEG.

A representative force–distance curve is shown in Figure S 4.1. With retraction of the cantilever, the force–distance curve first exhibits a typical appearance of elastic extension of the tethered PEG chain, which can be well fitted with the extended freely jointed chain (E-FJC) model shown by the red curve.[49-50] Then the force reaches a local maximum associated with the detachment of TBO from the GO surface. Single molecule force experiments have been carried out systematically at different locations across the GO surfaces under various retraction speeds (*i.e.*, ~300 to ~4700 nm/s) at pH 2 and pH 5.6, and the bond dissociation forces obtained from the force-distance curves have been collected. The histograms of the bond dissociation forces have been fitted using the Gaussian distribution to provide the most probable bond dissociation forces. It is found that the most probable bond dissociation forces F increase with increasing the loading rate r under the same pH condition. Fitting the data of F *vs.* ln (r) (Figure 4.4a and 4.4b) using the Bell-Evans model (Equation 4.1)[51-52] provides useful information about activation Gibbs energy for bond dissociation (ΔG) (Equation 4.2) and the bond dissociation distance from the equilibrium position (Δx),

$$F = \frac{k_B T}{\Delta x} ln\left(\frac{\Delta x}{k_0 k_B T}\right) + \frac{k_B T}{\Delta x} ln(r) \qquad (4.1)$$

$$\Delta G = RT ln\left(\frac{k_0}{A}\right) \qquad (4.2)$$

where k_B is the Boltzmann constant, T is the absolute temperature, and k_0 is the spontaneous dissociation rate of the bond. ΔG is bond dissociation energy, R is the gas constant and A is the Arrhenius prefactor or the frequency factor, which is chosen as 10^6 s^{-1} in the calculation according to previous reports.[53-54]

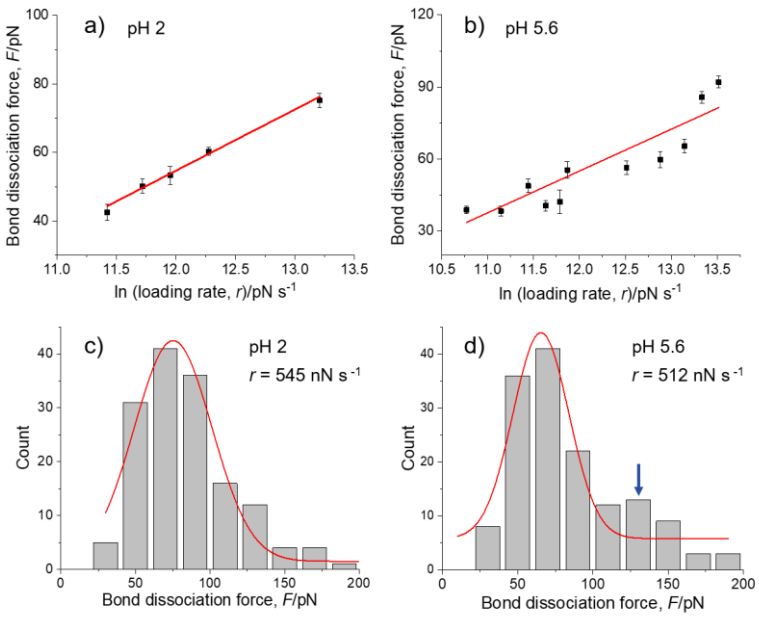

Figure 4.4 The most probable bond dissociation forces between TBO and GO under different loading rates at a) pH 2 and b) pH 5.6, where the red line corresponds to the fitting by the Bell-Evans model. Representative histograms of bond dissociation force values for TBO-GO at c) pH 2 and d) pH 5.6 (red curve: Gaussian fitting to give the most probable bond dissociation force).

At pH 2 (Figure 4.4a), the linear fitting of F versus ln(r) reveals a ΔG of -4.61 kcal/mol and a Δx of 2.3 Å for TBO-GO dissociation, and the representative histogram of bond dissociation forces (Figure 4.4c) shows a single peak at r=545 nN/s, in which the involved interaction should not be ascribed to electrostatic interaction due to the electrically neutral carboxylic groups on GO. (More histograms under different loading rates at pH 2 and pH 5.6 are shown in Figure S 4.2a and S 4.2b.) At pH 5.6 (Figure 4.4b), similar linear fitting gives ΔG = -4.57 kcal/mol and Δx = 2.3 Å, indicating the same type of interaction as that under pH 2 (further discussed in the next section). It is noted that a second local maximum appears as r increases to 512 nN/s (as indicated by the blue arrow) in Figure 4.4d, which is most likely ascribed to the electrostatic interaction between

the negatively charged ionized carboxylic groups of GO and cationic TBO. It is noted that the count attributing to the main peak is much higher that of the second maximum, yet the specific interactions involved still remain to be ravelled, as further discussed in the following section.

4.4 Theoretical calculations

The interactions between MB and a series of graphene surfaces (*i.e.*, pristine graphene, graphene with an epoxy group (epoxy-graphene) and an unionized/ionized carboxylic group (unionized/ionized carboxyl-graphene), according to the XPS and SMF results) have been simulated, and the electrostatic potential (ESP) surfaces of each single molecules have been computed and mapped using B3LYP/6-31G* level. All the geometries were optimized in vacuum and the energies in water were calculated by the single-point energy calculation based on the optimized geometry in vacuum using polarizable continuum model (PCM) with zero-point vibrational correction, and all these calculations were performed using the Gaussian 09 Program package.[55] The optimized configurations of single molecules are shown in Figure S 4.3. All these molecules possessing multi-cyclic aromatic structures lead to planar structures with slight distortion and the results are consistent with previous reports.[26, 56-57] The adsorption energies (E_{ad}) of MB molecule on different graphene surfaces were calculated by Equation 4.3 based the optimized geometries.[57-58]

$$E_{ad} = E_{complex} - (E_{graphene\ surface} + E_{MB}) \qquad (4.3)$$

where $E_{complex}$, $E_{graphene\ surface}$ and E_{MB} are the total ground state energies with zero-point vibrational correction of MB/each type of graphene surface, each type of graphene surface and MB molecule, respectively.

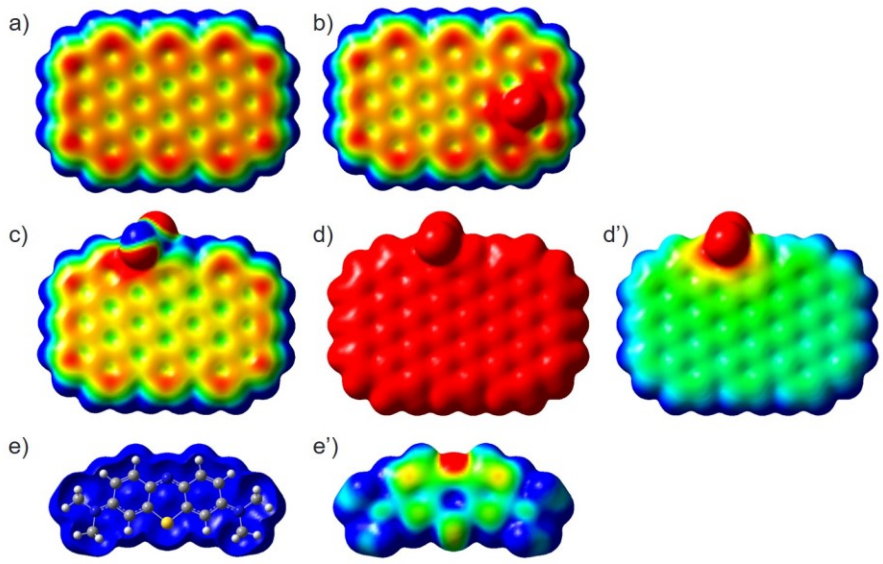

Figure 4.5 Electrostatic potential (ESP) surfaces of (a) graphene, (b) epoxy-graphene, (c) unionized carboxyl-graphene, (d) ionized carboxyl-graphene and (e) MB with a color scale of -12.55 (red) to 12.55 kcal/mol (blue). The ESP surface of MB is clipped to reveal the molecule structure. The grey, white, blue and yellow balls stand for carbon, hydrogen, nitrogen and sulfur atoms, respectively. ESP surfaces of (d') ionized carboxyl-graphene with a color scale of -94.125 (red) to -18.825 kcal/mol (blue), and e') MB with a scale of 50.2 (red) to 75.3 kcal/mol (blue). All electrostatic potentials are mapped on 0.002 electrons/Bohr^3 electron density isosurface.

As shown in Figure 4.5, on the ESP surfaces, the regions with ESP values less than or equal to the minimum ESP (ESP_{min}) are coded with red color, while the regions with ESP values larger than or equal to the maximum ESP (ESP_{max}) are coded with blue color. In Figure 4.5a-5e, the ESP surfaces are colored in the same scale (ESP_{min} = -12.55 and ESP_{max} = 12.55 kcal/mol). To observe the ESP difference of the atoms on each molecule more clearly, negatively charged ionized carboxyl-graphene (Figure 4.5d', ESP_{min} = -94.125 and ESP_{max} = -18.825 kcal/mol) and cationic MB molecule (Figure 4.5e', ESP_{min} = 50.2 and ESP_{max} = 75.3 kcal/mol) are also coded in other color scales. As shown in Figure 4.5a, for graphene, as well as other electrically neutral aromatic

molecules, the upper and bottom sides should be electron rich (red) due to the π electron cloud, while the hydrogen atoms (or σ framework) on the edge (blue) are electron deficient. Thus, the repulsion between π electron clouds and attraction between hydrogen (or σ framework) and π electrons of the two stacking aromatic molecules lead to an offset π stacking.[59-61] As shown in Figure 4.5b, with electron rich oxygen atom, the epoxy group on graphene is electron-donating which leads to high local π-electron density of the graphene. The electronic neutral carboxylic group on graphene (Figure 4.5c), also with electron rich oxygen atoms, is electron-withdrawing, which decreases the π-electron density of graphene. Ionized carboxyl-graphene shows negative potential (Figure 4.5d) with the highest negative potential locating at the oxygen atoms of carboxylic group (Figure 4.5d'). The cationic MB molecule is positively charged (Figure 4.5e), and its amine nitrogen is electron-withdrawing and decreases the π-electron density in the methyl groups (Figure 4.5e').

The configurations of an MB molecule adsorbed on different graphene surfaces are shown in Figure 4.6.[62] The distances between MB and different graphene surfaces, adsorption energy in vacuum ($E_{ad,\ vacuum}$) and adsorption energy in water ($E_{ad,\ water}$) are listed in Table 4-1. It can be observed that MB molecule forms an offset parallel stacking to the basal plane of graphene (Figure 4.6a), unionized (Figure 4.6c) and ionized carboxyl-graphene surfaces (Figure 4.6d) with vertical distances of ~3.8 Å (Table 4-1), and a T-shaped π stacking on epoxy-graphene with ~4.9 Å distance between the centers of rings, which agrees with literatures regarding the criteria for defining π- π interaction.[59-60, 63-64] The interaction between cationic MB with π system includes not only π- π interaction, but also cation- π interaction. The $E_{ad.\ vacuum}$ between cationic MB and different neutral graphene surfaces is in the range of -8.77 to -11.22 kcal/mol, which is reasonable according to previous reports on the $E_{ad.\ vacuum}$ between cationic aromatic molecule and neutral aromatic

molecule.[14] The $E_{ad,\ vacuum}$ between cationic MB and anionic deionized carboxyl-graphene is -62.24 kcal/mol, which is in the same order of the electrostatic interaction energy between organic dimmers as reported previously.[65] Table 4-1 shows that $E_{ad,\ water}$ is much weaker than $E_{ad,\ vacuum}$ between cationic MB and different graphene surfaces, which follows the same trend: E_{ad} of MB/graphene < E_{ad} of MB/unionized carboxyl-graphene < E_{ad} of MB/epoxy-graphene < E_{ad} of MB/ionize carboxyl-graphene. The possible reason for lower E_{ad} in water than in vacuum is that the cationic ionized MB molecule and anionic ionized carboxyl-graphene are surrounded by polar water molecules, thus their attractive interaction with their dimmers will be weakened.[59] As shown in Table 4-1, the affinity of MB to pristine graphene is the lowest and all the functional groups on graphene can further stabilize the stacking configuration in different degrees. For MB/unionized carboxyl-graphene, the π interactions of graphene with cationic MB are weakened by the decreased π electron density of graphene. In contrast, the electron rich oxygen on the carboxylic group can have polar interaction with cationic MB, thus the binding strength of MB/unionized carboxyl-graphene $E_{ad,\ water}$ = -0.07 kcal/mol is slightly higher than that of MB/graphene, suggesting the contribution of unionized carboxylic group to the interaction between MB and graphene is not significant. For MB/epoxy-graphene (Figure 4.6b), the electron rich epoxy group can attract electron deficient methyl groups of MB via polar interaction and its increased π-electron density enhances the π interaction with cationic MB.[66-67] The polar interaction might alter the configuration of MB molecule on epoxy-graphene surface from parallel π stacking to T-shaped π stacking. When the carboxylic group is unionized, MB/epoxy-graphene possesses the strongest binding strength with $E_{ad,\ water}$ of -0.96 kcal/mol which should dominate the GO-MB interaction. Thus, the main peaks in the bond dissociation histograms obtained in the SMF experiments at both pH 2 and 5.6 should be attributed to the interaction between TBO and the regions with epoxy

groups on GO, and the carboxylic group on the edge of GO has almost negligible contribution to the attraction between TBO molecule and the basal plane of GO. The E_{ad} between MB and ionized carboxyl-graphene is strongest among all the complexes, which is possibly due to the electrostatic attraction between the ionized positively charged MB and negatively charged carboxyl-graphene, and the enhanced π interactions between MB with low π electron density and graphene with high π-electron density. The computation results also support that the appearance of the second local maximum in histograms of bond dissociation forces for TBO-GO in the SMF measurements at pH 5.6 (Figure 4.4d) should be attributed to the dissociation between deionized TBO and carboxylic groups on GO, suggesting that the affinity of TBO to ionized carboxylic group is strong enough to attract TBO molecule to the vicinity of the carboxylic group on graphene edge. At pH 5.6, the DFT simulation results show that MB/epoxy-graphene possesses the second strongest binding strength, which further substantiates that the interaction between TBO and the regions with epoxy groups on GO attributes to the main peaks in bond dissociation histograms in the SMF experiments. The much higher counts for the primary maximum compared to that of the second maximum suggests that though the interaction between ionized carboxylic groups on GO and AOCs has the highest strength, the epoxy groups on GO dominate in enhancing the interactions between GO and AOCs, under both neutral and ionized conditions of carboxylic groups, due to their high content and relatively strong interaction with AOCs. The calculated $E_{ad,\ water}$ for MB/epoxy-graphene complex is in the same order of magnitude with bond dissociation energies ΔG (-4.57 kcal/mol) in SMFS results, and the lower value of calculated $E_{ad,\ water}$ is possibly because of the neglected thermal effects and treatment of correlation energy in function. Nevertheless, it should be noted that the trend of E_{ad} in DFT results fully support and interpretate the SMFS results.

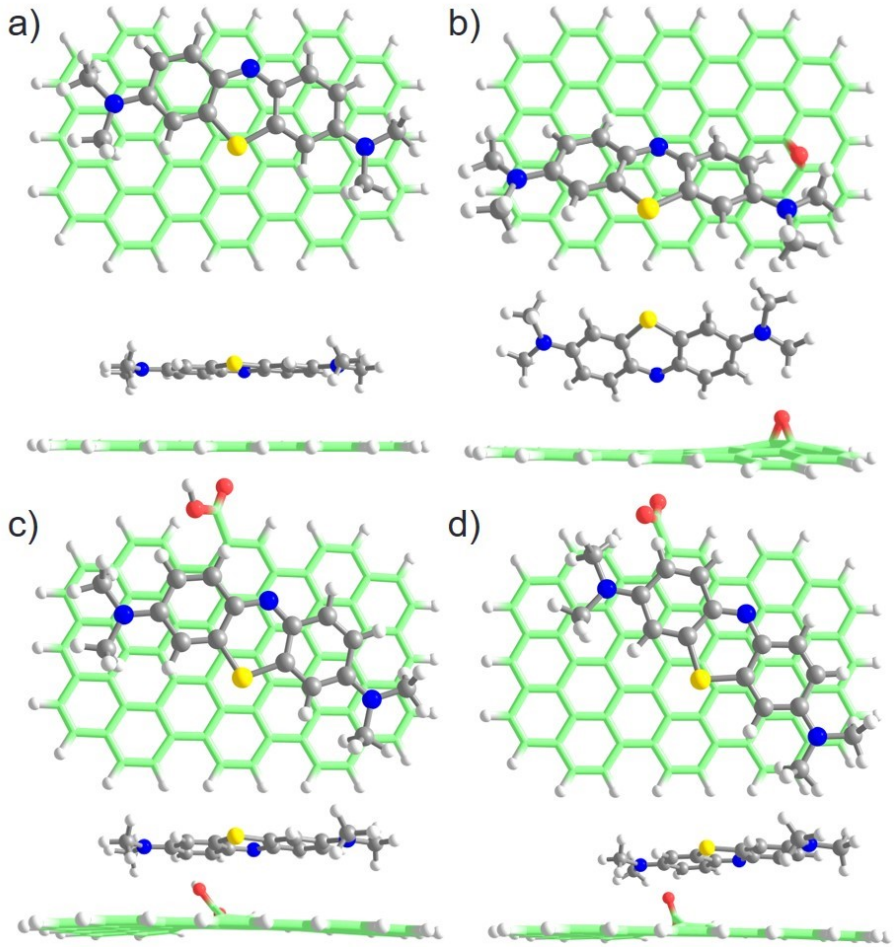

Figure 4.6 Optimized geometries of MB adsorbed on different graphene surfaces. (a) MB/graphene. (b) MB/epoxy-graphene. (c) MB/unionized carboxyl-graphene. (d) MB/ionized carboxyl-graphene. Grey: carbon; white: hydrogen; red: oxygen; blue: nitrogen and yellow: sulfur.

Table 4-1 E_{ad} of MB on different graphene surfaces.

Name	**Distance[a] (Å)**	$E_{ad.\ vacuum}$ **(kcal/mol)**	$E_{ad,\ water}$ **(kcal/mol)**
MB/graphene	3.9	-8.77	0.28
MB/epoxy-graphene	4.9	-11.22	-0.96
MB/unionized carboxyl-graphene	3.8	-9.13	-0.07
MB/ionized carboxyl-graphene	3.8	-62.24	-2.44

[a] *Vertical distance between parallel stacking dimer and distance between the centers of rings of the T-shaped stacking dimmer.*

4.5 Conclusions

In this work, SMFS and DFT calculations have been applied to systematically and quantitatively investigate the nanomechanical interaction mechanism of a model AOC molecule and GO surface. Electrostatic interaction and π- π interaction have been traditionally considered as the main driving interactions for the formation of AOCs/GO complexes. Interestingly, our results reveal that the role of electrostatic interaction between the negatively charged ionized carboxylic groups on GO and cationic AOC molecule has been overestimated, while the role of epoxy groups has been overlooked. It was found that most binding events in the formation of AOC/GO complex should be contributed to the presence of epoxy groups on GO due to their much higher content. The associated activation Gibbs energy for bond dissociation (ΔG) is determined as -4.61 kcal/mol and the bond dissociation distance from the equilibrium position (Δx) is 2.3 Å. The epoxy groups facilitate the adsorption of the AOCs on GO through polar interaction and enhanced π interactions. Our findings shed light on the design and development of novel GO based nanocomposites with tunable nanostructures and surface properties. For example, aromatic functional groups ended molecules (*e.g.*, double stranded DNA) can be possibly immobilized around the epoxy groups on GO, and the immobilization locations can be further manipulated by tuning the distribution of epoxy groups on GO as achieved by annealing treatment.[68] The methodology used in this work can be readily extended to the investigation of molecular interaction mechanisms of various GO based nanocomposites and their applications.

Supporting Information

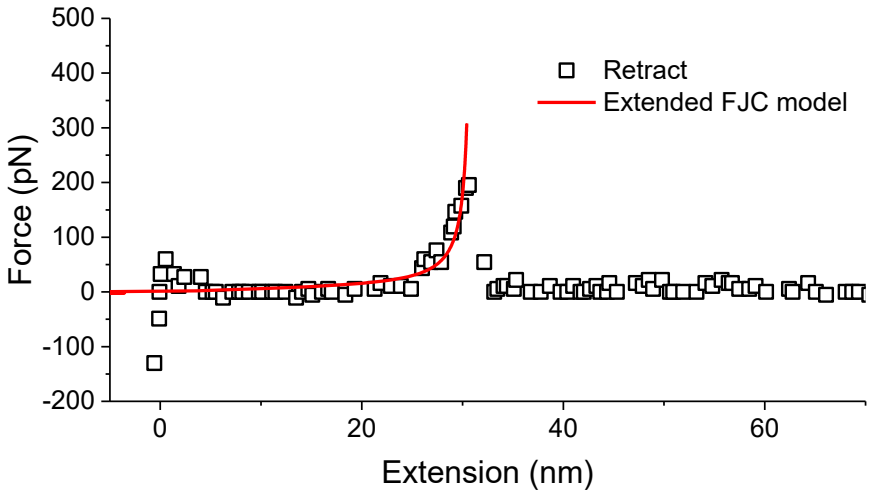

Figure S 4.1 A typical force-extension curve for the rupture between TBO and GO. The red corresponds to the fitting with extended freely-jointed chain (FJC) model.

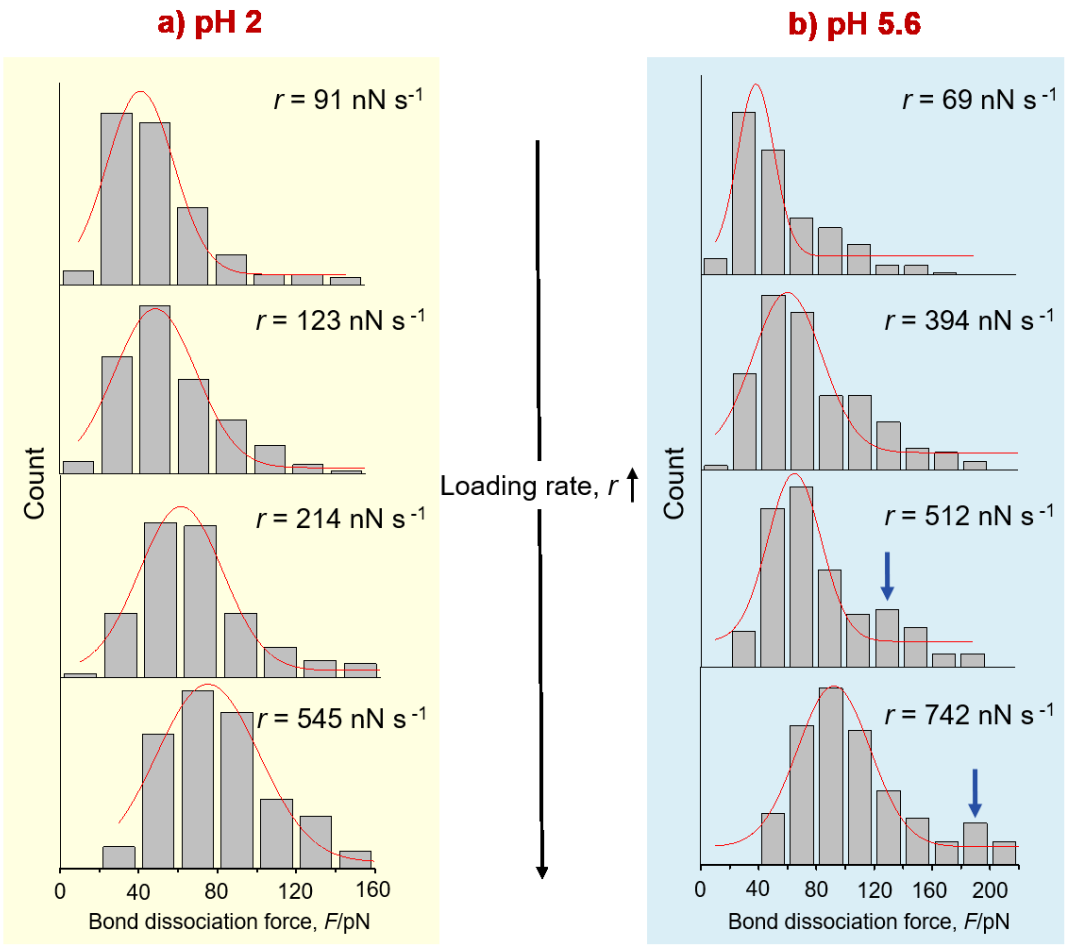

Figure S 4.2 Representatives histograms of bond dissociation force values for TBO-GO at increasing loading rates at **(a)** pH 2 and **(b)** pH 5.6 (red curve: Gaussian fitting to give the most probable bond dissociation force).

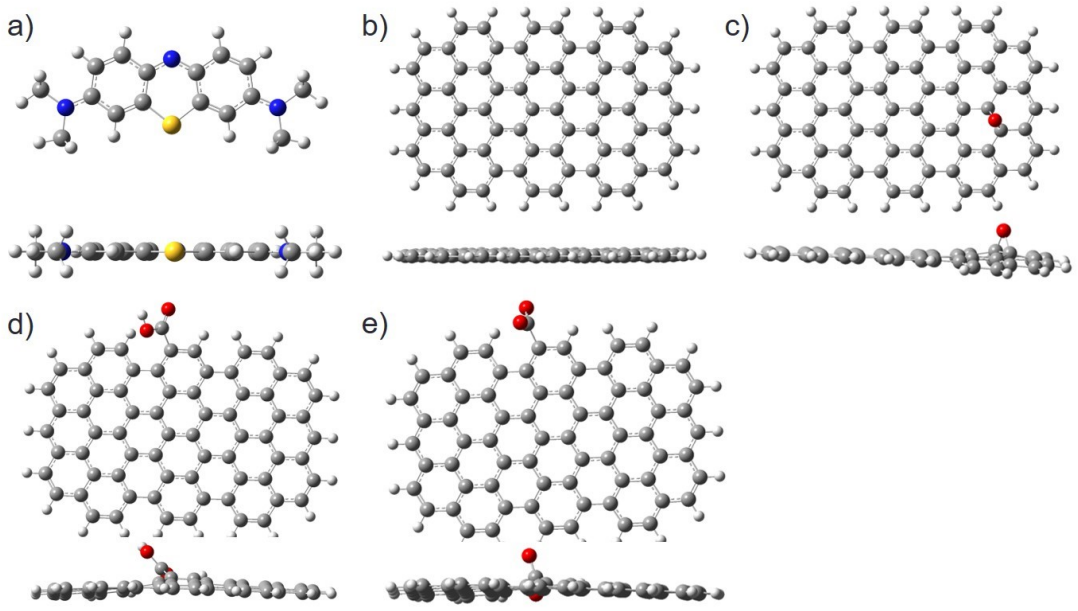

Figure S 4.3 Optimized geometries of **(a)** methylene blue, **(b)** graphene, **(c)** epoxy-graphene, **(d)** neutral (unionized) and **(e)** ionized carboxyl-graphene. Grey: carbon; white: hydrogen; red: oxygen; blue: nitrogen and yellow: sulfur.

Synthesis of Tip Modification Agents

CH_3-PEG_{1900}-TA: CH_3-PEG_{1900}-OH (1.9 g, 1 mmol), DCC (0.248 g, 1.2 mmol), and DMAP (1.2 mg, 0.01 mmol) were dissolved in 10 mL of DCM. The reaction mixture was protected by N_2 and cooled to 0°C in an ice bath. A solution of TA (0.206 g, 1 mmol) in 5 mL of DCM was added slowly. After kept in ice bath for 1 h, the reaction mixture was stirred at room temperature for 24 h. The reaction solution was filtered, and the organic layer was concentrated. The product was precipitated by the addition of ethyl ether into the resulting mixture. The precipitation was dissolved and precipitated again to obtain. The final product was achieved by vacuum desolvation.

HO-PEG_{4000}-TA: HO-PEG_{4000}-OH (4 g, 1 mmol), DCC (0.248 g, 1.2 mmol) and DMAP (1.2 mg, 0.01 mmol) were dissolved in 25 mL of DCM. The reaction mixture was protected by N_2

and cooled to 0ºC in an ice bath. A solution of TA (0.206 g, 1 mmol) in 5 mL of DCM was added slowly. After kept in ice bath for 1 h, the reaction mixture was stirred at room temperature for 24 h. The reaction solution was filtered, and the organic layer was concentrated. The product was precipitated by the addition of ethyl ether into the resulting mixture. The precipitation was dissolved and precipitated again to obtain. The final product was achieved by vacuum desolvation.

HOOC-PEG_{4000}-TA: HO-PEG_{4000}-TA (804 mg, 0.2 mmol), DMAP (2.5 mg, 0.02 mmol), and succinic anhydride (21 mg, 0.21 mmol) were dissolved in 15 mL of 1,4-dioxane and protected by N_2. The reaction mixture was stirred at room temperature for 48 h. The reaction solution was filtered, and the organic layer was concentrated. The product was precipitated by the addition of ethyl ether into the resulting mixture. The precipitation was dissolved in DCM and precipitated by ethyl ether to obtain. The final product was achieved by vacuum desolvation.

Dye-PEG_{4000}-TA: HOOC-PEG_{4000}-TA (92 mg, 0.02 mmol), TBO (8.3 mg, 0.02 mmol), DMAP (1 mg, 0.008 mmol) were dissolved in 50 mL of DCM and protected by N_2 and cooled to 0ºC in an ice bath. A solution of DCC (4.53 mg, 0.02 mmol) in 5 mL of DCM was added slowly. After kept in ice bath for 1 h, the reaction mixture was stirred at room temperature for 48 h. The reaction solution was filtered, and the organic layer was concentrated. The product was precipitated by the addition of ethyl ether into the resulting mixture. The precipitation was dissolved and precipitated again to be obtained. The final product was achieved by vacuum desolvation. Its successful synthesis was proved by the ^{1}H NMR spectrum (d_6-DMSO, 400 MHz, δ): 7.94-7.2 (5H, aromatic H), 4.51(4H, O=COC$\mathbf{H_2}$$CH_2$O), 4.08 (1H, SSC$\mathbf{H}$$(CH_2)_2$), 3.42-3.62 (~412H, PEG_{4000}), 3.39 (6H, NH(C$\mathbf{H_3}$)$_2$), 3.13 (2H, SSC$\mathbf{H_2}$$CH_2$), 2.91 (2H, OC=O$CH_2C\mathbf{H_2}$C=ON), 2.75 (2H, OC=OC$\mathbf{H_2}$$CH_2$C=ON), 2.30 (2H, SS$CH_2C\mathbf{H_2}$CH), 2.28 (2H, OC=OC$\mathbf{H_2}$$CH_2CH_2$), 2.24

(3H, phenyl-C**H$_3$**), 1.67 (2H, OC=OCH$_2$C**H$_2$**CH$_2$), 1.39 (2H, OC=OCH$_2$CH$_2$C**H$_2$**), 1.53 (2H, SSCHC**H$_2$**CH$_2$).

References

1. Yin, P. T.; Shah, S.; Chhowalla, M.; Lee, K.-B., Design, Synthesis, and Characterization of Graphene–Nanoparticle Hybrid Materials for Bioapplications. *Chem. Rev.* **2015,** *115*, 2483-2531.

2. Huang, W.; Wu, Y.; Qiu, L.; Dong, C.; Ding, J.; Li, D., Tuning Rheological Performance of Silica Concentrated Shear Thickening Fluid by Using Graphene Oxide. *Adv. Condens. Matter Phys.* **2015,** *2015*.

3. Li, D.; Müller, M. B.; Gilje, S.; Kaner, R. B.; Wallace, G. G., Processable Aqueous Dispersions of Graphene Nanosheets. *Nat. Nanotechnol.* **2008,** *3*, 101-105.

4. Li, P.; Wong, M.; Zhang, X.; Yao, H.; Ishige, R.; Takahara, A.; Miyamoto, M.; Nishimura, R.; Sue, H.-J., Tunable Lyotropic Photonic Liquid Crystal Based on Graphene Oxide. *ACS photonics* **2014,** *1*, 79-86.

5. Wan, S.; Li, Y.; Peng, J.; Hu, H.; Cheng, Q.; Jiang, L., Synergistic Toughening of Graphene Oxide–Molybdenum Disulfide–Thermoplastic Polyurethane Ternary Artificial Nacre. *ACS Nano* **2015,** *9*, 708-714.

6. Shi, Y.; Pramanik, A.; Tchounwou, C.; Pedraza, F.; Crouch, R. A.; Chavva, S. R.; Vangara, A.; Sinha, S. S.; Jones, S.; Sardar, D., Multifunctional Biocompatible Graphene Oxide Quantum Dots Decorated Magnetic Nanoplatform for Efficient Capture and Two-Photon Imaging of Rare Tumor Cells. *ACS Appl. Mater. Interfaces* **2015,** *7*, 10935-10943.

7. Zhang, M.; Zhao, Y.; Yan, L.; Peltier, R.; Hui, W.; Yao, X.; Cui, Y.; Chen, X.; Sun, H.; Wang, Z., Interfacial Engineering of Bimetallic Ag/Pt Nanoparticles on Reduced Graphene Oxide Matrix for Enhanced Antimicrobial Activity. *ACS Appl. Mater. Interfaces* **2016,** *8*, 8834-8840.

8. Shi, L.; Wang, Y.; Zhang, L.; Wang, P., Rational Design of a Bi-Layered Reduced Graphene Oxide Film on Polystyrene Foam for Solar-Driven Interfacial Water Evaporation. *J. Mater. Chem. A* **2017**.

9. Yang, X.; Zhang, X.; Ma, Y.; Huang, Y.; Wang, Y.; Chen, Y., Superparamagnetic Graphene Oxide–Fe 3 O 4 Nanoparticles Hybrid for Controlled Targeted Drug Carriers. *J. Mater. Chem.* **2009,** *19*, 2710-2714.

10. Koninti, R. K.; Sengupta, A.; Gavvala, K.; Ballav, N.; Hazra, P., Loading of an Anti-Cancer Drug onto Graphene Oxide and Subsequent Release to DNA/Rna: A Direct Optical Detection. *Nanoscale* **2014,** *6*, 2937-2944.

11. Yang, K.; Feng, L.; Liu, Z., The Advancing Uses of Nano-Graphene in Drug Delivery. *Expert Opin. Drug Deliv.* **2015,** *12*, 601-612.

12. Lu, C. H.; Yang, H. H.; Zhu, C. L.; Chen, X.; Chen, G. N., A Graphene Platform for Sensing Biomolecules. *Angew. Chem.* **2009,** *121*, 4879-4881.

13. Wang, Y.; Li, Z.; Hu, D.; Lin, C.-T.; Li, J.; Lin, Y., Aptamer/Graphene Oxide Nanocomplex for in Situ Molecular Probing in Living Cells. *J. Am. Chem. Soc.* **2010,** *132*, 9274-9276.

14. Georgakilas, V.; Tiwari, J. N.; Kemp, K. C.; Perman, J. A.; Bourlinos, A. B.; Kim, K. S.; Zboril, R., Noncovalent Functionalization of Graphene and Graphene Oxide for Energy Materials, Biosensing, Catalytic, and Biomedical Applications. *Chem. Rev.* **2016,** *116*, 5464-5519.

15. Wang, Y.; Li, Z.; Wang, J.; Li, J.; Lin, Y., Graphene and Graphene Oxide: Biofunctionalization and Applications in Biotechnology. *Trends Biotechnol.* **2011,** *29*, 205-212.

16. Lee, J.; Kim, J.; Kim, S.; Min, D. H., Biosensors Based on Graphene Oxide and Its Biomedical Application. *Adv. Drug Deliv. Rev.* **2016**.

17. Liu, J.; Liu, Z.; Barrow, C. J.; Yang, W., Molecularly Engineered Graphene Surfaces for Sensing Applications: A Review. *Anal. Chim. Acta* **2015,** *859*, 1-19.

18. Hummers Jr, W. S.; Offeman, R. E., Preparation of Graphitic Oxide. *J. Am. Chem. Soc.* **1958,** *80*, 1339-1339.

19. Yan, H.; Wu, H.; Li, K.; Wang, Y.; Tao, X.; Yang, H.; Li, A.; Cheng, R., Influence of the Surface Structure of Graphene Oxide on the Adsorption of Aromatic Organic Compounds from Water. *ACS Appl. Mater. Interfaces* **2015,** *7*, 6690-6697.

20. Compton, O. C.; Jain, B.; Dikin, D. A.; Abouimrane, A.; Amine, K.; Nguyen, S. T., Chemically Active Reduced Graphene Oxide with Tunable C/O Ratios. *ACS Nano* **2011,** *5*, 4380-4391.

21. Lerf, A.; He, H.; Forster, M.; Klinowski, J., Structure of Graphite Oxide Revisited. *J. Phys. Chem. B* **1998,** *102*, 4477-4482.

22. Szabó, T.; Berkesi, O.; Dékány, I., Drift Study of Deuterium-Exchanged Graphite Oxide. *Carbon* **2005,** *43*, 3186-3189.

23. Cai, W.; Piner, R. D.; Stadermann, F. J.; Park, S.; Shaibat, M. A.; Ishii, Y.; Yang, D.; Velamakanni, A.; An, S. J.; Stoller, M., Synthesis and Solid-State Nmr Structural Characterization of 13c-Labeled Graphite Oxide. *Science* **2008,** *321*, 1815-1817.

24. Szabó, T.; Berkesi, O.; Forgó, P.; Josepovits, K.; Sanakis, Y.; Petridis, D.; Dékány, I., Evolution of Surface Functional Groups in a Series of Progressively Oxidized Graphite Oxides. *Chem. Mater.* **2006,** *18*, 2740-2749.

25. Montes-Navajas, P.; Asenjo, N. G.; Santamaria, R.; Menendez, R.; Corma, A.; Garcia, H., Surface Area Measurement of Graphene Oxide in Aqueous Solutions. *Langmuir* **2013,** *29*, 13443-13448.

26. Haubner, K.; Murawski, J.; Olk, P.; Eng, L. M.; Ziegler, C.; Adolphi, B.; Jaehne, E., The Route to Functional Graphene Oxide. *Chemphyschem* **2010,** *11*, 2131-2139.

27. Ramesha, G.; Kumara, A. V.; Muralidhara, H.; Sampath, S., Graphene and Graphene Oxide as Effective Adsorbents toward Anionic and Cationic Dyes. *J. Colloid Interface Sci.* **2011,** *361*, 270-277.

28. Balapanuru, J.; Yang, J. X.; Xiao, S.; Bao, Q.; Jahan, M.; Polavarapu, L.; Wei, J.; Xu, Q. H.; Loh, K. P., A Graphene Oxide–Organic Dye Ionic Complex with DNA-Sensing and Optical-Limiting Properties. *Angew. Chem.* **2010,** *122*, 6699-6703.

29. Liu, X.; Leng, C.; Yu, L.; He, K.; Brown, L. J.; Chen, Z.; Cho, J.; Wang, D., Ion-Specific Oil Repellency of Polyelectrolyte Multilayers in Water: Molecular Insights into the Hydrophilicity of Charged Surfaces. *Angew. Chem.* **2015,** *127*, 4933-4938.

30. Chen, L.; Yang, J.; Zeng, X.; Zhang, L.; Yuan, W., Adsorption of Methylene Blue in Water by Reduced Graphene Oxide: Effect of Functional Groups. *Mater. Express* **2013,** *3*, 281-290.

31. Paek, S.-M.; Yoo, E.; Honma, I., Enhanced Cyclic Performance and Lithium Storage Capacity of Sno_2/Graphene Nanoporous Electrodes with Three-Dimensionally Delaminated Flexible Structure. *Nano lett.* **2009,** *9*, 72-75.

32. Hutter, J. L.; Bechhoefer, J., Calibration of Atomic-Force Microscope Tips. *Rev. Sci. Instrum.* **1993,** *64*, 1868-1873.

33. Lin, A.; Brunner, R.; Chen, P.; Talke, F.; Meyers, M., Underwater Adhesion of Abalone: The Role of Van Der Waals and Capillary Forces. *Acta Mater.* **2009,** *57*, 4178-4185.

34. Canto, M. I. F.; Setrakian, S.; Petras, R. E.; Blades, E.; Chak, A.; Sivak, M. V., Methylene Blue Selectively Stains Intestinal Metaplasia in Barrett's Esophagus. *Gastrointest. Endosc.* **1996,** *44*, 1-7.

35. Wainwright, M.; Crossley, K., Methylene Blue-a Therapeutic Dye for All Seasons? *J. Chemother.* **2002,** *14*, 431-443.

36. Schultz, E., Inactivation of Staphyloccus Bacteriophage by Methylene Blue. *Proc. Soc. Exp. Biol. Med.* **1928,** *26*, 100-101.

37. Chen, J. R.; Jiao, X. X.; Luo, H. Q.; Li, N. B., Probe-Label-Free Electrochemical Aptasensor Based on Methylene Blue-Anchored Graphene Oxide Amplification. *J. Mater. Chem. B* **2013,** *1*, 861-864.

38. Yang, S.-T.; Chen, S.; Chang, Y.; Cao, A.; Liu, Y.; Wang, H., Removal of Methylene Blue from Aqueous Solution by Graphene Oxide. *J. Colloid Interface Sci.* **2011,** *359*, 24-29.

39. Park, S.; Ruoff, R. S., Chemical Methods for the Production of Graphenes. *Nat. Nanotechnol.* **2009,** *4*, 217-224.

40. Stankovich, S.; Dikin, D. A.; Piner, R. D.; Kohlhaas, K. A.; Kleinhammes, A.; Jia, Y.; Wu, Y.; Nguyen, S. T.; Ruoff, R. S., Synthesis of Graphene-Based Nanosheets Via Chemical Reduction of Exfoliated Graphite Oxide. *Carbon* **2007,** *45*, 1558-1565.

41. Fu, Y.; Wang, J.; Liu, Q.; Zeng, H., Water-Dispersible Magnetic Nanoparticle–Graphene Oxide Composites for Selenium Removal. *Carbon* **2014,** *77*, 710-721.

42. Some, S.; Kim, Y.; Yoon, Y.; Yoo, H.; Lee, S.; Park, Y.; Lee, H., High-Quality Reduced Graphene Oxide by a Dual-Function Chemical Reduction and Healing Process. *Sci. Rep.* **2013,** *3*, 1929.

43. Fu, Y. Water-Dispersible Magnetic Particle-Graphene Oxide Composites: Synthesis, Characterization and Application in the Removal of Selenium. University of Alberta, 2014.

44. Konkena, B.; Vasudevan, S., Understanding Aqueous Dispersibility of Graphene Oxide and Reduced Graphene Oxide through Pka Measurements. *J. Phys. Chem. Lett.* **2012,** *3*, 867-872.

45. Zhang, Y.; Liu, C.; Shi, W.; Wang, Z.; Dai, L.; Zhang, X., Direct Measurements of the Interaction between Pyrene and Graphite in Aqueous Media by Single Molecule Force Spectroscopy: Understanding the Π-Π Interactions. *Langmuir* **2007,** *23*, 7911-7915.

46. Lee, H.; Scherer, N. F.; Messersmith, P. B., Single-Molecule Mechanics of Mussel Adhesion. *Proc. Natl. Acad. Sci. U. S. A.* **2006,** *103*, 12999-13003.

47. Stock, P.; Monroe, J. I.; Utzig, T.; Smith, D. J.; Shell, M. S.; Valtiner, M., Unraveling Hydrophobic Interactions at the Molecular Scale Using Force Spectroscopy and Molecular Dynamics Simulations. *ACS Nano* **2017,** *11*, 2586-2597.

48. Hinterdorfer, P.; Dufrêne, Y. F., Detection and Localization of Single Molecular Recognition Events Using Atomic Force Microscopy. *Nat. Methods* **2006,** *3*, 347-355.

49. Zhang, Y.; Liu, C.; Shi, W.; Wang, Z.; Dai, L.; Zhang, X., Direct Measurements of the Interaction between Pyrene and Graphite in Aqueous Media by Single Molecule Force Spectroscopy: Understanding the Π− Π Interactions. *Langmuir* **2007,** *23*, 7911-7915.

50. Zhang, W.; Zhang, X., Single Molecule Mechanochemistry of Macromolecules. *Prog. Polym. Sci.* **2003,** *28*, 1271-1295.

51. Bell, G. I., Models for the Specific Adhesion of Cells to Cells. *Science* **1978,** *200*, 618-627.

52. Evans, E.; Ritchie, K., Strength of a Weak Bond Connecting Flexible Polymer Chains. *Biophys. J.* **1999,** *76*, 2439-2447.

53. Li, Y.; Qin, M.; Li, Y.; Cao, Y.; Wang, W., Single Molecule Evidence for the Adaptive Binding of Dopa to Different Wet Surfaces. *Langmuir* **2014,** *30*, 4358-4366.

54. Das, P.; Reches, M., Revealing the Role of Catechol Moieties in the Interactions between Peptides and Inorganic Surfaces. *Nanoscale* **2016,** *8*, 15309-15316.

55. Frisch, M.; Trucks, G.; Schlegel, H.; Scuseria, G.; Robb, M.; Cheeseman, J.; Scalmani, G.; Barone, V.; Mennucci, B.; Petersson, G.; et al., Gaussian 09, Revision D. 01*, Gaussian Inc., Wallingford CT* **2016**.

56. Taylor, W. H., The Crystal Structure of Methylene Blue. *J. Chem. Technol. Biotechnol.* **1935**, 732-734.

57. Kong, X.; Chen, Q., The Positive Influence of Boron-Doped Graphene with Pyridine as a Probe Molecule on Sers: A Density Functional Theory Study. *J. Mater. Chem.* **2012,** *22*, 15336.

58. Balamurugan, K.; Subramanian, V., Adsorption of Chlorobenzene onto (5,5) Armchair Single-Walled Carbon Nanotube and Graphene Sheet: Toxicity Versus Adsorption Strength. *J. Phys. Chem. C* **2013,** *117*, 21217-21227.

59. Janiak, C., A Critical Account on Π–Π Stacking in Metal Complexes with Aromatic Nitrogen-Containing Ligands. *J. Chem. Soc., Dalton Trans.* **2000**, 3885-3896.

60. Martinez, C. R.; Iverson, B. L., Rethinking the Term "Pi-Stacking". *Chem. Sci.* **2012,** *3*, 2191.

61. Higaki, Y.; Kiyoshima, Y.; Suzuki, K.; Kabayama, H.; Ohta, N.; Seo, Y.; Takahara, A., Elastomers Built up through the Π–Π Stacking Association of Polycyclic Planar Aromatic Diimides. *RSC Adv.* **2017,** *7*, 46195-46200.

62. ChemCraft program: http://www.chemcraftprog.com.

63. McGaughey, G. B.; Gagné, M.; Rappé, A. K., Π-Stacking Interactions Alive and Well in Proteins. *J. Biol. Chem.* **1998,** *273*, 15458-15463.

64. Ringer, A. L.; Sinnokrot, M. O.; Lively, R. P.; Sherrill, C. D., The Effect of Multiple Substituents on Sandwich and T-Shaped Π–Π Interactions. *Chem.-Eur. J.* **2006,** *12*, 3821-3828.

65. Volkov, A.; Coppens, P., Calculation of Electrostatic Interaction Energies in Molecular Dimers from Atomic Multipole Moments Obtained by Different Methods of Electron Density Partitioning. *J. Comput. Chem.* **2004,** *25*, 921-934.

66. Mecozzi, S.; West, A. P.; Dougherty, D. A., Cation-Pi Interactions in Aromatics of Biological and Medicinal Interest: Electrostatic Potential Surfaces as a Useful Qualitative Guide. *Proc. Natl. Acad. Sci. U. S. A.* **1996,** *93*, 10566-10571.

67. Hawker, C. J.; Fréchet, J. M., Monodispersed Dendritic Polyesters with Removable Chain Ends: A Versatile Approach to Globular Macromolecules with Chemically Reversible Polarities. *J. Chem. Soc., Perkin Trans. 1* **1992**, 2459-2469.

68. Bardhan, N. M.; Kumar, P. V.; Li, Z.; Ploegh, H. L.; Grossman, J. C.; Belcher, A. M.; Chen, G.-Y., Enhanced Cell Capture on Functionalized Graphene Oxide Nanosheets through Oxygen Clustering. *ACS Nano* **2017**.

Chapter 5 Regenerable Functionalized Sponge Composite Materials for Removal of Water from Oil

5.1 Introduction

Zwitterions widely exist in living creatures and in nature, including cell membranes,[1] peptides,[2] proteins[3] and osmolytes.[4] The cell's nonfouling nature is believed to be contributed by the zwitterionic headgroups of phospholipids, which are the main component of external face of the mammalian cell.[5] As an ubiquitous class of materials, zwitterion materials integrate both positive and negative ionic groups and remain charge neutral,[6-7] which can superiorly bind water molecules and prevent fouling adhesion by hydration introduced by electrostatic interaction, compared to other hydrophilic materials achieving hydration via hydrogen bonding, such as poly(ethylene glycol) (PEG), dextran and tetraglyme.[8-9] Zwitterionic polyelectrolytes, as a polymer form of zwitterions with strong hydration strength and long chain that weakens the attraction between substrates and fouling, have been widely applied in surface modification to achieve various functionalities, such as nonfouling,[10-11] lubrication,[12] underwater superoleophobicity[13] and oil/water separation.[14] In the application of oil/water separation, zwitterionic polymers, as well as other hydrophilic polymer with hydration ability, have been coated on various substrates or directly fabricated as devices to filtrate the oil/water mixture and high separation efficiency has been achieved due to their decent oil resistant performance when being hydrated. The oil filtrated from water includes a large family of light oils, such as hexadecane, ether, toluene, hexane, soybean oil and even light crude oil.[13-16]

Global demands for crude oil steadily increase over the last quarter of the 20th century, and with declining production of middle and light oil, the production of heavy oil is rising and will

become more and more important.[17-18] Handling and transport of heavy oil is widely recognized as a challenging topic due to its heavy fractions (asphaltenes) and formed water residues during extraction.[19] Asphaltenes are the heaviest components of crude oil with aromatic structures and heteroatoms, that tend to aggregate, precipitate and adsorb on the surface of reservoirs and pipelines, resulting difficulties for transportation and petroleum recovery.[20-23] Besides, the existence of asphaltenes in heavy oil can stabilize the water-in-oil emulsions, and the water residues can lead to corrosion of appliances and impair the production of refined petroleum. Thus, innovative approaches and technologies are required to clean asphaltenes contaminated surface and remove water from heavy oil in petroleum industry. Using hydrated surfaces, as in previous studies for the case of light oils, to resist the heavy oil adhesion is not practical because the involved water would lead to appliance corrosion and refining difficulties. Therefore, it will be of great interest and importance to develop a surface that after contacted with heavy oil in dry state and the oil contaminants can still be cleaned by water with good regenerability, which has not been accomplished before to our best knowledge. The displacement of oil by water on the solid interface requires the solid surfaces exhibiting a strong affinity toward water. Very recently, an unexpected and superior long-range attraction has been observed between zwitterionic polyelectrolyte surfaces and water droplet in oil compared with other kinds of single-charged polyelectrolytes (cationic and anionic) by our group. The attraction is supposed due to the strong dipole interaction introduced by the large dipole moment of the polyzwitterion. [24] Herein, in this work, it is found that the zwitterionic poly(3-[dimethyl(2-methacryloyloxyethyl) ammonium] propanesulfonate) (PMAPS) coating on polydopamine (PDA) modified silicon wafer surface shows outstanding underwater self-cleaning property and recyclability after heavy oil contamination (using asphaltenes solution as a model heavy oil) under its dry state compared with cationic poly(2-(methacryloyloxy)ethyl

trimethylammonium chloride) (PMTAC) and anionic poly(3-sulfopropyl acrylate potassium) (PSPAK) polyelectrolytes, which implies its promising application for self-cleaning coating on various instruments, including reservoirs, pipelines and other handling appliances.

The anti-fouling property and affinity to water of the zwitterionic coating also inspires its application in the removal of water in heavy oil. Recently, two-dimensional (2D) filtration membranes, including steel meshes[25] and fabrics,[26] have attracted great attentions, because they can continuously and effectively separate oil/water mixtures. Unfortunately, asphaltenes in heavy oil tend to precipitate and could easily clog the membranes, reducing their performance in permeation flux and separation efficiency. Therefore, research efforts for facile, low-cost and efficient materials that can remove water from heavy oil are significantly desired. Herein, zwitterionic PMAPS has been grafted on PDA modified polyurethane (PU) sponge to adsorb water from model heavy oil (asphaltene toluene solution) with high separation efficiency for the first time to our best knowledge. After removing the water from oil, the sponge is taken out, washed by water and ready for reuse, which is a promising technology for the application of water removal from heavy oil.

5.2 Experiments and materials

5.2.1 Materials

3-[dimethyl(2-methacryloyloxyethyl)ammonium] propanesulfonate (MAPS), 2-(methacryloyloxy)ethyl trimethylammonium chloride (MTAC), dopamine hydrochloride, tris(hydroxymethyl)aminomethane, and 3-sulfopropyl acrylate potassium (SPAK) were purchased from Sigma Aldrich. 4,4'- azobis(4-cyanopentanoic acid) (V501) was obtained from Aldrich. The polyurethane (PU) sponge is commercial available. Sodium borohydride was purchase from Alfa Aesar. PMAPS, PMTAC and PSPAK polyelectrolytes were synthesized by RAFT polymerization

method (mole ratio of monomer to 4-cyanopentanoic acid dithiobenzoate (RAFT agent) equals to 50:1).[24]

5.2.2 Preparation of PDA coated silicon wafer substrates and sponges

Before coating, silicon wafer substrates were rinsed by ethanol and Milli-Q water repeatedly, dried by nitrogen gas and cleaned by UV-ozone for 15 min. PDA coated silicon wafer substrates were prepared by immersing silicon wafer substrates in dopamine solution (2 mg mL^{-1}, pH 8.5 tris buffer) under magnetic stirring for 24 h. After coating, the silicon wafer substrates were taken out from the solution, rinsed by Milli-Q water and dried by nitrogen gas.

The PU sponges were cut into blocks with mass of 25 mg and cleaned by Milli-Q water and ethanol repeatedly. And then three pieces of PU sponges were immersed in dopamine solution (2 mg mL^{-1}, pH 8.5 tris buffer) for 24 h under magnetic stirring. Then the PDA coated sponges were removed from the solution, washed by Milli-Q water and dried by lyophilization.

5.2.3 Synthesis of polyelectrolytes-grafted PDA coated silicon wafer substrates and sponges

30 mg of different polyelectrolytes (PMAPS, PMTAC and PSPAK) were dissolved into 15 mL pH 8.5 tris buffer. Then, reducing agent $NaBH_4$ was added into the previous solution and the mixture was stirred for 1 hr. After that, 5 pieces of PDA coated silicon wafer substrates were put into the solution under stirring for 24 h.

Different polyelectrolytes (PMAPS, PMTAC and PSPAK, 120 mg) were dissolved into 40 mL of tris buffer (pH 8.5), to which $NaBH_4$ was added. The stirring was kept for 1 hr. After that, 3 pieces of PDA coated sponges were put into the solution with stirring for 24 h.

5.2.4 Characterization

Atomic force microscope (AFM) images of the silicon wafer substrates were obtained using a Dimension Icon AFM (Bruker, Santa Barbara, CA) by tapping mode. A scanning electronic

microscopy (SEM, Tescan Vega-3, Czech Republic) was used to characterize the topography of the substrates. X-ray photoelectron spectroscopy (XPS) measurements were employed to characterize the chemical composition using a spectrometer (Kratos Axis Ultra, NY) with Al Kα radiation (12 mA, 14 kV). Water contents of oil/water mixture was measured by a Karl Fischer titrator (Mettler Toledo, OH).

5.2.5 Anti-asphaltenes performance study of polyelectrolytes PDA coated silicon wafer surfaces

For recyclable test, in each cycle, dry silicon wafer surfaces, PDA coated silicon wafer surfaces, and different polyelectrolytes-PDA coated silicon wafer surfaces were immersed in 1000 ppm asphaltene toluene solution for 1 h. After that, the surfaces were taken out and washed by Milli-Q water for underwater oil contact angle measurement. Then, the surfaces were dried by nitrogen gas for next cycle.

To study the pH effect of water, dry silicon wafer surfaces, PDA-coated surfaces, and different polyelectrolytes PDA-coated silicon wafer surfaces were immersed in 1000 ppm asphaltene toluene solution for 24 h, taken out and washed by water (pH 2, 5.6 and 11). Then the underwater oil contact angle on different surfaces were obtained.

5.2.6 Water removal performance in asphaltene toluene solution

0.7 mL Milli-Q water was added into 10 mL 500 ppm asphaltene toluene solution and shaken for 30 s to form a water-in-oil (W/O) emulsion solution. Then the pre-wetted different polyelectrolytes modified PDA coated sponges were put into the W/O emulsion solution and shaken. Then the sponge was manipulated by tweezer to access the water droplet in the edge of container. The sponge was then taken out and washed in water for recycling tests.

5.3 Results and discussion

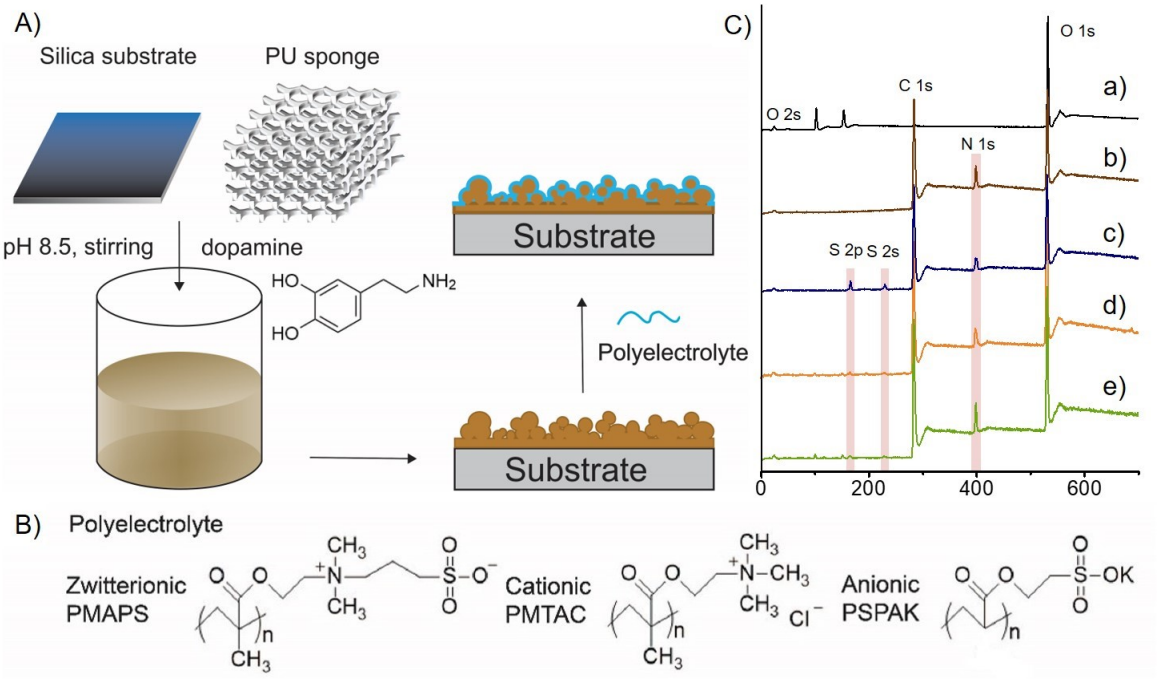

Figure 5.1 (A) Schematic illustration for the fabrication of polyelectrolyte-polydopamine (PDA) coating on silicon wafer and sponge substrates. **(B)** Chemical structures of polyelectrolytes: poly(3-[dimethyl(2-methacryloyloxy)ethyl ammonium] propanesulfonate) (PMAPS), poly(2-(methacryloyloxy)ethyl trimethylammonium chloride) (PMTAC) and poly(3-sulfopropyl acrylate potassium) (PSPAK). **(C)** XPS spectra of (a) blank, (b) PDA, (c) PMAPS-PDA, (d) PMTAC-PDA and (e) PSPAK-PDA coated silicon wafer surfaces.

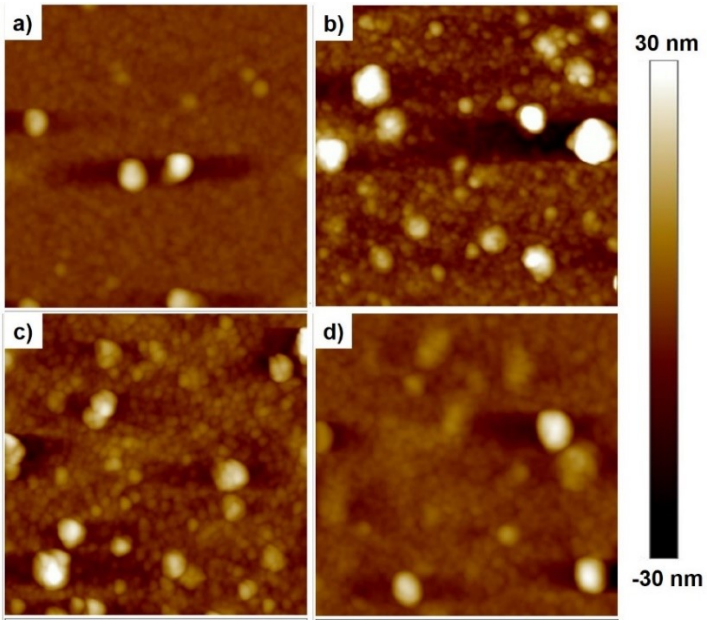

Figure 5.2 Atomic force microscopy (AFM) topographic images (1×1 μm^2) of a) PDA, b) PMAPS-PDA, c) PMTAC-PDA and d) PSPAK-PDA coated silicon wafer surfaces.

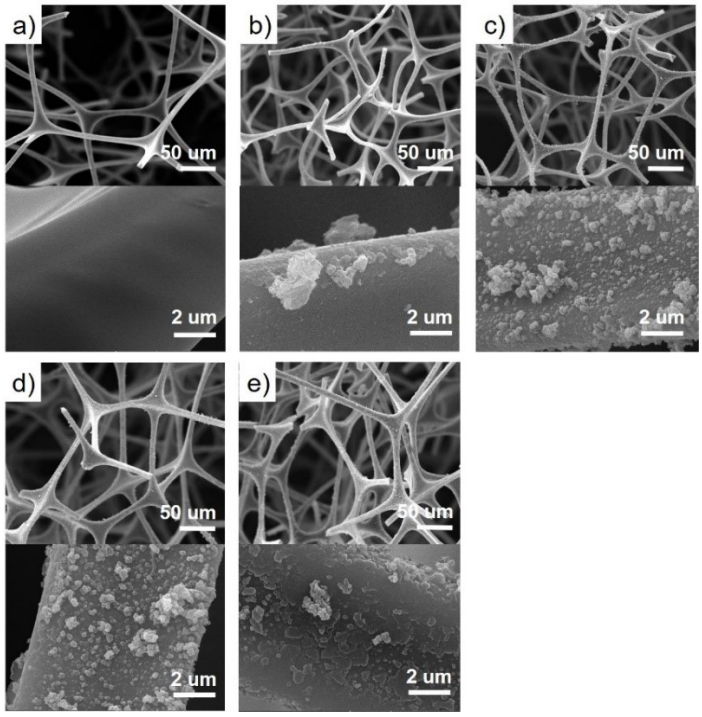

Figure 5.3 Scanning electronic microscopy (SEM) images of a) PDA, b) PMAPS-PDA, c) PMTAC-PDA and d) PSPAK-PDA coated polyurethane (PU) sponges.

Zwitterionic PMAPS, cationic PMTAC and anionic PSPAK polyelectrolyte-PDA coatings have been fabricated by a facile method. As shown in Figure 5.1A, to achieve substrate-independent surface modification, PDA has been coated on the substrates (silicon wafer surfaces and PU sponges) first, of which the catechol derivatives can deposit on various organic and inorganic substrates via covalent and non-covalent interactions.[27-29] Then, zwitterionic PMAPS, cationic PMTAC and anionic PSPAK polyelectrolytes are grafted to the PDA coated substrates. The chemical structures of zwitterionic PMAPS, cationic PMTAC and anionic PSPAK polyelectrolytes are shown in Figure 5.1B. The elemental compositions of PDA and polyelectrolytes-PDA coatings have been characterized by X-ray photoelectron spectroscopy (XPS) and the spectra are shown in Figure 1C. Successful deposition of PDA is confirmed by the appearance of N 1s peak at 398.4 eV, which is absent in pure silicon wafer surface. After the grafting of polyelectrolytes, two signal peaks of S 2p and S 2s at 166.0 eV and 229.6 eV appear due to the sulfur containing end groups of polyelectrolytes. Atomic force microscopy (AFM) topographic images PDA, PMAPS-PDA, PMTAC-PDA and PSPAK-PDA coated silicon wafer surfaces, and scanning electronic microscopy (SEM) images of PU sponges with PDA, PMAPS-PDA, PMTAC-PDA and PSPAK-PDA coatings are shown in Figure 5.2 and Figure 5.3, responsively. It can be observed that PDA aggregates appear on the surface of coatings with high coverage, and there are no obvious changes after the further modification of polyelectrolytes.

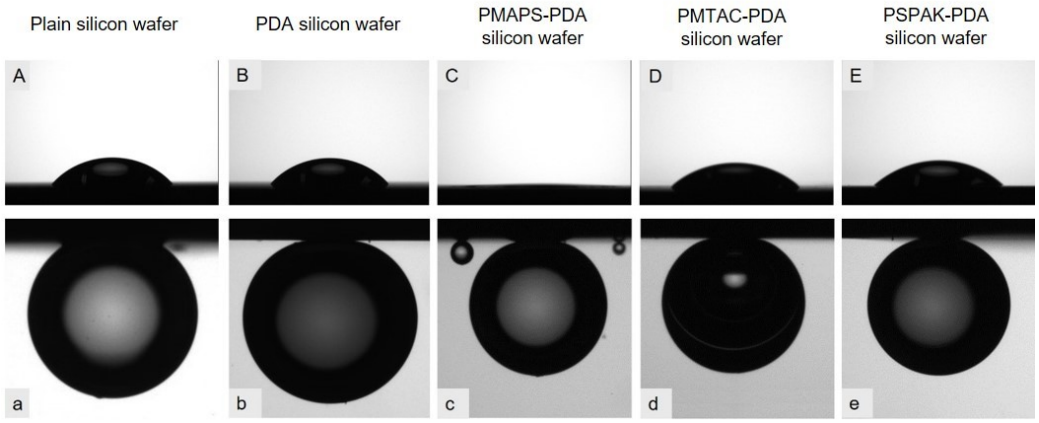

Figure 5.4 Water contact angle in oil (WCA-A **(A-E)** and oil contact angle in water (OCA-W) **(a-e)** on different silicon wafer surfaces.

The water contact angles in air (WCA-A) and oil contact angles in water (OCA-W) of different silicon wafer substrates are shown in Figure 5.4. The oil phase is 1000 ppm asphaltene toluene solution. The PDA coated silicon wafer substrate is hydrophilic with WCA-A of 45.7° ± 1.1°, which is consisted with previous reports.[28, 30] After the grafting of polyelectrolytes, only zwitterionic PMAPS-PDA coated silicon wafer substrate shows superhydrophilicity with WCA-A < 5°, while cationic PMTAC and anionic PSPAK-PDA coated silicon wafer substrates show hydrophilicity with WCA-A ~ 40°, which indicates that PMAPS-PDA coated silicon wafer substrate is more hydrophilic in air compared with PMTAC-PDA and PSPAK-PDA coated silicon wafer substrates. With the grafting of the three kinds of polyelectrolytes on the PDA coated silicon wafer substrates, all substrates show underwater superoleophobicity, which is possibly due to the hydrated water introduced by the ionic groups of polyelectrolytes that prevent the oil fouling.

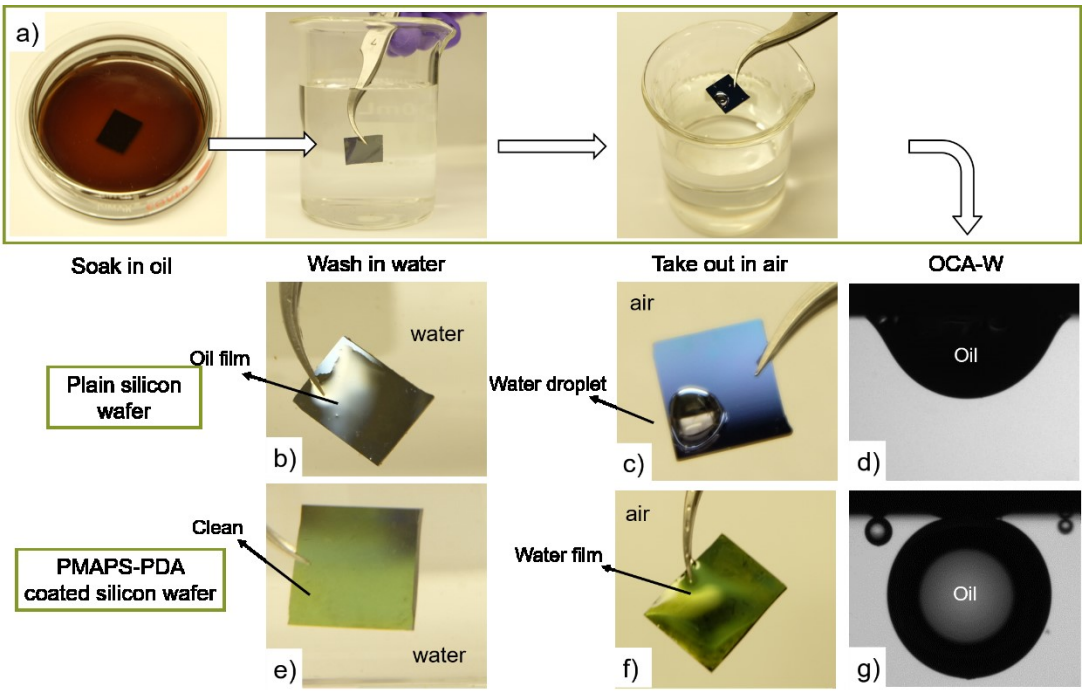

Figure 5.5 (a) A series of photos to illustrate the process to clean different asphaltenes contaminated substrates (plain silicon wafer, PDA, PMAPS-PDA, PMTAC-PDA and PSPAK-PDA coated silicon wafer substrates). The substrates are first soaked in asphaltene toluene solution under dry state, then washed in water and taken out in air. When being washed in water, **(b)** the oil film stays on the surface of plain silicon wafer, while **(e)** the oil on the PMAPS-PDA coated silicon wafer surface leaves and there is no oil can be observed. When the substrates are taken out from water, **(c)** the attached water on plain silicon wafer substrate shrinks into a single water droplet, **(f)** while the water stays as film on PSPAK-PDA coated silicon wafer substrate. The OCA-W on **(d)** plain silicon wafer and **(g)** PMAPS-PDA coated silicon wafer surface after first time cleaning.

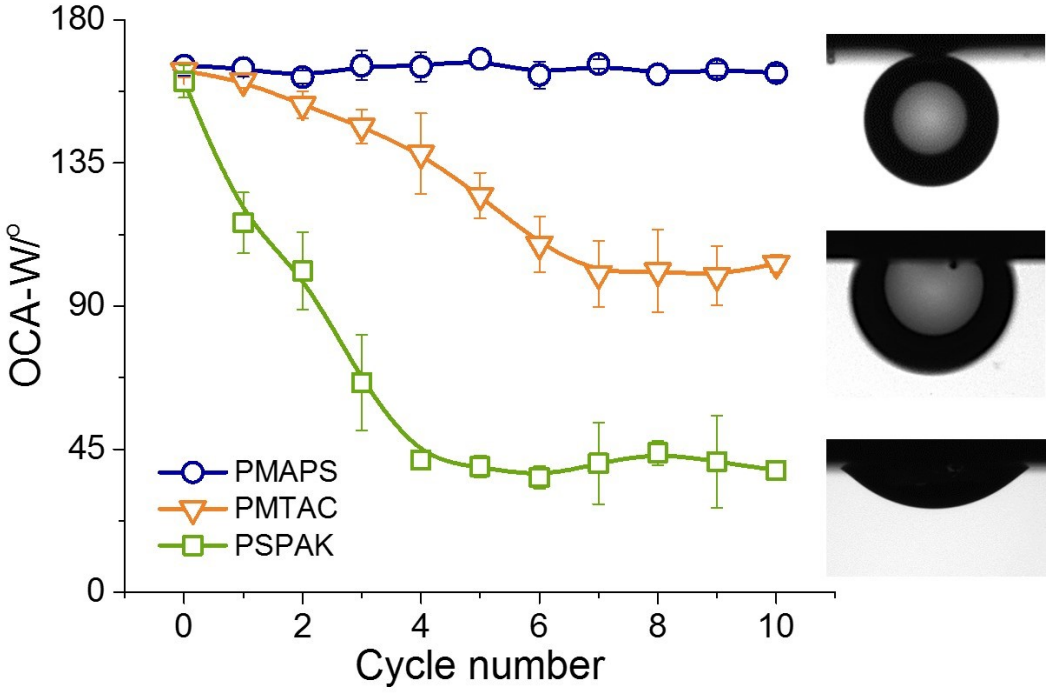

Figure 5.6 OCA-W on zwitterionic PMAPS, cationic PMTAC and anionic PSPAK-PDA coated silicon wafer substrates after being soaked in 1000 ppm asphaltene toluene solution under dry state and washed by water over ten cycles.

As the major source of pipeline fouling, asphaltenes in heavy oil are a class of aromatic and polar macromolecules that can aggregate and adsorb onto a wide range of solid surfaces.[31-34] Thus the surface fouled by heavy oil requires to have strong attraction for water that the water molecules can penetrate and displace the adsorbed heavy oil film to achieve self-cleaning. To assess the self-cleaning ability, anti-fouling ability after cleaning by water and recyclability of the as-prepared surfaces, as shown in Figure 5.5a, the OCA-W were measured after the nitrogen-dried substrates been soaked in asphaltene toluene solution (1000 ppm) for one hour and washed in water, repeatedly. It can be observed that after been soaked in asphaltene toluene solution for the

first time, when the oil contaminated silicon wafer surface is washed in water (Figure 5.5b), the oil film remains stable on the silicon wafer surface, resulting reduced hydrophilicity in air (Figure 5.5c) and underwater oleophobicity (Figure 5.5d). In contrast, when the zwitterionic PMAPS-PDA surface is washed in water (Figure 5.5e), the oil quickly releases from the surface with no oil residues on the surface that can be observed (Figure 5.5f) and the surface still show superoleophobicity (Figure 5.5g). After ten times recycle, it is found that the underwater oleophobicity of both cationic PMTAC and anionic PSPAK-PDA surfaces decrease gradually, while zwitterionic PMAPS-PDA surface remains remarkable superoleophobicity. The reduced oleophobicity may be due to the gradual oil fouling of cationic PMTAC and anionic PSPAK-PDA surfaces resulted from the failing of self-cleaning by water, which is in accordance with previous report that zwitterions can bind water molecules superiorly via ion-dipole interaction than single-charged groups[4, 35] and the long-range attraction between zwitterionic polyelectrolytes and water in oil is stronger than that between single-charged polyelectrolytes and water in oil.[24]

For industrial application, the polyelectrolyte coatings need to maintain their self-cleaning and anti-heavy oil property in environment with wide pH range. However, asphaltenes in heavy oil contain hydroxyl groups (-SOH) and carboxylic groups, thus asphaltenes at oil/water interface would carry different charges under various pH.[36] Asphaltenes at oil/water interface with variable charging properties might change their interactions with the coating surfaces and impair their self-cleaning and anti-fouling property under certain pH condition. Herein, the self-cleaning and anti-fouling property of zwitterionic PMAPS, cationic PMTAC and anionic PSPAK-PDA surfaces is characterized under acidic, neutral and alkaline pH. It can be observed in Figure 5.7a that under pH 2, 5.6 and 11, zwitterionic PMAPS, cationic PMTAC and anionic PSPAK-PDA substrates all show underwater superoleophobicity. However, after being soaked in 1000 ppm asphaltene

toluene solution for 24 h under dry state and washed by water with different pH, only zwitterionic PMAPS-PDA silicon wafer substrates show superoleophobic property at all pH values, while both cationic PMTAC and anionic PSPAK-PDA substrates lose superoleophobicity at certain pH values (Figure 5.7b). This might be due to the high hydration strength of zwitterionic polyelectrolytes under wide pH range that water molecules can clean and replace the oil foulings on the surface, which lead to the recovered superoleophobicity, while the hydration strength of cationic PMTAC and anionic PMTAC polyelectrolytes is impaired at some certain pH due to their single-charged groups.

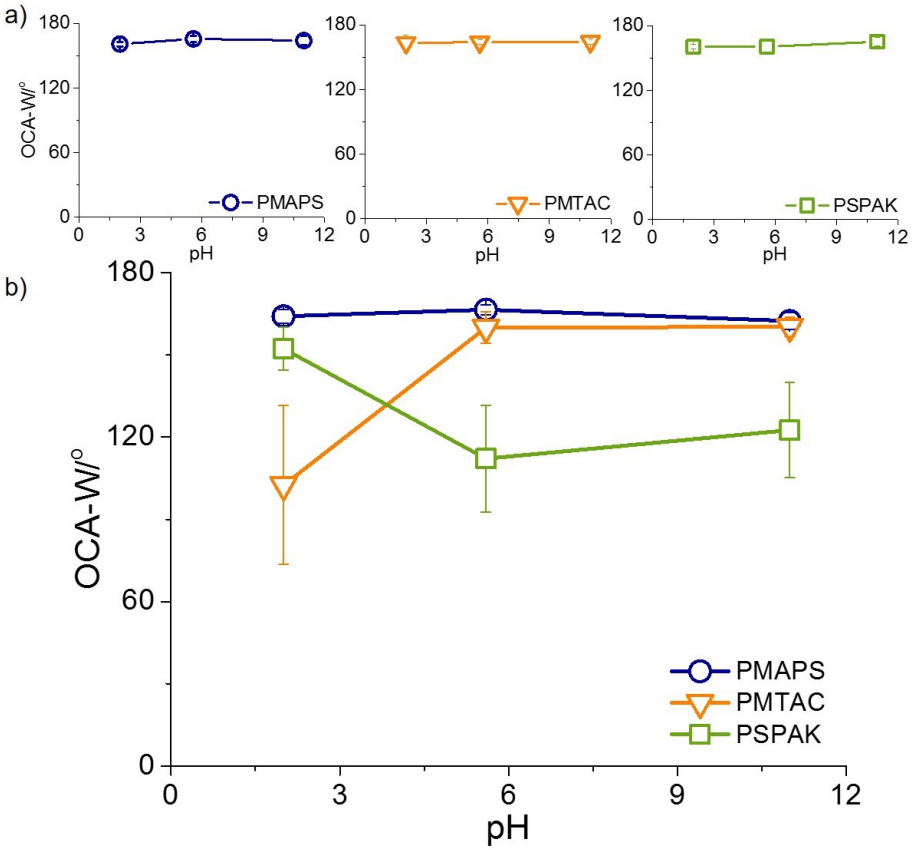

Figure 5.7 OCA-W values taken for zwitterionic PMAPS, cationic PMTAC and anionic PSPAK-PDA coated silicon wafer substrates **(a)** before and **(b)** after being soaked in 1000 ppm asphaltene toluene solution under dry state and washed by water (pH=2, 5.6 and 11).

In practical industry, the removal of water from heavy oil is highly required, however, asphaltenes components incline to precipitate and may clog the membrane, which limits the application of membranes in heavy oil/water separation. In this work, zwitterionic PMAPS, cationic PMTAC and anionic PSPAK-PDA coated sponges are fabricated and applied to remove water from asphaltene toluene solution. In a typical illustrative experiment, the PMAPS-PDA coated sponge is added to the W/O emulsion solution to adsorb water, and then the sponge is taken out and washed in water for recycling (Figure 5.8). Figure 5.9 shows the recycling performance of the three kinds of polyelectrolytes-PDA coated sponges in the removal of water from oil, it can be observed that during 10 cycles of usage, the removal percentages of water by cationic PMTAC and anionic PSPAK grafted PDA sponges gradually decrease, while the percentages of water removed by zwitterionic PMAPS sponge maintains higher than 90%.

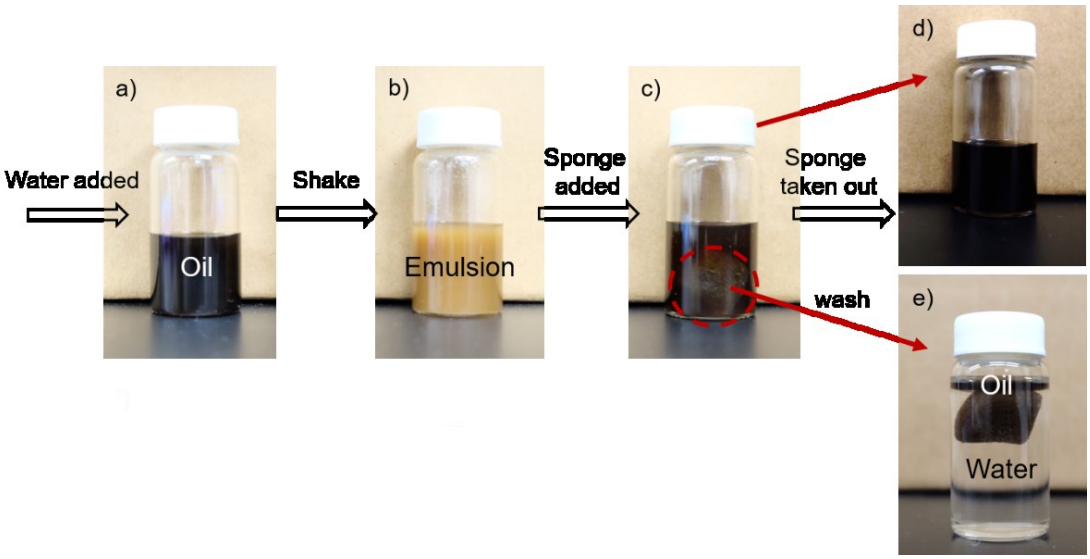

Figure 5.8 A series of implementing processes to demonstrate the water removal ability and anti-fouling property of PMAPS-PDA coated sponge.

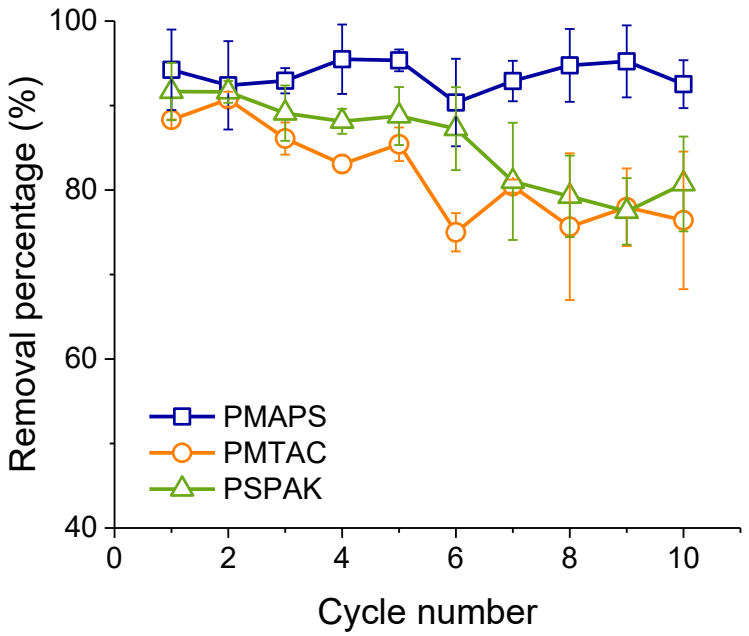

Figure 5.9 Removal percentage when adsorbing water from water-in-oil (W/O) emulsion solutions over 10 cycles by PMAPS, PMTAC and PSPAK-PDA coated sponges. After application in each cycle, sponges are washed in water.

5.4 Conclusions

In summary, we have successfully fabricated zwitterionic PMAPS, cationic PMTAC and anionic PSPAK-PDA coated silicon wafer substrates and sponges. It was found that though soaked in model heavy oil under dry state, the zwitterionic PMAPS-PDA coated silicon wafer surfaces still can be cleaned by water and maintain underwater superoleophobicity after ten-time cycles. However, the oleophobicity of cationic PMTAC and anionic PSPAK-PDA coated silicon wafer substrates gradually decrease with increasing cycle number. This remarkable underwater self-cleaning ability and superoleophobicity might be due to the superior water binding ability and long-range attraction for water of zwitterionic polyelectrolyte coating in oil. Applying the PMAPS-PDA coating on inner surfaces of heavy oil transportation pipelines, and the surfaces of other

related appliances can make these surfaces be easily cleaned by water, which has not been realized before to our best knowledge. In addition, the zwitterionic PMAPS-PDA coated sponges can remove more than 90% water from water-in-model heavy oil emulsion for ten cycles, which is a promising technology in heavy oil industry for practical application.

References

1. Xue, Q.; Cao, H.; Meng, F.; Quan, M.; Gong, Y.-K., Cell Membrane Mimetic Coating Immobilized by Mussel-Inspired Adhesion on Commercial Ultrafiltration Membrane to Enhance Antifouling Performance. *J. Membr. Sci.* **2017**.

2. Garbis, S. D.; Roumeliotis, T. I.; Tyritzis, S. I.; Zorpas, K. M.; Pavlakis, K.; Constantinides, C. A., A Novel Multidimensional Protein Identification Technology Approach Combining Protein Size Exclusion Prefractionation, Peptide Zwitterion− Ion Hydrophilic Interaction Chromatography, and Nano-Ultraperformance Rp Chromatography/Nesi-Ms2 for the in-Depth Analysis of the Serum Proteome and Phosphoproteome: Application to Clinical Sera Derived from Humans with Benign Prostate Hyperplasia. *Anal. Chem.* **2010,** *83*, 708-718.

3. Harris, L. J.; Birch, T. W., Zwitterions: Proof of the Zwitterion Constitution of the Amino-Acid Molecule. Ii. Amino-Acids, Polypeptides, Etc., and Proteins as Zwitterions, with Instances of Non-Zwitterion Ampholytes. *Biochem. J.* **1930,** *24*, 1080.

4. Eiberweiser, A.; Nazet, A.; Kruchinin, S. E.; Fedotova, M. V.; Buchner, R., Hydration and Ion Binding of the Osmolyte Ectoine. *J. Phys. Chem. B* **2015,** *119*, 15203-15211.

5. Bretscher, M. S., Mammalian Plasma Membranes. *Nature* **1975,** *258*, 43-49.

6. Kobayashi, M.; Terayama, Y.; Kikuchi, M.; Takahara, A., Chain Dimensions and Surface Characterization of Superhydrophilic Polymer Brushes with Zwitterion Side Groups. *Soft Matter* **2013,** *9*, 5138-5148.

7. Murakami, D.; Kobayashi, M.; Moriwaki, T.; Ikemoto, Y.; Jinnai, H.; Takahara, A., Spreading and Structuring of Water on Superhydrophilic Polyelectrolyte Brush Surfaces. *Langmuir* **2013,** *29*, 1148-1151.

8. Zhang, P.; Lin, L.; Zang, D.; Guo, X.; Liu, M., Designing Bioinspired Anti-Biofouling Surfaces Based on a Superwettability Strategy. *Small* **2016**.

9. Jiang, S.; Cao, Z., Ultralow-Fouling, Functionalizable, and Hydrolyzable Zwitterionic Materials and Their Derivatives for Biological Applications. *Adv. Mater.* **2010,** *22*, 920-932.

10. Schlenoff, J. B., Zwitteration: Coating Surfaces with Zwitterionic Functionality to Reduce Nonspecific Adsorption. *Langmuir* **2014,** *30*, 9625-9636.

11. Ji, Y.-L.; An, Q.-F.; Guo, Y.-S.; Hung, W.-S.; Lee, K.-R.; Gao, C.-J., Bio-Inspired Fabrication of High Perm-Selectivity and Anti-Fouling Membranes Based on Zwitterionic Polyelectrolyte Nanoparticles. *Journal of Materials Chemistry A* **2016,** *4*, 4224-4231.

12. Chen, M.; Briscoe, W. H.; Armes, S. P.; Klein, J., Lubrication at Physiological Pressures by Polyzwitterionic Brushes. *Science* **2009,** *323*, 1698-1701.

13. Liu, Q.; Patel, A. A.; Liu, L., Superhydrophilic and Underwater Superoleophobic Poly (Sulfobetaine Methacrylate)-Grafted Glass Fiber Filters for Oil–Water Separation. *ACS Appl. Mater. Interfaces* **2014,** *6*, 8996-9003.

14. Zhu, Y.; Zhang, F.; Wang, D.; Pei, X. F.; Zhang, W.; Jin, J., A Novel Zwitterionic Polyelectrolyte Grafted Pvdf Membrane for Thoroughly Separating Oil from Water with Ultrahigh Efficiency. *J. Mater. Chem. A* **2013,** *1*, 5758-5765.

15. Gao, S.; Sun, J.; Liu, P.; Zhang, F.; Zhang, W.; Yuan, S.; Li, J.; Jin, J., A Robust Polyionized Hydrogel with an Unprecedented Underwater Anti-Crude-Oil-Adhesion Property. *Adv. Mater.* **2016,** *28*, 5307-5314.

16. Huang, K.-T.; Yeh, S.-B.; Huang, C.-J., Surface Modification for Superhydrophilicity and Underwater Superoleophobicity: Applications in Antifog, Underwater Self-Cleaning, and Oil–Water Separation. *ACS Appl. Mater. Interfaces* **2015,** *7*, 21021-21029.

17. Martínez-Palou, R.; de Lourdes Mosqueira, M.; Zapata-Rendón, B.; Mar-Juárez, E.; Bernal-Huicochea, C.; de la Cruz Clavel-López, J.; Aburto, J., Transportation of Heavy and Extra-Heavy Crude Oil by Pipeline: A Review. *J. Pet. Sci. Eng.* **2011,** *75*, 274-282.

18. Ferreira, S. R.; Louzada, H. F.; Dip, R. M. M.; González, G.; Lucas, E. F., Influence of the Architecture of Additives on the Stabilization of Asphaltene and Water-in-Oil Emulsion Separation. *Energy Fuels* **2015,** *29*, 7213-7220.

19. Yang, F.; Tchoukov, P.; Pensini, E.; Dabros, T.; Czarnecki, J.; Masliyah, J.; Xu, Z., Asphaltene Subfractions Responsible for Stabilizing Water-in-Crude Oil Emulsions. Part 1: Interfacial Behaviors. *Energy Fuels* **2014,** *28*, 6897-6904.

20. Goual, L.; Sedghi, M.; Zeng, H.; Mostowfi, F.; McFarlane, R.; Mullins, O. C., On the Formation and Properties of Asphaltene Nanoaggregates and Clusters by Dc-Conductivity and Centrifugation. *Fuel* **2011,** *90*, 2480-2490.

21. Hoepfner, M. P.; Vilas Bôas Fávero, C. u.; Haji-Akbari, N.; Fogler, H. S., The Fractal Aggregation of Asphaltenes. *Langmuir* **2013,** *29*, 8799-8808.

22. González, G.; Sousa, M. A.; Lucas, E. F., Asphaltenes Precipitation from Crude Oil and Hydrocarbon Media. *Energy Fuels* **2006,** *20*, 2544-2551.

23. Syunyaev, R.; Balabin, R.; Akhatov, I.; Safieva, J., Adsorption of Petroleum Asphaltenes onto Reservoir Rock Sands Studied by near-Infrared (Nir) Spectroscopy. *Energy Fuels* **2009,** *23*, 1230-1236.

24. Shi, C.; Yan, B.; Xie, L.; Zhang, L.; Wang, J.; Takahara, A.; Zeng, H., Long-Range Hydrophilic Attraction between Water and Polyelectrolyte Surfaces in Oil. *Angew. Chem. Int. Ed.* **2016,** *55*, 15017-15021.

25. Xue, Z.; Wang, S.; Lin, L.; Chen, L.; Liu, M.; Feng, L.; Jiang, L., A Novel Superhydrophilic and Underwater Superoleophobic Hydrogel-Coated Mesh for Oil/Water Separation. *Adv. Mater.* **2011,** *23*, 4270-4273.

26. Zhou, X.; Zhang, Z.; Xu, X.; Guo, F.; Zhu, X.; Men, X.; Ge, B., Robust and Durable Superhydrophobic Cotton Fabrics for Oil/Water Separation. *ACS Appl. Mater. Interfaces* **2013,** *5*, 7208-7214.

27. Dalsin, J. L.; Hu, B.-H.; Lee, B. P.; Messersmith, P. B., Mussel Adhesive Protein Mimetic Polymers for the Preparation of Nonfouling Surfaces. *J. Am. Chem. Soc.* **2003,** *125*, 4253-4258.

28. Lee, H.; Dellatore, S. M.; Miller, W. M.; Messersmith, P. B., Mussel-Inspired Surface Chemistry for Multifunctional Coatings. *Science* **2007,** *318*, 426-430.

29. Lee, H.; Scherer, N. F.; Messersmith, P. B., Single-Molecule Mechanics of Mussel Adhesion. *Proc. Natl. Acad. Sci. U. S. A.* **2006,** *103*, 12999-13003.

30. Yang, H.-C.; Liao, K.-J.; Huang, H.; Wu, Q.-Y.; Wan, L.-S.; Xu, Z.-K., Mussel-Inspired Modification of a Polymer Membrane for Ultra-High Water Permeability and Oil-in-Water Emulsion Separation. *J. Mater. Chem. A* **2014,** *2*, 10225-10230.

31. Alboudwarej, H.; Pole, D.; Svrcek, W. Y.; Yarranton, H. W., Adsorption of Asphaltenes on Metals. *Ind. Eng. Chem. Res.* **2005,** *44*, 5585-5592.

32. Akhlaq, M. S.; Götze, P.; Kessel, D.; Dornow, W., Adsorption of Crude Oil Colloids on Glass Plates: Measurements of Contact Angles and the Factors Influencing Glass Surface Properties. *Colloids Surf. Physicochem. Eng. Aspects* **1997,** *126*, 25-32.

33. Higaki, Y.; Hatae, K.; Ishikawa, T.; Takanohashi, T.; Hayashi, J.-i.; Takahara, A., Adsorption and Desorption Behavior of Asphaltene on Polymer-Brush-Immobilized Surfaces. *ACS Appl. Mater. Interfaces* **2014,** *6*, 20385-20389.

34. Turgman-Cohen, S.; Fischer, D. A.; Kilpatrick, P. K.; Genzer, J., Asphaltene Adsorption onto Self-Assembled Monolayers of Alkyltrichlorosilanes of Varying Chain Length. *ACS Appl. Mater. Interfaces* **2009,** *1*, 1347-1357.

35. Chen, S.; Li, L.; Zhao, C.; Zheng, J., Surface Hydration: Principles and Applications toward Low-Fouling/Nonfouling Biomaterials. *Polymer* **2010,** *51*, 5283-5293.

36. Das, S.; Thundat, T.; Mitra, S. K., Analytical Model for Zeta Potential of Asphaltene. *Fuel* **2013,** *108*, 543-549.

Chapter 6 Conclusions and Suggestions

6.1 Major conclusions

(1) Poly (acrylic acid) modified magnetic graphene oxide composite (PAA/MGO) was synthesized successfully by a facile method, which was substantiated by Fourier transform infrared spectroscopy (FTIR), X-ray photoelectron spectroscopy (XPS), X-ray diffraction (XRD), thermogravimetric analysis (TGA) and high-resolution transmission electron microscopy (HRTEM) results. The batch tests of the adsorption of a model cationic dye, methylene blue (MB), on PAA/MGO and magnetic graphene oxide (MGO) were carried out. After the functionalization of Poly (acrylic acid) (PAA) to MGO, the maximum adsorption capacity of MB (pH ~7) increased from ~70 mg g^{-1} to ~291 mg g^{-1}. It was observed that, with increased pH (from 3 to 11), zeta potential of both PAA/MGO and MGO decreased, and the adsorption capacity of MB on both PAA/MGO and MGO increased, implying that electrostatic interaction played an essential role during adsorption and the increased adsorption capacity of PAA/MGO compared to MGO was due to the rich contents of anionic carboxylic groups of PAA.

(2) The adsorption behavior of aromatic organic compounds (AOCs), using MB as a model compound, on graphene (GO) was systematically and quantitatively investigated by single-molecular force spectroscopy (SMFS) combined with Density Functional Theory (DFT) simulations. Our results showed that epoxy groups were the dominative functional groups that facilitated the GO-AOCs interaction. Derived from SMFS results, the bond dissociation events between AOC and the regions on graphene with epoxy groups had a bond dissociation energy ΔG of ~-4.6 kcal/mol and bond dissociation distance Δx of 2.3 Å. It was revealed by the simulation results that the epoxy groups facilitated the adsorption of the AOC on GO through polar interaction and enhanced π interactions.

(3) Zwitterionic poly (3-[dimethyl(2-methacryloyloxyethyl) ammonium] propanesulfonate) (PMAPS), cationic poly (2-(methacryloyloxy)ethyl trimethylammonium chloride) (PMTAC) and anionic poly (3-sulfopropyl acrylate potassium) (PSPAK) grafted polydopamine (PDA) coated silicon wafer substrates and polyurethane (PU) sponges were fabricated successfully. It was found that PMAPS-PDA coating showed superiorly anti-fouling performance compared with PMTAC and PSPAK-PDA coatings. After being soaked in model heavy oil under dry state, the PMAPS-PDA coated silicon wafer substrates could be easily cleaned by water (pH 2, 5.6 and 11). The PMAPS-PDA coated sponges could remove more than 90% of water from the model heavy oil for ten cycles.

6.2 Major contributions

(1) PAA/MGO shows higher maximum adsorption capacity of MB than the previous reported magnetic graphene or MGO composites (~44 to 190 mg g^{-1}) under similar experimental conditions with rapid adsorption rate. As a highly effective and efficient adsorbent, it is promising to utilize PAA/MGO to remove cationic organic pollutants from wastewater.

(2) It is the first time that employing SMFS and DFT simulations to study interaction mechanism between AOCs and GO at single molecular scale. The adsorption energy and morphology derived from the experimental and theoretic results have the potential to provide guidance to tune the adsorption behavior of AOCs on GO and to fabricate new AOCs/GO composites in the future. Besides, the method to combing SMFS and DFT calculations are supposed to be effective to survey the adsorption mechanism of various molecules on GO and other 2-D materials, such as MoS_2.

(3) For the first time to our best knowledge, the underwater self-cleaning of substrates being fouled by model heavy oil under dry state is realized and the removal of water from model heavy oil by adsorption is achieved. This PMAPS-PDA coating can be easily fabricated and is promising to be applied in industries to minimize the fouling concerns in handling and transporting heavy oil, and to remove the water residues, which can avoid the corrosion problem and benefit petroleum recovery.

6.3 Suggestions for future work

(1) Tune the number and variety of functional groups on GO for selective adsorption for some specific kinds of pollutants.

(2) Fabricate PMAPS-PDA coated sponges with larger size for large-scale application, or to apply PMAPS-PDA coating in more real industrial conditions. Toluene was used as the diluting agent for asphaltenes in this study, while in the future, the dilutes that applied in industries can be used.

Bibliography

1. Kelly, E. N.; Schindler, D. W.; Hodson, P. V.; Short, J. W.; Radmanovich, R.; Nielsen, C. C., Oil Sands Development Contributes Elements Toxic at Low Concentrations to the Athabasca River and Its Tributaries. *Proc. Natl. Acad. Sci. U. S. A.* **2010,** *107*, 16178-16183.

2. Kelly, E. N.; Short, J. W.; Schindler, D. W.; Hodson, P. V.; Ma, M.; Kwan, A. K.; Fortin, B. L., Oil Sands Development Contributes Polycyclic Aromatic Compounds to the Athabasca River and Its Tributaries. *Proc. Natl. Acad. Sci. U. S. A.* **2009,** *106*, 22346-22351.

3. Allen, E. W., Process Water Treatment in Canada's Oil Sands Industry: I. Target Pollutants and Treatment Objectives. *J. Environ. Eng. Sci.* **2008,** *7*, 123-138.

4. Bajpai, P., *Bleach Plant Effluents from the Pulp and Paper Industry*. Springer: 2013.

5. Ozcan, A.; Ozcan, A.; Gok, O., Adsorption Kinetics and Isotherms of Anionic Dye of Reactive Blue 19 from Aqueous Solutions onto Dtma-Sepiolite. In *Hazardous Materials and Wastewater—Treatment, Removal and Analysis*, Nova Science Publishers: New York, 2007.

6. Prasad, A. L.; Santhi, T., Adsorption of Hazardous Cationic Dyes from Aqueous Solution onto Acacia Nilotica Leaves as an Eco Friendly Adsorbent. *Sustain. Environ. Res.* **2012,** *22*, 113-122.

7. Martínez-Palou, R.; de Lourdes Mosqueira, M.; Zapata-Rendón, B.; Mar-Juárez, E.; Bernal-Huicochea, C.; de la Cruz Clavel-López, J.; Aburto, J., Transportation of Heavy and Extra-Heavy Crude Oil by Pipeline: A Review. *J. Pet. Sci. Eng.* **2011,** *75*, 274-282.

8. Grassi, M.; Kaykioglu, G.; Belgiorno, V.; Lofrano, G., Removal of Emerging Contaminants from Water and Wastewater by Adsorption Process. In *Emerging Compounds Removal from Wastewater*, Springer: 2012; pp 15-37.

9. Singh, S. N., *Microbial Degradation of Synthetic Dyes in Wastewaters*. Springer: 2014.

10. Abrahart, E. N., *Dyes and Their Intermediates*. Chemical Publishing: New York, 1977.

11. Pereira, L.; Alves, M., Dyes—Environmental Impact and Remediation. In *Environmental Protection Strategies for Sustainable Development*, Springer: 2012; pp 111-162.

12. Vaidya, A.; Datye, K., Environmental-Pollution During Chemical-Processing of Synthetic-Fibers. *Colourage* **1982,** *29*, 3-10.

13. Bhatnagar, A.; Jain, A., A Comparative Adsorption Study with Different Industrial Wastes as Adsorbents for the Removal of Cationic Dyes from Water. *J. Colloid Interface Sci.* **2005,** *281*, 49-55.

14. Garg, V. K., Green Chemistry for Dyes Removal from Waste Water. *Green Process. Synth.* **2015,** *4*, 507-508.

15. Raghavacharya, C., Colour Removal from Industrial Effluents: A Comparative Review of Available Technologies. *Chem. Eng. World* **1997,** *32*, 53-54.

16. Robinson, T.; McMullan, G.; Marchant, R.; Nigam, P., Remediation of Dyes in Textile Effluent: A Critical Review on Current Treatment Technologies with a Proposed Alternative. *Bioresour. Technol.* **2001,** *77*, 247-255.

17. Ding, Z.; Hu, X.; Zimmerman, A. R.; Gao, B., Sorption and Cosorption of Lead (Ii) and Methylene Blue on Chemically Modified Biomass. *Bioresour. Technol.* **2014,** *167*, 569-573.

18. Forgacs, E.; Cserhati, T.; Oros, G., Removal of Synthetic Dyes from Wastewaters: A Review. *Environ. Int.* **2004,** *30*, 953-971.

19. Bhattacharyya, K. G.; Sarma, A., Adsorption Characteristics of the Dye, Brilliant Green, on Neem Leaf Powder. *Dyes Pigm.* **2003,** *57*, 211-222.

20. Kumar, V.; Wati, L.; Nigam, P.; Banat, I.; Yadav, B.; Singh, D.; Marchant, R., Decolorization and Biodegradation of Anaerobically Digested Sugarcane Molasses Spent Wash Effluent from Biomethanation Plants by White-Rot Fungi. *Process Biochem.* **1998,** *33*, 83-88.

21. Dąbrowski, A., Adsorption—from Theory to Practice. *Adv. Colloid Interface Sci.* **2001,** *93*, 135-224.

22. Iqbal, M. J.; Ashiq, M. N., Adsorption of Dyes from Aqueous Solutions on Activated Charcoal. *J. Hazard. Mater.* **2007,** *139*, 57-66.

23. Xu, Y.; Lebrun, R. E.; Gallo, P.-J.; Blond, P., Treatment of Textile Dye Plant Effluent by Nanofiltration Membrane. *Sep. Sci. Technol.* **1999,** *34*, 2501-2519.

24. Mishra, G.; Tripathy, M., A Critical Review of the Treatments for Decolourization of Textile Effluent. *Colourage* **1993,** *40*, 35-35.

25. Mantzavinos, D.; Hellenbrand, R.; Livingston, A. G.; Metcalfe, I. S., Beneficial Combination of Wet Oxidation, Membrane Separation and Biodegradation Processes for Treatment of Polymer Processing Wastewaters. *Can. J. Chem. Eng.* **2000,** *78*, 418-422.

26. Slokar, Y. M.; Le Marechal, A. M., Methods of Decoloration of Textile Wastewaters. *Dyes Pigm.* **1998,** *37*, 335-356.

27. Namasivayam, C.; Kavitha, D., Removal of Congo Red from Water by Adsorption onto Activated Carbon Prepared from Coir Pith, an Agricultural Solid Waste. *Dyes Pigm.* **2002,** *54*, 47-58.

28. Ramesha, G.; Kumara, A. V.; Muralidhara, H.; Sampath, S., Graphene and Graphene Oxide as Effective Adsorbents toward Anionic and Cationic Dyes. *J. Colloid Interface Sci.* **2011,** *361*, 270-277.

29. Hamilton, C. E. Functionalization, Coordination, and Coating of Carbon Nanomaterials. Rice University, 2009.

30. Ai, L.; Zhang, C.; Chen, Z., Removal of Methylene Blue from Aqueous Solution by a Solvothermal-Synthesized Graphene/Magnetite Composite. *J. Hazard. Mater.* **2011,** *192*, 1515-1524.

31. Xie, G.; Xi, P.; Liu, H.; Chen, F.; Huang, L.; Shi, Y.; Hou, F.; Zeng, Z.; Shao, C.; Wang, J., A Facile Chemical Method to Produce Superparamagnetic Graphene Oxide–Fe_3o_4 Hybrid Composite and Its Application in the Removal of Dyes from Aqueous Solution. *J. Mater. Chem.* **2012,** *22*, 1033-1039.

32. He, F.; Fan, J.; Ma, D.; Zhang, L.; Leung, C.; Chan, H. L., The Attachment of Fe 3 O 4 Nanoparticles to Graphene Oxide by Covalent Bonding. *Carbon* **2010,** *48*, 3139-3144.

33. Shi, H.; Li, W.; Zhong, L.; Xu, C., Methylene Blue Adsorption from Aqueous Solution by Magnetic Cellulose/Graphene Oxide Composite: Equilibrium, Kinetics, and Thermodynamics. *Ind. Eng. Chem. Res.* **2014,** *53*, 1108-1118.

34. Li, L.; Fan, L.; Luo, C.; Duan, H.; Wang, X., Study of Fuchsine Adsorption on Magnetic Chitosan/Graphene Oxide. *RSC Adv.* **2014,** *4*, 24679-24685.

35. Kang, T. W.; Jeon, S. J.; Kim, H. I.; Park, J. H.; Yim, D.; Lee, H. R.; Ju, J. M.; Kim, M. J.; Kim, J. H., Optical Detection of Enzymatic Activity and Inhibitors on Non-Covalently Functionalized Fluorescent Graphene Oxide. *ACS Nano* **2016,** *10*, 5346-5353.

36. Georgakilas, V.; Tiwari, J. N.; Kemp, K. C.; Perman, J. A.; Bourlinos, A. B.; Kim, K. S.; Zboril, R., Noncovalent Functionalization of Graphene and Graphene Oxide for Energy Materials, Biosensing, Catalytic, and Biomedical Applications. *Chem. Rev.* **2016,** *116*, 5464-5519.

37. Yan, H.; Wu, H.; Li, K.; Wang, Y.; Tao, X.; Yang, H.; Li, A.; Cheng, R., Influence of the Surface Structure of Graphene Oxide on the Adsorption of Aromatic Organic Compounds from Water. *ACS Appl. Mater. Interfaces* **2015,** *7*, 6690-6697.

38. Wang, Y.; Li, Z.; Hu, D.; Lin, C.-T.; Li, J.; Lin, Y., Aptamer/Graphene Oxide Nanocomplex for in Situ Molecular Probing in Living Cells. *Journal of the American Chemical Society* **2010,** *132*, 9274-9276.

39. Chen, X.; Chen, B., Macroscopic and Spectroscopic Investigations of the Adsorption of Nitroaromatic Compounds on Graphene Oxide, Reduced Graphene Oxide, and Graphene Nanosheets. *Environ. Sci. Technol.* **2015,** *49*, 6181-6189.

40. Kyzas, G. Z.; Deliyanni, E. A.; Matis, K. A., Graphene Oxide and Its Application as an Adsorbent for Wastewater Treatment. *Journal of Chemical Technology and Biotechnology* **2014,** *89*, 196-205.

41. Sharma, P.; Hussain, N.; Borah, D. J.; Das, M. R., Kinetics and Adsorption Behavior of the Methyl Blue at the Graphene Oxide/Reduced Graphene Oxide Nanosheet–Water Interface: A Comparative Study. *J. Chem. Eng. Data* **2013,** *58*, 3477-3488.

42. Yang, S.-T.; Chen, S.; Chang, Y.; Cao, A.; Liu, Y.; Wang, H., Removal of Methylene Blue from Aqueous Solution by Graphene Oxide. *J. Colloid Interface Sci.* **2011,** *359*, 24-29.

43. Zhang, J.; Azam, M. S.; Shi, C.; Huang, J.; Yan, B.; Liu, Q.; Zeng, H., Poly(Acrylic Acid) Functionalized Magnetic Graphene Oxide Nanocomposite for Removal of Methylene Blue. *RSC Adv.* **2015,** *5*, 32272-32282.

44. Wang, Y.; Li, Z.; Wang, J.; Li, J.; Lin, Y., Graphene and Graphene Oxide: Biofunctionalization and Applications in Biotechnology. *Trends Biotechnol.* **2011,** *29*, 205-212.

45. Yang, K.; Feng, L.; Liu, Z., The Advancing Uses of Nano-Graphene in Drug Delivery. *Expert opinion on drug delivery* **2015,** *12*, 601-612.

46. Lee, J.; Kim, J.; Kim, S.; Min, D. H., Biosensors Based on Graphene Oxide and Its Biomedical Application. *Adv Drug Deliv Rev* **2016**.

47. Liu, J.; Liu, Z.; Barrow, C. J.; Yang, W., Molecularly Engineered Graphene Surfaces for Sensing Applications: A Review. *Anal. Chim. Acta* **2015,** *859*, 1-19.

48. Kong, X.-k.; Chen, Q.-w.; Lun, Z.-y., Probing the Influence of Different Oxygenated Groups on Graphene Oxide's Catalytic Performance. *J. Mater. Chem. A* **2014,** *2*, 610-613.

49. Compton, O. C.; Jain, B.; Dikin, D. A.; Abouimrane, A.; Amine, K.; Nguyen, S. T., Chemically Active Reduced Graphene Oxide with Tunable C/O Ratios. *ACS nano* **2011,** *5*, 4380-4391.

50. Lerf, A.; He, H.; Forster, M.; Klinowski, J., Structure of Graphite Oxide Revisited. *J. Phys. Chem. B* **1998,** *102*, 4477-4482.

51. Szabó, T.; Berkesi, O.; Dékány, I., Drift Study of Deuterium-Exchanged Graphite Oxide. *Carbon* **2005,** *43*, 3186-3189.

52. Cai, W.; Piner, R. D.; Stadermann, F. J.; Park, S.; Shaibat, M. A.; Ishii, Y.; Yang, D.; Velamakanni, A.; An, S. J.; Stoller, M., Synthesis and Solid-State Nmr Structural Characterization of 13c-Labeled Graphite Oxide. *Science* **2008,** *321*, 1815-1817.

53. Szabó, T.; Berkesi, O.; Forgó, P.; Josepovits, K.; Sanakis, Y.; Petridis, D.; Dékány, I., Evolution of Surface Functional Groups in a Series of Progressively Oxidized Graphite Oxides. *Chemistry of materials* **2006,** *18*, 2740-2749.

54. Montes-Navajas, P.; Asenjo, N. G.; Santamaria, R.; Menendez, R.; Corma, A.; Garcia, H., Surface Area Measurement of Graphene Oxide in Aqueous Solutions. *Langmuir* **2013,** *29*, 13443-13448.

55. Haubner, K.; Murawski, J.; Olk, P.; Eng, L. M.; Ziegler, C.; Adolphi, B.; Jaehne, E., The Route to Functional Graphene Oxide. *Chemphyschem* **2010,** *11*, 2131-2139.

56. Chen, L.; Yang, J.; Zeng, X.; Zhang, L.; Yuan, W., Adsorption of Methylene Blue in Water by Reduced Graphene Oxide: Effect of Functional Groups. *Mater. Express* **2013,** *3*, 281-290.

57. Ramesha, G. K.; Kumara, A. V.; Muralidhara, H. B.; Sampath, S., Graphene and Graphene Oxide as Effective Adsorbents toward Anionic and Cationic Dyes. *J. Colloid Interface Sci.* **2011,** *361*, 270-277.

58. Balapanuru, J.; Yang, J. X.; Xiao, S.; Bao, Q.; Jahan, M.; Polavarapu, L.; Wei, J.; Xu, Q. H.; Loh, K. P., A Graphene Oxide–Organic Dye Ionic Complex with DNA-Sensing and Optical-Limiting Properties. *Angew. Chem.* **2010,** *122*, 6699-6703.

59. Ferreira, S. R.; Louzada, H. F.; Dip, R. M. M.; González, G.; Lucas, E. F., Influence of the Architecture of Additives on the Stabilization of Asphaltene and Water-in-Oil Emulsion Separation. *Energy Fuels* **2015,** *29*, 7213-7220.

60. Goual, L.; Sedghi, M.; Zeng, H.; Mostowfi, F.; McFarlane, R.; Mullins, O. C., On the Formation and Properties of Asphaltene Nanoaggregates and Clusters by Dc-Conductivity and Centrifugation. *Fuel* **2011,** *90*, 2480-2490.

61. Hoepfner, M. P.; Vilas Bôas Fávero, C. u.; Haji-Akbari, N.; Fogler, H. S., The Fractal Aggregation of Asphaltenes. *Langmuir* **2013,** *29*, 8799-8808.

62. González, G.; Sousa, M. A.; Lucas, E. F., Asphaltenes Precipitation from Crude Oil and Hydrocarbon Media. *Energy Fuels* **2006,** *20*, 2544-2551.

63. Syunyaev, R.; Balabin, R.; Akhatov, I.; Safieva, J., Adsorption of Petroleum Asphaltenes onto Reservoir Rock Sands Studied by near-Infrared (Nir) Spectroscopy. *Energy Fuels* **2009,** *23*, 1230-1236.

64. He, K.; Duan, H.; Chen, G. Y.; Liu, X.; Yang, W.; Wang, D., Cleaning of Oil Fouling with Water Enabled by Zwitterionic Polyelectrolyte Coatings: Overcoming the Imperative Challenge of Oil–Water Separation Membranes. *ACS Nano* **2015,** *9*, 9188-9198.

65. Sztukowski, D. M.; Yarranton, H. W., Oilfield Solids and Water-in-Oil Emulsion Stability. *J. Colloid Interface Sci.* **2005,** *285*, 821-833.

66. Czarnecki, J.; Moran, K., On the Stabilization Mechanism of Water-in-Oil Emulsions in Petroleum Systems. *Energy Fuels* **2005,** *19*, 2074-2079.

67. Kallevik, H.; Kvalheim, O. M.; Sjöblom, J., Quantitative Determination of Asphaltenes and Resins in Solution by Means of near-Infrared Spectroscopy. Correlations to Emulsion Stability. *J. Colloid Interface Sci.* **2000,** *225*, 494-504.

68. Dai, Q.; Chung, K. H., Hot Water Extraction Process Mechanism Using Model Oil Sands. *Fuel* **1996,** *75*, 220-226.

69. Chen, G., Electrochemical Technologies in Wastewater Treatment. *Sep. Purif. Technol.* **2004,** *38*, 11-41.

70. Kwon, W.-T.; Park, K.; Han, S. D.; Yoon, S. M.; Kim, J. Y.; Bae, W.; Rhee, Y. W., Investigation of Water Separation from Water-in-Oil Emulsion Using Electric Field. *J Ind. Eng. Chem.* **2010,** *16*, 684-687.

71. Eow, J. S.; Ghadiri, M., Electrostatic Enhancement of Coalescence of Water Droplets in Oil: A Review of the Technology. *Chem. Eng. J.* **2002,** *85*, 357-368.

72. P. Kajitvichyanukul, Y.-T. H., L. Wang, *Handbook of Environmental Engineering*. 2006; Vol. 4, p 521.

73. Chan, Y. J.; Chong, M. F.; Law, C. L.; Hassell, D., A Review on Anaerobic–Aerobic Treatment of Industrial and Municipal Wastewater. *Chem. Eng. J.* **2009,** *155*, 1-18.

74. Suzuki, Y.; Maruyama, T., Removal of Emulsified Oil from Water by Coagulation and Foam Separation. *Sep. Sci. Technol.* **2005,** *40*, 3407-3418.

75. Xue, Z.; Cao, Y.; Liu, N.; Feng, L.; Jiang, L., Special Wettable Materials for Oil/Water Separation. *Journal of Materials Chemistry A* **2014,** *2*, 2445-2460.

76. Liu, M.; Wang, S.; Wei, Z.; Song, Y.; Jiang, L., Bioinspired Design of a Superoleophobic and Low Adhesive Water/Solid Interface. *Adv. Mater.* **2009,** *21*, 665-669.

77. Jung, Y. C.; Bhushan, B., Wetting Behavior of Water and Oil Droplets in Three-Phase Interfaces for Hydrophobicity/Philicity and Oleophobicity/Philicity. *Langmuir* **2009,** *25*, 14165-14173.

78. Gupta, R. K.; Dunderdale, G. J.; England, M. W.; Hozumi, A., Oil/Water Separation Techniques: A Review of Recent Progresses and Future Directions. *Journal of Materials Chemistry A* **2017**.

79. Huang, W.; Lei, M.; Huang, H.; Chen, J.; Chen, H., Effect of Polyethylene Glycol on Hydrophilic Tio 2 Films: Porosity-Driven Superhydrophilicity. *Surf. Coat. Technol.* **2010,** *204*, 3954-3961.

80. Xu, L.; Liu, N.; Cao, Y.; Lu, F.; Chen, Y.; Zhang, X.; Feng, L.; Wei, Y., Mercury Ion Responsive Wettability and Oil/Water Separation. *ACS Appl. Mater. Interfaces* **2014,** *6*, 13324-13329.

81. Zhang, W.; Zhu, Y.; Liu, X.; Wang, D.; Li, J.; Jiang, L.; Jin, J., Salt-Induced Fabrication of Superhydrophilic and Underwater Superoleophobic Paa-G-Pvdf Membranes for Effective Separation of Oil-in-Water Emulsions. *Angew. Chem. Int. Ed.* **2014,** *53*, 856-860.

82. Kobayashi, M.; Terayama, Y.; Kikuchi, M.; Takahara, A., Chain Dimensions and Surface Characterization of Superhydrophilic Polymer Brushes with Zwitterion Side Groups. *Soft Matter* **2013,** *9*, 5138-5148.

83. Murakami, D.; Kobayashi, M.; Moriwaki, T.; Ikemoto, Y.; Jinnai, H.; Takahara, A., Spreading and Structuring of Water on Superhydrophilic Polyelectrolyte Brush Surfaces. *Langmuir* **2013,** *29*, 1148-1151.

84. Xue, Q.; Cao, H.; Meng, F.; Quan, M.; Gong, Y.-K., Cell Membrane Mimetic Coating Immobilized by Mussel-Inspired Adhesion on Commercial Ultrafiltration Membrane to Enhance Antifouling Performance. *J. Membr. Sci.* **2017**.

85. Garbis, S. D.; Roumeliotis, T. I.; Tyritzis, S. I.; Zorpas, K. M.; Pavlakis, K.; Constantinides, C. A., A Novel Multidimensional Protein Identification Technology Approach Combining Protein Size Exclusion Prefractionation, Peptide Zwitterion− Ion Hydrophilic Interaction Chromatography, and Nano-Ultraperformance Rp Chromatography/Nesi-Ms2 for the in-Depth Analysis of the Serum Proteome and Phosphoproteome: Application to Clinical Sera Derived from Humans with Benign Prostate Hyperplasia. *Anal. Chem.* **2010,** *83*, 708-718.

86. Harris, L. J.; Birch, T. W., Zwitterions: Proof of the Zwitterion Constitution of the Amino-Acid Molecule. Ii. Amino-Acids, Polypeptides, Etc., and Proteins as Zwitterions, with Instances of Non-Zwitterion Ampholytes. *Biochem. J.* **1930,** *24*, 1080.

87. Eiberweiser, A.; Nazet, A.; Kruchinin, S. E.; Fedotova, M. V.; Buchner, R., Hydration and Ion Binding of the Osmolyte Ectoine. *J. Phys. Chem. B* **2015,** *119*, 15203-15211.

88. Bretscher, M. S., Mammalian Plasma Membranes. *Nature* **1975,** *258*, 43-49.

89. Zhang, P.; Lin, L.; Zang, D.; Guo, X.; Liu, M., Designing Bioinspired Anti-Biofouling Surfaces Based on a Superwettability Strategy. *Small* **2016**.

90. Jiang, S.; Cao, Z., Ultralow-Fouling, Functionalizable, and Hydrolyzable Zwitterionic Materials and Their Derivatives for Biological Applications. *Adv. Mater.* **2010,** *22*, 920-932.

91. Chen, S.; Li, L.; Zhao, C.; Zheng, J., Surface Hydration: Principles and Applications toward Low-Fouling/Nonfouling Biomaterials. *Polymer* **2010,** *51*, 5283-5293.

92. Liu, Q.; Patel, A. A.; Liu, L., Superhydrophilic and Underwater Superoleophobic Poly (Sulfobetaine Methacrylate)-Grafted Glass Fiber Filters for Oil–Water Separation. *ACS Appl. Mater. Interfaces* **2014,** *6*, 8996-9003.

93. Zhu, Y.; Zhang, F.; Wang, D.; Pei, X. F.; Zhang, W.; Jin, J., A Novel Zwitterionic Polyelectrolyte Grafted Pvdf Membrane for Thoroughly Separating Oil from Water with Ultrahigh Efficiency. *Journal of Materials Chemistry A* **2013,** *1*, 5758-5765.

94. Gao, S.; Sun, J.; Liu, P.; Zhang, F.; Zhang, W.; Yuan, S.; Li, J.; Jin, J., A Robust Polyionized Hydrogel with an Unprecedented Underwater Anti-Crude-Oil-Adhesion Property. *Adv. Mater.* **2016,** *28*, 5307-5314.

95. Huang, K.-T.; Yeh, S.-B.; Huang, C.-J., Surface Modification for Superhydrophilicity and Underwater Superoleophobicity: Applications in Antifog, Underwater Self-Cleaning, and Oil–Water Separation. *ACS Appl. Mater. Interfaces* **2015,** *7*, 21021-21029.

96. Shi, C.; Yan, B.; Xie, L.; Zhang, L.; Wang, J.; Takahara, A.; Zeng, H., Long-Range Hydrophilic Attraction between Water and Polyelectrolyte Surfaces in Oil. *Angew. Chem. Int. Ed.* **2016,** *55*, 15017-15021.

97. Zeng, H., *Polymer Adhesion, Friction, and Lubrication*. John Wiley & Sons: 2013.

98. Bennig, G. K., Atomic Force Microscope and Method for Imaging Surfaces with Atomic Resolution. U.S. Patent: 1988.

99. Zhang, L.; Zeng, H.; Liu, Q., Probing Molecular and Surface Interactions of Comb-Type Polymer Polystyrene-Graft-Poly (Ethylene Oxide)(Ps-G-Peo) with an SFA. *J. Phys. Chem. C* **2012,** *116*, 17554-17562.

100. Wang, J.; Li, J.; Xie, L.; Shi, C.; Liu, Q.; Zeng, H., Interactions between Elemental Selenium and Hydrophilic/Hydrophobic Surfaces: Direct Force Measurements Using AFM. *Chem. Eng. J.* **2016,** *303*, 646-654.

101. Bell, G. I., Models for the Specific Adhesion of Cells to Cells. *Science* **1978,** *200*, 618-627.

102. Evans, E.; Ritchie, K., Strength of a Weak Bond Connecting Flexible Polymer Chains. *Biophys. J.* **1999,** *76*, 2439-2447.

103. Puntheeranurak, T.; Neundlinger, I.; Kinne, R. K.; Hinterdorfer, P., Single-Molecule Recognition Force Spectroscopy of Transmembrane Transporters on Living Cells. *Nat. Protoc.* **2011,** *6*, 1443.

104. Skoog, D. A.; Holler, F. J.; Crouch, S. R., *Principles of Instrumental Analysis*. Cengage learning: 2017.

105. Hollander, J. M.; Jolly, W. L., X-Ray Photoelectron Spectroscopy. *Acc. Chem. Res.* **1970,** *3*, 193-200.

106. Coats, A.; Redfern, J., Thermogravimetric Analysis. A Review. *Analyst* **1963,** *88*, 906-924.

107. Kirby, B. J., *Micro-and Nanoscale Fluid Mechanics: Transport in Microfluidic Devices*. Cambridge University Press: 2010.

108. Fischer, K., Neues Verfahren Zur Maßanalytischen Bestimmung Des Wassergehaltes Von Flüssigkeiten Und Festen Körpern. *Angew. Chem.* **1935,** *48*, 394-396.

109. Tavčar, E.; Turk, E.; Kreft, S., Simple Modification of Karl-Fischer Titration Method for Determination of Water Content in Colored Samples. *J Anal. Methods Chem.* **2012,** *2012*.

110. Zhu, S.; Jiao, S.; Liu, Z.; Pang, G.; Feng, S., High Adsorption Capacity for Dye Removal by Cuzn Hydroxyl Double Salts. *Environ. Sci.: Nano* **2014,** *1*, 172-180.

111. Crini, G., Non-Conventional Low-Cost Adsorbents for Dye Removal: A Review. *Bioresour. Technol.* **2006,** *97*, 1061-1085.

112. Ozcan, A.; Ozcan, A. S.; Gok, O., *Adsorption Kinetics and Isotherms of Anionic Dye of Reactive Blue 19 from Aqueous Solutions onto Dtma-Sepiolite*. 2007; p 25.

113. Prasad, A. L.; Santhi, T., Adsorption of Hazardous Cationic Dyes from Aqueous Solution onto Acacia Nilotica Leaves as an Eco Friendly Adsorbent. *Sustain. Environ. Res.* **2012,** *22*, 113-122.

114. Garg, V. K.; Gupta, R.; Bala Yadav, A.; Kumar, R., Dye Removal from Aqueous Solution by Adsorption on Treated Sawdust. *Bioresour. Technol.* **2003,** *89*, 121-124.

115. Shi, B.; Li, G.; Wang, D.; Feng, C.; Tang, H., Removal of Direct Dyes by Coagulation: The Performance of Preformed Polymeric Aluminum Species. *J. Hazard. Mater.* **2007,** *143*, 567-574.

116. Guibal, E.; Roussy, J., Coagulation and Flocculation of Dye-Containing Solutions Using a Biopolymer (Chitosan). *React. Funct. Polym.* **2007,** *67*, 33-42.

117. Lachheb, H.; Puzenat, E.; Houas, A.; Ksibi, M.; Elaloui, E.; Guillard, C.; Herrmann, J.-M., Photocatalytic Degradation of Various Types of Dyes (Alizarin S, Crocein Orange G, Methyl Red, Congo Red, Methylene Blue) in Water by Uv-Irradiated Titania. *Appl. Catal., B* **2002,** *39*, 75-90.

118. Zhao, D.; Sheng, G.; Chen, C.; Wang, X., Enhanced Photocatalytic Degradation of Methylene Blue under Visible Irradiation on Graphene@ TiO_2 Dyade Structure. *Appl. Catal., B* **2012,** *111*, 303-308.

119. Zhang, N.; Zhang, Y.; Xu, Y.-J., Recent Progress on Graphene-Based Photocatalysts: Current Status and Future Perspectives. *Nanoscale* **2012,** *4*, 5792-5813.

120. Purkait, M.; DasGupta, S.; De, S., Removal of Dye from Wastewater Using Micellar-Enhanced Ultrafiltration and Recovery of Surfactant. *Sep. Purif. Technol.* **2004,** *37*, 81-92.

121. Zaghbani, N.; Hafiane, A.; Dhahbi, M., Separation of Methylene Blue from Aqueous Solution by Micellar Enhanced Ultrafiltration. *Sep. Purif. Technol.* **2007,** *55*, 117-124.

122. Zhuang, X.; Wan, Y.; Feng, C.; Shen, Y.; Zhao, D., Highly Efficient Adsorption of Bulky Dye Molecules in Wastewater on Ordered Mesoporous Carbons. *Chem. Mater.* **2009,** *21*, 706-716.

123. Wang, C.; Feng, C.; Gao, Y.; Ma, X.; Wu, Q.; Wang, Z., Preparation of a Graphene-Based Magnetic Nanocomposite for the Removal of an Organic Dye from Aqueous Solution. *Chem. Eng. J.* **2011,** *173*, 92-97.

124. Iram, M.; Guo, C.; Guan, Y.; Ishfaq, A.; Liu, H., Adsorption and Magnetic Removal of Neutral Red Dye from Aqueous Solution Using Fe_3O_4 Hollow Nanospheres. *J. Hazard. Mater.* **2010,** *181*, 1039-1050.

125. Gupta, V. K., Application of Low-Cost Adsorbents for Dye Removal--a Review. *J. Environ. Manage.* **2009,** *90*, 2313-2342.

126. Li, Q.; Yue, Q.-Y.; Sun, H.-J.; Su, Y.; Gao, B.-Y., A Comparative Study on the Properties, Mechanisms and Process Designs for the Adsorption of Non-Ionic or Anionic Dyes onto Cationic-Polymer/Bentonite. *J. Environ. Manage.* **2010,** *91*, 1601-1611.

127. Alpat, S. K.; Özbayrak, Ö.; Alpat, Ş.; Akçay, H., The Adsorption Kinetics and Removal of Cationic Dye, Toluidine Blue O, from Aqueous Solution with Turkish Zeolite. *J. Hazard. Mater.* **2008,** *151*, 213-220.

128. Hameed, B.; Din, A. M.; Ahmad, A., Adsorption of Methylene Blue onto Bamboo-Based Activated Carbon: Kinetics and Equilibrium Studies. *J. Hazard. Mater.* **2007,** *141*, 819-825.

129. Ramesha, G.; Vijaya Kumara, A.; Muralidhara, H.; Sampath, S., Graphene and Graphene Oxide as Effective Adsorbents toward Anionic and Cationic Dyes. *J. Colloid Interface Sci.* **2011,** *361*, 270-277.

130. Hamilton, C. E. Functionalization, Coordination, and Coating of Carbon Nanomaterials Ph.D Thesis, University of Rice, 2009.

131. Zhao, G.; Wen, T.; Chen, C.; Wang, X., Synthesis of Graphene-Based Nanomaterials and Their Application in Energy-Related and Environmental-Related Areas. *RSC Adv.* **2012,** *2*, 9286-9303.

132. Wang, H.; Yuan, X.; Wu, Y.; Huang, H.; Peng, X.; Zeng, G.; Zhong, H.; Liang, J.; Ren, M., Graphene-Based Materials: Fabrication, Characterization and Application for the Decontamination of Wastewater and Wastegas and Hydrogen Storage/Generation. *Adv. Colloid Interface Sci.* **2013,** *195*, 19-40.

133. Wang, S.; Sun, H.; Ang, H. M.; Tadé, M. O., Adsorptive Remediation of Environmental Pollutants Using Novel Graphene-Based Nanomaterials. *Chem. Eng. J.* **2013,** *226*, 336-347.

134. Zhao, G.; Jiang, L.; He, Y.; Li, J.; Dong, H.; Wang, X.; Hu, W., Sulfonated Graphene for Persistent Aromatic Pollutant Management. *Adv. Mater.* **2011,** *23*, 3959-3963.

135. Zhang, W.; Zhou, C.; Zhou, W.; Lei, A.; Zhang, Q.; Wan, Q.; Zou, B., Fast and Considerable Adsorption of Methylene Blue Dye onto Graphene Oxide. *Bull. Environ. Contam. Toxicol.* **2011,** *87*, 86-90.

136. Stankovich, S.; Piner, R. D.; Chen, X.; Wu, N.; Nguyen, S. T.; Ruoff, R. S., Stable Aqueous Dispersions of Graphitic Nanoplatelets Via the Reduction of Exfoliated Graphite Oxide in the Presence of Poly(Sodium 4-Styrenesulfonate). *J. Mater. Chem.* **2006,** *16*, 155.

137. Stankovich, S.; Dikin, D. A.; Piner, R. D.; Kohlhaas, K. A.; Kleinhammes, A.; Jia, Y.; Wu, Y.; Nguyen, S. T.; Ruoff, R. S., Synthesis of Graphene-Based Nanosheets Via Chemical Reduction of Exfoliated Graphite Oxide. *Carbon* **2007,** *45*, 1558-1565.

138. Travlou, N. A.; Kyzas, G. Z.; Lazaridis, N. K.; Deliyanni, E. A., Functionalization of Graphite Oxide with Magnetic Chitosan for the Preparation of a Nanocomposite Dye Adsorbent. *Langmuir* **2013,** *29*, 1657-1668.

139. Madadrang, C. J.; Kim, H. Y.; Gao, G.; Wang, N.; Zhu, J.; Feng, H.; Gorring, M.; Kasner, M. L.; Hou, S., Adsorption Behavior of Edta-Graphene Oxide for Pb (Ii) Removal. *ACS Appl. Mater. Interfaces* **2012,** *4*, 1186-1193.

140. He, F.; Fan, J.; Ma, D.; Zhang, L.; Leung, C.; Chan, H. L., The Attachment of Fe_3o_4 Nanoparticles to Graphene Oxide by Covalent Bonding. *Carbon* **2010,** *48*, 3139-3144.

141. Meral, K.; Metin, Ö., Graphene Oxide--Magnetite Nanocomposite as an Efficient and Magnetically Separable Adsorbent for Methylene Blue Removal from Aqueous Solution. *Turk. J. Chem.* **2014,** *38*, 775-782.

142. Huang, S.-H.; Chen, D.-H., Rapid Removal of Heavy Metal Cations and Anions from Aqueous Solutions by an Amino-Functionalized Magnetic Nano-Adsorbent. *J. Hazard. Mater.* **2009,** *163*, 174-179.

143. Kan, L.; Xu, Z.; Gao, C., General Avenue to Individually Dispersed Graphene Oxide-Based Two-Dimensional Molecular Brushes by Free Radical Polymerization. *Macromolecules* **2010,** *44*, 444-452.

144. Yang, Y.; Xie, Y.; Pang, L.; Li, M.; Song, X.; Wen, J.; Zhao, H., Preparation of Reduced Graphene Oxide/Poly(Acrylamide) Nanocomposite and Its Adsorption of Pb(Ii) and Methylene Blue. *Langmuir* **2013,** *29*, 10727-10736.

145. Liu, J.; Cao, H.; Xiong, J.; Cheng, Z., Ferromagnetic Hematite@ Graphene Nanocomposites for Removal of Rhodamine B Dye Molecules from Water. *CrystEngComm* **2012,** *14*, 5140-5144.

146. Chandra, V.; Park, J.; Chun, Y.; Lee, J. W.; Hwang, I.-C.; Kim, K. S., Water-Dispersible Magnetite-Reduced Graphene Oxide Composites for Arsenic Removal. *ACS Nano* **2010,** *4*, 3979-3986.

147. Neises, B.; Steglich, W., Simple Method for the Esterification of Carboxylic Acids. *Angew. Chem., Int. Ed. Engl.* **1978,** *17*, 522-524.

148. Durdureanu-Angheluta, A.; Ardeleanu, R.; Pinteala, M.; Harabagiu, V.; Chiriac, H.; Simionescu, B., Silane Covered Magnetite Particles. Preparation and Characterisation. *Dig. J. Nanomater. Bios.* **2008,** *3*, 33-40.

149. Everaerts, F.; Torrianni, M.; Hendriks, M.; Feijen, J., Biomechanical Properties of Carbodiimide Crosslinked Collagen: Influence of the Formation of Ester Crosslinks. *J. Biomed. Mater. Res. A* **2007,** *85*, 547-555.

150. Liao, M.-H.; Chen, D.-H., Preparation and Characterization of a Novel Magnetic Nano-Adsorbent. *J. Mater. Chem.* **2002,** *12*, 3654-3659.

151. Mak, S.-Y.; Chen, D.-H., Fast Adsorption of Methylene Blue on Polyacrylic Acid-Bound Iron Oxide Magnetic Nanoparticles. *Dyes Pigm.* **2004,** *61*, 93-98.

152. Yao, Y.; Miao, S.; Yu, S.; Ma, L. P.; Sun, H.; Wang, S., Fabrication of Fe_3O_4/Sio_2 Core/Shell Nanoparticles Attached to Graphene Oxide and Its Use as an Adsorbent. *J. Colloid Interface Sci.* **2012,** *379*, 20-26.

153. Yao, Y.; Miao, S.; Liu, S.; Ma, L. P.; Sun, H.; Wang, S., Synthesis, Characterization, and Adsorption Properties of Magnetic Fe_3O_4@Graphene Nanocomposite. *Chem. Eng. J.* **2012,** *184*, 326-332.

154. Li, L.; Liu, X. L.; Gao, M.; Hong, W.; Liu, G. Z.; Fan, L.; Hu, B.; Xia, Q. H.; Liu, L.; Song, G. W.; Xu, Z. S., The Adsorption on Magnetic Hybrid Fe_3o_4/Hkust-1/Go of Methylene Blue from Water Solution. *J. Mater. Chem. A* **2014,** *2*, 1795.

155. Paek, S.-M.; Yoo, E.; Honma, I., Enhanced Cyclic Performance and Lithium Storage Capacity of Sno_2/Graphene Nanoporous Electrodes with Three-Dimensionally Delaminated Flexible Structure. *Nano letters* **2009,** *9*, 72-75.

156. Xie, Y.; Yan, B.; Xu, H.; Chen, J.; Liu, Q.; Deng, Y.; Zeng, H., Highly Regenerable Mussel-Inspired Fe3o4@ Polydopamine-Ag Core-Shell Microspheres as Catalyst and Adsorbent for Methylene Blue Removal. *ACS Appl. Mater. Interfaces* **2014,** *6*, 8845-8852.

157. Fu, Y.; Wang, J.; Liu, Q.; Zeng, H., Water-Dispersible Magnetic Nanoparticle–Graphene Oxide Composites for Selenium Removal. *Carbon* **2014,** *77*, 710-721.

158. Wang, G.; Yang, S.; Wei, Z.; Dong, X.; Wang, H.; Qi, M., Facile Preparation of Poly(E-Caprolactone)/Fe_3o_4@Graphene Oxide Superparamagnetic Nanocomposites. *Polym. Bull.* **2013,** *70*, 2359-2371.

159. Yang, Z.; Chen, X.-H.; Xia, S.-Z.; Pu, Y.-X.; Xu, H.-Y.; Li, W.-H.; Xu, L.-S.; Yi, B.; Pan, W.-Y., Covalent Attachment of Poly (Acrylic Acid) onto Multiwalled Carbon Nanotubes Functionalized with Formaldehyde Via Electrophilic Substitution Reaction. *J. Mater. Sci.* **2007,** *42*, 9447-9452.

160. Zhang, J.; Yang, H.; Shen, G.; Cheng, P.; Zhang, J.; Guo, S., Reduction of Graphene Oxide Via L-Ascorbic Acid. *Chem. Commun.* **2010,** *46*, 1112-1114.

161. Dong, Y.; Hu, M.; Ma, R.; Cheng, H.; Yang, S.; Li, Y. Y.; Zapien, J. A., Evaporation-Induced Synthesis of Carbon-Supported Fe_3O_4 Nanocomposites as Anode Material for Lithium-Ion Batteries. *CrystEngComm* **2013,** *15*, 1324-1331.

162. Jin, Y.; Jia, C.; Huang, S.-W.; O'Donnell, M.; Gao, X., Multifunctional Nanoparticles as Coupled Contrast Agents. *Nat. Commun.* **2010,** *1*, 41.

163. Reimer, L.; Kohl, H., *Transmission Electron Microscopy: Physics of Image Formation*. Springer Science & Business Media: 2008; Vol. 36.

164. Gentsch, P.; Gilde, H.; Reimer, L., Measurement of the Top Bottom Effect in Scanning Transmission Electron Microscopy of Thick Amorphous Specimens. *J. Microsc.* **1974,** *100*, 81-92.

165. Socrates, G., *Infrared and Raman Characteristic Group Frequencies: Tables and Charts*. John Wiley & Sons: 2004.

166. Larkin, P., *Infrared and Raman Spectroscopy; Principles and Spectral Interpretation*. Elsevier: 2011.

167. Shimanouchi, T. *Tables of Molecular Vibrational Frequencies Consolidated. Volume I*; DTIC Document: 1972.

168. Some, S.; Kim, Y.; Yoon, Y.; Yoo, H.; Lee, S.; Park, Y.; Lee, H., High-Quality Reduced Graphene Oxide by a Dual-Function Chemical Reduction and Healing Process. *Sci. Rep.* **2013,** *3*, 1929.

169. Fu, Y. Water-Dispersible Magnetic Particle-Graphene Oxide Composites: Synthesis, Characterization and Application in the Removal of Selenium. Master Thesis, University of Alberta, 2014.

170. Novoselov, K. S.; Geim, A. K.; Morozov, S. V.; Jiang, D.; Zhang, Y.; Dubonos, S. V.; Grigorieva, I. V.; Firsov, A. A., Electric Field Effect in Atomically Thin Carbon Films. *Science* **2004,** *306*, 666-669.

171. Connors, K. A., *Chemical Kinetics: The Study of Reaction Rates in Solution*. John Wiley & Sons: 1990.

172. Toth, J., *Adsorption*. CRC Press: 2002.

173. Langmuir, I., The Constitution and Fundamental Properties of Solids and Liquids. Part I. Solids. *J. Am. Chem. Soc.* **1916,** *38*, 2221-2295.

174. Freundlich, H., Uber Die Adsorption in Losungen. *Zeitschrift für Physikalische* **1906,** *57*, 384-470.

175. Masel, R. I., *Principles of Adsorption and Reaction on Solid Surfaces*. John Wiley & Sons: 1996; Vol. 3.

176. Tuite, E. M.; Kelly, J. M., New Trends in Photobiology: Photochemical Interactions of Methylene Blue and Analogues with DNA and Other Biological Substrates. *J. Photochem. Photobiol., B* **1993,** *21*, 103-124.

177. He, F.; Fan, J.; Ma, D.; Zhang, L.; Leung, C.; Chan, H. L., The Attachment of Fe_3O_4 Nanoparticles to Graphene Oxide by Covalent Bonding. *Carbon* **2010,** *48*, 3139-3144.

178. Li, L.; Liu, X. L.; Gao, M.; Hong, W.; Liu, G. Z.; Fan, L.; Hu, B.; Xia, Q. H.; Liu, L.; Song, G. W., The Adsorption on Magnetic Hybrid Fe_3O_4/Hkust-1/Go of Methylene Blue from Water Solution. *J. Mater. Chem. A* **2014,** *2*, 1795-1801.

179. Yin, P. T.; Shah, S.; Chhowalla, M.; Lee, K.-B., Design, Synthesis, and Characterization of Graphene–Nanoparticle Hybrid Materials for Bioapplications. *Chem. Rev.* **2015,** *115*, 2483-2531.

180. Huang, W.; Wu, Y.; Qiu, L.; Dong, C.; Ding, J.; Li, D., Tuning Rheological Performance of Silica Concentrated Shear Thickening Fluid by Using Graphene Oxide. *Adv. Condens. Matter Phys.* **2015,** *2015*.

181. Li, D.; Müller, M. B.; Gilje, S.; Kaner, R. B.; Wallace, G. G., Processable Aqueous Dispersions of Graphene Nanosheets. *Nat. Nanotechnol.* **2008,** *3*, 101-105.

182. Li, P.; Wong, M.; Zhang, X.; Yao, H.; Ishige, R.; Takahara, A.; Miyamoto, M.; Nishimura, R.; Sue, H.-J., Tunable Lyotropic Photonic Liquid Crystal Based on Graphene Oxide. *ACS photonics* **2014,** *1*, 79-86.

183. Wan, S.; Li, Y.; Peng, J.; Hu, H.; Cheng, Q.; Jiang, L., Synergistic Toughening of Graphene Oxide–Molybdenum Disulfide–Thermoplastic Polyurethane Ternary Artificial Nacre. *ACS Nano* **2015,** *9*, 708-714.

184. Shi, Y.; Pramanik, A.; Tchounwou, C.; Pedraza, F.; Crouch, R. A.; Chavva, S. R.; Vangara, A.; Sinha, S. S.; Jones, S.; Sardar, D., Multifunctional Biocompatible Graphene Oxide Quantum Dots Decorated Magnetic Nanoplatform for Efficient Capture and Two-Photon Imaging of Rare Tumor Cells. *ACS Appl. Mater. Interfaces* **2015,** *7*, 10935-10943.

185. Zhang, M.; Zhao, Y.; Yan, L.; Peltier, R.; Hui, W.; Yao, X.; Cui, Y.; Chen, X.; Sun, H.; Wang, Z., Interfacial Engineering of Bimetallic Ag/Pt Nanoparticles on Reduced Graphene Oxide Matrix for Enhanced Antimicrobial Activity. *ACS Appl. Mater. Interfaces* **2016,** *8*, 8834-8840.

186. Shi, L.; Wang, Y.; Zhang, L.; Wang, P., Rational Design of a Bi-Layered Reduced Graphene Oxide Film on Polystyrene Foam for Solar-Driven Interfacial Water Evaporation. *J. Mater. Chem. A* **2017**.

187. Yang, X.; Zhang, X.; Ma, Y.; Huang, Y.; Wang, Y.; Chen, Y., Superparamagnetic Graphene Oxide–Fe 3 O 4 Nanoparticles Hybrid for Controlled Targeted Drug Carriers. *J. Mater. Chem.* **2009,** *19*, 2710-2714.

188. Koninti, R. K.; Sengupta, A.; Gavvala, K.; Ballav, N.; Hazra, P., Loading of an Anti-Cancer Drug onto Graphene Oxide and Subsequent Release to DNA/Rna: A Direct Optical Detection. *Nanoscale* **2014,** *6*, 2937-2944.

189. Yang, K.; Feng, L.; Liu, Z., The Advancing Uses of Nano-Graphene in Drug Delivery. *Expert Opin. Drug Deliv.* **2015,** *12*, 601-612.

190. Lu, C. H.; Yang, H. H.; Zhu, C. L.; Chen, X.; Chen, G. N., A Graphene Platform for Sensing Biomolecules. *Angew. Chem.* **2009,** *121*, 4879-4881.

191. Hummers Jr, W. S.; Offeman, R. E., Preparation of Graphitic Oxide. *J. Am. Chem. Soc.* **1958,** *80*, 1339-1339.

192. Liu, X.; Leng, C.; Yu, L.; He, K.; Brown, L. J.; Chen, Z.; Cho, J.; Wang, D., Ion-Specific Oil Repellency of Polyelectrolyte Multilayers in Water: Molecular Insights into the Hydrophilicity of Charged Surfaces. *Angew. Chem.* **2015,** *127*, 4933-4938.

193. Hutter, J. L.; Bechhoefer, J., Calibration of Atomic - Force Microscope Tips. *Rev. Sci. Instrum.* **1993,** *64*, 1868-1873.

194. Lin, A.; Brunner, R.; Chen, P.; Talke, F.; Meyers, M., Underwater Adhesion of Abalone: The Role of Van Der Waals and Capillary Forces. *Acta Mater.* **2009,** *57*, 4178-4185.

195. Canto, M. I. F.; Setrakian, S.; Petras, R. E.; Blades, E.; Chak, A.; Sivak, M. V., Methylene Blue Selectively Stains Intestinal Metaplasia in Barrett's Esophagus. *Gastrointest. Endosc.* **1996,** *44*, 1-7.

196. Wainwright, M.; Crossley, K., Methylene Blue-a Therapeutic Dye for All Seasons? *J. Chemother.* **2002,** *14*, 431-443.

197. Schultz, E., Inactivation of Staphyloccus Bacteriophage by Methylene Blue. *Proc. Soc. Exp. Biol. Med.* **1928,** *26*, 100-101.

198. Chen, J. R.; Jiao, X. X.; Luo, H. Q.; Li, N. B., Probe-Label-Free Electrochemical Aptasensor Based on Methylene Blue-Anchored Graphene Oxide Amplification. *J. Mater. Chem. B* **2013,** *1*, 861-864.

199. Park, S.; Ruoff, R. S., Chemical Methods for the Production of Graphenes. *Nature nanotechnology* **2009,** *4*, 217-224.

200. Some, S.; Kim, Y.; Yoon, Y.; Yoo, H.; Lee, S.; Park, Y.; Lee, H., High-Quality Reduced Graphene Oxide by a Dual-Function Chemical Reduction and Healing Process. *Sci. Rep.* **2013,** *3*, 1929.

201. Konkena, B.; Vasudevan, S., Understanding Aqueous Dispersibility of Graphene Oxide and Reduced Graphene Oxide through Pka Measurements. *J. Phys. Chem. Lett.* **2012,** *3*, 867-872.

202. Zhang, Y.; Liu, C.; Shi, W.; Wang, Z.; Dai, L.; Zhang, X., Direct Measurements of the Interaction between Pyrene and Graphite in Aqueous Media by Single Molecule Force Spectroscopy: Understanding the Π-Π Interactions. *Langmuir* **2007,** *23*, 7911-7915.

203. Lee, H.; Scherer, N. F.; Messersmith, P. B., Single-Molecule Mechanics of Mussel Adhesion. *Proc. Natl. Acad. Sci. U. S. A.* **2006,** *103*, 12999-13003.

204. Stock, P.; Monroe, J. I.; Utzig, T.; Smith, D. J.; Shell, M. S.; Valtiner, M., Unraveling Hydrophobic Interactions at the Molecular Scale Using Force Spectroscopy and Molecular Dynamics Simulations. *ACS Nano* **2017,** *11*, 2586-2597.

205. Hinterdorfer, P.; Dufrêne, Y. F., Detection and Localization of Single Molecular Recognition Events Using Atomic Force Microscopy. *Nat. Methods* **2006,** *3*, 347-355.

206. Zhang, Y.; Liu, C.; Shi, W.; Wang, Z.; Dai, L.; Zhang, X., Direct Measurements of the Interaction between Pyrene and Graphite in Aqueous Media by Single Molecule Force Spectroscopy: Understanding the Π− Π Interactions. *Langmuir* **2007,** *23*, 7911-7915.

207. Zhang, W.; Zhang, X., Single Molecule Mechanochemistry of Macromolecules. *Prog. Polym. Sci.* **2003,** *28*, 1271-1295.

208. Li, Y.; Qin, M.; Li, Y.; Cao, Y.; Wang, W., Single Molecule Evidence for the Adaptive Binding of Dopa to Different Wet Surfaces. *Langmuir* **2014,** *30*, 4358-4366.

209. Das, P.; Reches, M., Revealing the Role of Catechol Moieties in the Interactions between Peptides and Inorganic Surfaces. *Nanoscale* **2016,** *8*, 15309-15316.

210. Frisch, M.; Trucks, G.; Schlegel, H.; Scuseria, G.; Robb, M.; Cheeseman, J.; Scalmani, G.; Barone, V.; Mennucci, B.; Petersson, G., Gaussian 09, Revision D. 01*, Gaussian Inc., Wallingford CT* **2016**.

211. Taylor, W. H., The Crystal Structure of Methylene Blue. *J. Chem. Technol. Biotechnol.* **1935**, 732-734.

212. Kong, X.; Chen, Q., The Positive Influence of Boron-Doped Graphene with Pyridine as a Probe Molecule on Sers: A Density Functional Theory Study. *J. Mater. Chem.* **2012,** *22*, 15336.

213. Balamurugan, K.; Subramanian, V., Adsorption of Chlorobenzene onto (5,5) Armchair Single-Walled Carbon Nanotube and Graphene Sheet: Toxicity Versus Adsorption Strength. *J. Phys. Chem. C* **2013,** *117*, 21217-21227.

214. Janiak, C., A Critical Account on Π–Π Stacking in Metal Complexes with Aromatic Nitrogen-Containing Ligands. *J. Chem. Soc., Dalton Trans.* **2000**, 3885-3896.

215. Martinez, C. R.; Iverson, B. L., Rethinking the Term "Pi-Stacking". *Chem. Sci.* **2012,** *3*, 2191.

216. Higaki, Y.; Kiyoshima, Y.; Suzuki, K.; Kabayama, H.; Ohta, N.; Seo, Y.; Takahara, A., Elastomers Built up through the Π–Π Stacking Association of Polycyclic Planar Aromatic Diimides. *RSC Adv.* **2017,** *7*, 46195-46200.

217. ChemCraft program: http://www.chemcraftprog.com.

218. McGaughey, G. B.; Gagné, M.; Rappé, A. K., Π-Stacking Interactions Alive and Well in Proteins. *J. Biol. Chem.* **1998,** *273*, 15458-15463.

219. Ringer, A. L.; Sinnokrot, M. O.; Lively, R. P.; Sherrill, C. D., The Effect of Multiple Substituents on Sandwich and T‐Shaped ∏–∏ Interactions. *Chem.-Eur. J.* **2006,** *12*, 3821-3828.

220. Volkov, A.; Coppens, P., Calculation of Electrostatic Interaction Energies in Molecular Dimers from Atomic Multipole Moments Obtained by Different Methods of Electron Density Partitioning. *J. Comput. Chem.* **2004,** *25*, 921-934.

221. Mecozzi, S.; West, A. P.; Dougherty, D. A., Cation-Pi Interactions in Aromatics of Biological and Medicinal Interest: Electrostatic Potential Surfaces as a Useful Qualitative Guide. *Proc. Natl. Acad. Sci. U. S. A.* **1996,** *93*, 10566-10571.

222. Hawker, C. J.; Fréchet, J. M., Monodispersed Dendritic Polyesters with Removable Chain Ends: A Versatile Approach to Globular Macromolecules with Chemically Reversible Polarities. *J. Chem. Soc., Perkin Trans. 1* **1992**, 2459-2469.

223. Bardhan, N. M.; Kumar, P. V.; Li, Z.; Ploegh, H. L.; Grossman, J. C.; Belcher, A. M.; Chen, G.-Y., Enhanced Cell Capture on Functionalized Graphene Oxide Nanosheets through Oxygen Clustering. *ACS Nano* **2017**.

224. Schlenoff, J. B., Zwitteration: Coating Surfaces with Zwitterionic Functionality to Reduce Nonspecific Adsorption. *Langmuir* **2014,** *30*, 9625-9636.

225. Ji, Y.-L.; An, Q.-F.; Guo, Y.-S.; Hung, W.-S.; Lee, K.-R.; Gao, C.-J., Bio-Inspired Fabrication of High Perm-Selectivity and Anti-Fouling Membranes Based on Zwitterionic Polyelectrolyte Nanoparticles. *J. Mater. Chem. A* **2016,** *4*, 4224-4231.

226. Chen, M.; Briscoe, W. H.; Armes, S. P.; Klein, J., Lubrication at Physiological Pressures by Polyzwitterionic Brushes. *Science* **2009,** *323*, 1698-1701.

227. Yang, F.; Tchoukov, P.; Pensini, E.; Dabros, T.; Czarnecki, J.; Masliyah, J.; Xu, Z., Asphaltene Subfractions Responsible for Stabilizing Water-in-Crude Oil Emulsions. Part 1: Interfacial Behaviors. *Energy Fuels* **2014,** *28*, 6897-6904.

228. Xue, Z.; Wang, S.; Lin, L.; Chen, L.; Liu, M.; Feng, L.; Jiang, L., A Novel Superhydrophilic and Underwater Superoleophobic Hydrogel - Coated Mesh for Oil/Water Separation. *Adv. Mater.* **2011,** *23*, 4270-4273.

229. Zhou, X.; Zhang, Z.; Xu, X.; Guo, F.; Zhu, X.; Men, X.; Ge, B., Robust and Durable Superhydrophobic Cotton Fabrics for Oil/Water Separation. *ACS Appl. Mater. Interfaces* **2013,** *5*, 7208-7214.

230. Dalsin, J. L.; Hu, B.-H.; Lee, B. P.; Messersmith, P. B., Mussel Adhesive Protein Mimetic Polymers for the Preparation of Nonfouling Surfaces. *J. Am. Chem. Soc.* **2003,** *125*, 4253-4258.

231. Lee, H.; Dellatore, S. M.; Miller, W. M.; Messersmith, P. B., Mussel-Inspired Surface Chemistry for Multifunctional Coatings. *Science* **2007,** *318*, 426-430.

232. Lee, H.; Scherer, N. F.; Messersmith, P. B., Single-Molecule Mechanics of Mussel Adhesion. *Proc. Natl. Acad. Sci. U. S. A.* **2006,** *103*, 12999-13003.

233. Yang, H.-C.; Liao, K.-J.; Huang, H.; Wu, Q.-Y.; Wan, L.-S.; Xu, Z.-K., Mussel-Inspired Modification of a Polymer Membrane for Ultra-High Water Permeability and Oil-in-Water Emulsion Separation. *Journal of Materials Chemistry A* **2014,** *2*, 10225-10230.

234. Alboudwarej, H.; Pole, D.; Svrcek, W. Y.; Yarranton, H. W., Adsorption of Asphaltenes on Metals. *Ind. Eng. Chem. Res.* **2005,** *44*, 5585-5592.

235. Akhlaq, M. S.; Götze, P.; Kessel, D.; Dornow, W., Adsorption of Crude Oil Colloids on Glass Plates: Measurements of Contact Angles and the Factors Influencing Glass Surface Properties. *Colloids Surf. Physicochem. Eng. Aspects* **1997,** *126*, 25-32.

236. Higaki, Y.; Hatae, K.; Ishikawa, T.; Takanohashi, T.; Hayashi, J.-i.; Takahara, A., Adsorption and Desorption Behavior of Asphaltene on Polymer-Brush-Immobilized Surfaces. *ACS Appl. Mater. Interfaces* **2014,** *6*, 20385-20389.

237. Turgman-Cohen, S.; Fischer, D. A.; Kilpatrick, P. K.; Genzer, J., Asphaltene Adsorption onto Self-Assembled Monolayers of Alkyltrichlorosilanes of Varying Chain Length. *ACS Appl. Mater. Interfaces* **2009,** *1*, 1347-1357.

238. Das, S.; Thundat, T.; Mitra, S. K., Analytical Model for Zeta Potential of Asphaltene. *Fuel* **2013,** *108*, 543-549.